

---

Electronic Thesis and Dissertation Repository

---

January 2015

## A Study of Photon Trapping and the ac Stark Effect in Photonic Crystals and Dispersive Materials

Iftekharul Haque, *The University of Western Ontario*

Supervisor: Mahi R. Singh, *The University of Western Ontario*

A thesis submitted in partial fulfillment of the requirements for the Doctor of Philosophy degree in Physics

© Iftekharul Haque 2015

Follow this and additional works at: <https://ir.lib.uwo.ca/etd>

 Part of the [Condensed Matter Physics Commons](#)

---

### Recommended Citation

Haque, Iftekharul, "A Study of Photon Trapping and the ac Stark Effect in Photonic Crystals and Dispersive Materials" (2015). *Electronic Thesis and Dissertation Repository*. 2670.  
<https://ir.lib.uwo.ca/etd/2670>

This Dissertation/Thesis is brought to you for free and open access by Scholarship@Western. It has been accepted for inclusion in Electronic Thesis and Dissertation Repository by an authorized administrator of Scholarship@Western. For more information, please contact [wlsadmin@uwo.ca](mailto:wlsadmin@uwo.ca).

A STUDY OF PHOTON TRAPPING AND THE AC STARK EFFECT IN PHOTONIC  
CRYSTALS AND DISPERSIVE MATERIALS

(Thesis format: Monograph)

by

Iftekhar Haque

Graduate Program in Physics

A thesis submitted in partial fulfillment  
of the requirements for the degree of  
Doctor of Philosophy

The School of Graduate and Postdoctoral Studies  
The University of Western Ontario  
London, Ontario, Canada

© Iftekhar Haque 2014

# Abstract

In this thesis, we study light-matter interaction in the contexts of coherent population trapping (CPT) and the ac Stark effect in nanoparticles embedded (doped) in two important classes of reservoirs -- photonic crystals and dispersive materials. These materials have gaps in their energy spectra and are studied widely due to their unusual optical properties and potential for novel applications. We consider that the reservoirs are doped with an ensemble of five-level nanoparticles, each with a single  $\Lambda$  core (consisting of a lower doublet and an upper energy level), which interact with both the host reservoir and external radiation fields. We have also included studies of cases where the nanoparticles interact with each other as well via dipole-dipole interaction (DDI), which is included in the mean field approximation. This only happens when the doping concentration is high ( $\sim 10^{18}$  per cubic meter).

In studying CPT, we have developed a novel technique of optical switching by devising a system whereby the doped nanoparticles become stable against absorption from the radiation field(s) i.e. they switch to their ground states. We have confirmed the occurrence of CPT in both types of reservoir and have also identified a number of important contrasting features which have markedly different utilities. Most significantly, we have found that the strength of the DDI between the nanoparticles plays a very important role in determining the conditions required for CPT in both materials. In studying the ac Stark effect in photonic crystals, we have used an ensemble of five-level nanoparticles, each with a single cascade core [ladder configuration], both with and without DDI. We found that, in the ac Stark regime, resonance tuning of the transitions within the nanoparticles, in relation to the band structure of these crystals, offers a new mechanism for switching the nanoparticle system from an inverted to a non-inverted state. Specifically, a doped nanoparticle can effectively become transparent to any radiation field tuned to the probed transition. Under DDI, we found that the absorption in the system decreases with increasing DDI strength. These findings have very exciting potential for applications in optical switching.

## Keywords

Quantum coherence, quantum interference, photonic crystals, dispersive materials, coherent population trapping, ac Stark effect, dipole-dipole interaction

## Co-Authorship Statement

All publications and research presented in this thesis were co-authored with Prof. Mahi R. Singh. In all cases, without exception, the principle idea behind the research was developed by the first author. All calculations and numerical simulations, without exception, were performed by Iftekhar Haque. The analyses of the results of the calculations and simulations were carried, without exception, in equal collaboration between the authors.

## Acknowledgments

I want to thank my supervisor, Prof. Mahi R. Singh, for his guidance and the benefit of his singular wisdom, throughout the years.

I must extend my dutiful gratitude to the Ministry of Training, Colleges and Universities, Ontario, Canada for support in the form of an Ontario Graduate Scholarship and also to Natural Sciences and Engineering Research Council of Canada for the endowment of a Postgraduate Scholarship.

Lastly, I wish to convey my heartfelt appreciation to Peter and Laurie Komorowski, for their unconditional and much needed support in my hours of dire need. You were friends, indeed.

*To my brother,  
my keeper,  
and  
to my darling Olivia,  
my life.*

# Table of Contents

|   |     |
|---|-----|
| Abstract .....  | ii  |
| Co-Authorship Statement.....  | iii |
| Acknowledgments.....  | iv  |
| Table of Contents .....   | vi  |
| List of Figures .....   | ix  |
| List of Appendices .....  | xiv |
| Chapter 1 .....   | 1   |
| 1 Introduction .....  | 1   |
| 1.1 Photonic Crystals .....   | 1   |
| 1.2 Dispersive Materials .....  | 2   |
| 1.3 Dipole-dipole Interaction .....   | 4   |
| 1.4 Coherent Population Trapping.....   | 7   |
| 1.5 ac Stark Effect.....  | 14  |
| 1.6 Recent Related Developments in Photonic Crystals and Dispersive Materials.... | 16  |
| 1.7 Outline of the Thesis .....   | 20  |
| Chapter 2.....  | 23  |
| 2 Population Trapping in Photonic Crystals .....                                  | 23  |
| 2.1 Introduction.....   | 23  |
| 2.2 Photonic Crystals .....   | 25  |
| 2.3 Coherent Population Trapping.....   | 28  |
| 2.4 Population Density and Photon Trapping .....                                  | 31  |
| 2.5 Results and Discussions .....   | 39  |
| 2.6 Summary and Conclusion .....  | 43  |
| Chapter 3.....  | 44  |

|       |  |     |
|-------|--|-----|
| 3     | Population Trapping in Dispersive Materials .....  | 44  |
| 3.1   | Introduction.....  | 44  |
| 3.2   | Dispersive Materials .....   | 47  |
| 3.3   | Dispersive Materials as Reservoirs.....  | 52  |
| 3.4   | Population Density and Polariton Trapping.....   | 53  |
| 3.5   | Results and Discussions.....   | 54  |
| 3.6   | Summary and Conclusion .....   | 56  |
|       | Chapter 4.....   | 58  |
| 4     | Dipole-dipole Interaction and Coherent Trapping in Photonic Crystals and Dispersive Materials..... | 58  |
| 4.1   | Introduction.....  | 58  |
| 4.2   | Dipole-dipole Interaction .....  | 60  |
| 4.3   | Population Density and Coherent Population Trapping .....  | 62  |
| 4.4   | Results and Discussions.....   | 66  |
| 4.4.1 | Photonic Crystals .....  | 66  |
| 4.4.2 | Dispersive Materials .....   | 70  |
| 4.5   | Summary and Conclusion .....   | 74  |
|       | Chapter 5.....   | 77  |
| 5     | The ac Stark Effect in Photonic Crystals .....   | 77  |
| 5.1   | Introduction.....  | 77  |
| 5.2   | The ac Stark Effect.....   | 80  |
| 5.3   | Formulation of Susceptibility .....  | 82  |
| 5.4   | Results and Discussions.....   | 93  |
| 5.5   | Summary and Conclusion .....   | 104 |
|       | Chapter 6.....   | 106 |
| 6     | Dipole-dipole Interaction and the ac Stark Effect in Photonic Crystals .....                       | 106 |



|   |     |
|---|-----|
| 6.1 Introduction.....                               | 106 |
| 6.2 The Dipole-dipole Interaction Hamiltonian.....  | 108 |
| 6.3 Absorption Coefficient and Density Matrix ..... | 111 |
| 6.4 Results and Discussions.....                    | 113 |
| 6.5 Summary and Conclusion.....                     | 116 |
| Chapter 7.....                                      | 118 |
| 7 Concluding Remarks.....                           | 118 |
| Bibliography .....                                  | 123 |
| Appendices.....                                     | 136 |
| Curriculum Vitae .....                              | 147 |

## List of Figures

|  |    |
|--|----|
| Figure 2-1: Level scheme of a five-level nanoparticle; $\omega_{ij}$ is the energy difference between levels $ i\rangle$ and $ j\rangle$ . Here, $ i\rangle$ and $ j\rangle$ stand for $ a\rangle,  b\rangle,  c\rangle,  d\rangle$ and $ e\rangle$ . Levels $ b\rangle$ and $ c\rangle$ both spontaneously decay to level $ e\rangle$ and level $ a\rangle$ spontaneously decays to level $ d\rangle$ , due to nanoparticle-reservoir interaction. $\Gamma_a, \Gamma_b$ and $\Gamma_c$ denote the linewidths of levels $ a\rangle,  b\rangle$ and $ c\rangle$ , respectively. $\Omega_1$ and $\Omega_2$ are the magnitudes of the Rabi frequencies corresponding to the two fields..... | 24 |
| Figure 2-2: Schematic representation of a photonic crystal with three-dimensional periodicity. It consists of a periodic arrangement of dielectric spheres in air. The lattice constant is denoted as $L$ .....  | 26 |
| Figure 2-3: Plot of the photon energy $\varepsilon_k$ as a function of the wave vector $k$ for a photonic crystal. Note that there is an energy gap between $\varepsilon_c$ and $\varepsilon_v$ . .....  | 28 |
| Figure 2-4: Level scheme of a $\Lambda$ -type three-level nanoparticle. The energy difference between levels $ i\rangle$ and $ j\rangle$ is denoted as $\omega_{ij}$ . Levels $ a\rangle$ and $ b\rangle$ are coupled by a field of frequency $\nu_1$ and amplitude $E_1$ ; $ a\rangle$ and $ c\rangle$ are coupled by a probe field of frequency $\nu_2$ and amplitude $E_2$ .....  | 29 |
| Figure 2-5: Plot of the dispersion relation of the photonic crystal with $n = 1.082$ , $a/L = 0.24$ and $L = 300$ nm. The quantities $\varepsilon_v$ and $\varepsilon_c$ are the maximum energy of the valence band and the minimum energy of the conduction band, respectively. The horizontal axis is the ratio of the energy $\varepsilon_k$ to the maximum valence band energy $\varepsilon_v$ . The band gap of the crystal lies between $\varepsilon_k / \varepsilon_v = 1$ and $\varepsilon_c / \varepsilon_v$ , shown by the vertical dashed lines. ....   | 32 |
| Figure 2-6: Plot of the form factor $Z(\varepsilon_k)$ of the photonic crystal. The choices of the crystal parameters and the horizontal axis are identical to those for the dispersion relation in Fig. 2-5.....  | 35 |

|  |    |
|--|----|
| Figure 2-7: Plot of $\rho_{aa}$ against varying $\Omega_r$ and $\varepsilon_{ad}$ for the photonic crystal – displays symmetric response about the band gap. ....  | 41 |
| Figure 3-1: Level scheme of a five-level nanoparticle; $\omega_{ij}$ is the energy difference between levels $ i\rangle$ and $ j\rangle$ . Here, $ i\rangle$ and $ j\rangle$ stand for $ a\rangle,  b\rangle,  c\rangle,  d\rangle$ and $ e\rangle$ . Levels $ b\rangle$ and $ c\rangle$ both spontaneously decay to level $ e\rangle$ and level $ a\rangle$ spontaneously decays to level $ d\rangle$ , due to nanoparticle-reservoir interaction. $\Gamma_a, \Gamma_b$ and $\Gamma_c$ denote the linewidths of levels $ a\rangle,  b\rangle$ and $ c\rangle$ , respectively. $\Omega_1$ and $\Omega_2$ are the magnitudes of the Rabi frequencies corresponding to the two fields..... | 45 |
| Figure 3-2: Plot of the dispersion relation for SiC. The parameters used are $\varepsilon_v = 0.098$ eV, $\varepsilon_c = 0.118$ eV and $\kappa = 10^{-5}$ eV.....   | 50 |
| Figure 3-3: Plot of the form factor $Z(\varepsilon)$ of the dispersive material reservoir. The choices of parameters are identical to those for the dispersion relation shown in Fig. 3-2. ....  | 53 |
| Figure 3-4: Plot of $\rho_{aa}$ against $\Omega_r$ and $\varepsilon_{ad}$ for the dispersive material – shows different behaviors at the two band edges. ....  | 55 |
| Figure 4-1: Level scheme of a five-level nanoparticle. $\omega_{ij}$ is the energy difference between the levels $ i\rangle$ and $ j\rangle$ . Here $ i\rangle$ and $ j\rangle$ stand for $ a\rangle,  b\rangle,  c\rangle,  d\rangle$ and $ e\rangle$ . The levels $ b\rangle$ and $ c\rangle$ both spontaneously decay to level $ e\rangle$ and level $ a\rangle$ spontaneously decays to level $ d\rangle$ .....  | 60 |
| Figure 4-2: Plot of the form factor $Z(\varepsilon_k)$ of the photonic crystal. The choices of the crystal parameters and the horizontal axis are identical to those for the dispersion relation in Fig. 2-5.....  | 65 |
| Figure 4-3: Plot of the form factor $Z(\varepsilon)$ of the dispersive material reservoir. The choices of parameters are identical to those for the dispersion relation shown in Fig. 3-2. ....  | 65 |

|  |    |
|--|----|
| Figure 4-4: Plot of $\rho_{aa}$ against $\Omega_r$ for $N = 10^{18}$ (dash-dotted curve), $N = 2 \times 10^{18}$ (dotted curve) and $N = 3 \times 10^{18}$ (solid curve), for a photonic crystal reservoir.....  | 67 |
| Figure 4-5: Plot of $\rho_{aa}$ against $\varepsilon_{ad}$ for the values of $N$ as in Fig 4.4, for a photonic crystal reservoir. ....   | 68 |
| Figure 4-6: Three-dimensional plot of $\rho_{aa}$ against $\Omega_r$ (relative Rabi frequency) and $N$ (number density of doped nanoparticles), for a photonic crystal reservoir. ....   | 69 |
| Figure 4-7: Three-dimensional plot of $\rho_{aa}$ against $\varepsilon_{ad}$ (energy) and $N$ (number density of doped nanoparticles), for a photonic crystal reservoir. ....  | 70 |
| Figure 4-8: Plot of $\rho_{aa}$ against $\Omega_r$ for $N = 10^{18}$ (dotted curve), $N = 2 \times 10^{18}$ (dash-dotted curve) and $N = 3 \times 10^{18}$ (solid curve), for a dispersive material reservoir. ....  | 71 |
| Figure 4-9: Plots of $\rho_{aa}$ against $\varepsilon_{ad}$ for $N = 2.8 \times 10^{18}$ (dotted curve), $N = 2.9 \times 10^{18}$ (dash-dotted curve) and $N = 3.0 \times 10^{18}$ (solid curve) showing the lower energy band, for a dispersive material reservoir. ....  | 72 |
| Figure 4-10: Plots of $\rho_{aa}$ against $\varepsilon_{ad}$ for $N = 2.8 \times 10^{18}$ (dotted curve), $N = 2.9 \times 10^{18}$ (dash-dotted curve) and $N = 3.0 \times 10^{18}$ (solid curve) showing the upper energy band, for a dispersive material reservoir. The band gap is not shown. ....  | 73 |
| Figure 5-1: Schematic diagrams for the five-level atom, driven by two pump laser fields with Rabi frequencies $\Omega_\alpha$ and $\Omega_\beta$ . The levels are denoted as $ a\rangle$ , $ b\rangle$ , $ c\rangle$ , $ d\rangle$ and $ e\rangle$ . The probe field with Rabi frequency $\Omega_p$ drives the (a) $ c\rangle \rightarrow  e\rangle$ or (b) $ b\rangle \rightarrow  e\rangle$ transition. The detuning of the two pump fields and the probe field are denoted as $\Delta_{ab}$ , $\Delta_{bc}$ and (a) $\Delta_{ec}$ or (b) $\Delta_{eb}$ , respectively. The dashed arrows represent the decay channels and $\Gamma_i$ denotes the decay rate of level $ i\rangle$ . .... | 79 |

- Figure 5-2: Schematic representation of the two-level nanoparticle, with ground level  $|g\rangle$  and excited level  $|e\rangle$ , showing the bare and dressed states. The dashed, solid and dash-dotted arrows indicate transitions between the dressed states. .... 81
- Figure 5-3: Plot of the spectral intensity against the frequency, obtained by application of the probe beam, showing the Mollow triplet. .... 81
- Figure 5-4: Plots of the dispersion relation (top panel) and the form factor  $Z(\varepsilon_k)$  (bottom panel) of the photonic crystal with  $n=1.4$ ,  $a/L=0.2$  and  $L=300$  nm, where  $k$  denotes the wave vector. The quantities  $\varepsilon_v$  and  $\varepsilon_c$  are the maximum energy of the valence band and the minimum energy of the conduction band, respectively. The horizontal axis is the ratio of the energy  $\varepsilon_k$  to the maximum valence band energy  $\varepsilon_v$ . The band gap of the crystal lies between  $\varepsilon_k / \varepsilon_v = 1$  and  $\varepsilon_c / \varepsilon_v$ , shown by the vertical dashed lines. .... 83
- Figure 5-5: Numerical plots of the time evolution of the population densities (a)  $\rho_{aa}$  (b)  $\rho_{dd}$  (c)  $\rho_{bb}$  and (d)  $\rho_{cc}$  of the atom in Fig. 5-1(a). The horizontal axes show dimensionless time  $\gamma_0 t$ . The solid curves are drawn for the case where  $\varepsilon_{ad} / \varepsilon_v = 80.00\%$ . The dotted curves represent the case where  $\varepsilon_{ad} / \varepsilon_v = 99.99\%$ . All other resonance energies are kept far from either of the band edges. .... 94
- Figure 5-6: Numerical plots of the time evolution of  $\chi_1'' / \chi_0$  for  $\varepsilon_{ad} / \varepsilon_v = 80.00\%$  (solid curve) and  $\varepsilon_{ad} / \varepsilon_v = 99.99\%$  (dotted curve), using the atomic scheme in Fig. 5-1(a). All other resonance energies are kept away from either of the band edges at all times. The horizontal axis shows scaled time  $\gamma_0 t$ . .... 96
- Figure 5-7: Plots of  $\chi_1'' / \chi_0$  against probe field detuning  $\Delta_{ec} / \gamma_0$  for the atom in Fig. 5-1 (a), in steady state. In (a)  $\Delta_{ab} / \gamma_0 = \Delta_{bc} / \gamma_0 = 0$  and in (b)  $\Delta_{ab} / \gamma_0 = 2$  and  $\Delta_{bc} / \gamma_0 = 0$ . The Rabi frequencies of the laser fields are taken as  $\Omega_\alpha / \gamma_0 = \Omega_\beta / \gamma_0 = 10$  and  $\Omega_p / \gamma_0 = 0.2$ . The solid curves are drawn for the case where all resonance energies are away from either of the band

edges and  $\varepsilon_{ad} / \varepsilon_v = 80.00\%$ . The dash-dotted curves represent the case where  $\varepsilon_{ad} / \varepsilon_v = 99.99\%$  while all other energies remain far from the band edges. .... 97

Figure 5-8: Plots of  $\chi_2'' / \chi_0$  against probe field detuning  $\Delta_{eb} / \gamma_0$  for the atom in Fig. 5-1 (b), in steady state. In (a)  $\Delta_{ab} / \gamma_0 = \Delta_{bc} / \gamma_0 = 0$  and in (b)  $\Delta_{ab} / \gamma_0 = 2$  and  $\Delta_{bc} / \gamma_0 = 0$ . The Rabi frequencies of the laser fields are taken as  $\Omega_\alpha / \gamma_0 = \Omega_\beta / \gamma_0 = 10$  and  $\Omega_p / \gamma_0 = 0.2$ . The solid curves are drawn for the case where all resonance energies are away from either of the band edges and  $\varepsilon_{ad} / \varepsilon_v = 80.00\%$ . The dash-dotted curves represent the case where  $\varepsilon_{ad} / \varepsilon_v = 99.99\%$  while all other energies remain far from the band edges. .... 100

Figure 6-1: Schematic diagram for the five-level nanoparticle, driven by two pump laser fields with Rabi frequencies  $\Omega_\alpha$  and  $\Omega_\beta$ . The levels are denoted as  $|a\rangle$ ,  $|b\rangle$ ,  $|c\rangle$ ,  $|d\rangle$  and  $|e\rangle$ . The probe field with Rabi frequency  $\Omega_p$  drives the  $|c\rangle \rightarrow |e\rangle$  transition. The detuning of the two pump fields and the probe field are denoted as  $\Delta_{ab}$ ,  $\Delta_{bc}$  and  $\Delta_{ec}$ , respectively. The dashed arrows represent the decay channels and  $\Gamma_i$  denotes the decay rate of level  $|i\rangle$ . .... 109

Figure 6-2: Plots of the absorption coefficient against the detuning parameter. The solid and the dashed curves correspond to  $C_c = 0$  and  $C_c = 5$ , respectively. .... 114

Figure 6-3: Plots of the absorption coefficient against the detuning parameter. The solid and the dashed curves correspond to  $C_c = 5$  and  $C_c = 10$ , respectively. .... 115

Figure 6-4: Plots of the absorption coefficient against the detuning parameter when the relevant resonance energy of the nanoparticle lies away from (solid curve) and near a band edge (dashed curve) of the photonic crystal. The DDI parameter  $C_c = 5$ . .... 115

## List of Appendices

|  |     |
|--|-----|
| Appendix A: One-dimensional Scalar Wave Equation .....                         | 136 |
| Appendix B: Photon Dispersion Relation in the Photonic Crystal Reservoir ..... | 136 |
| Appendix C: Reservoir, Field, and Interaction Hamiltonians.....                | 138 |
| Appendix D: Hamiltonian of the Nanoparticle I.....                             | 139 |
| Appendix E: Dipole Approximation.....  | 140 |
| Appendix F: Rotating Wave Approximation (RWA).....                             | 140 |
| Appendix G: Photonic Crystal Form Factor .....                                 | 140 |
| Appendix H: The Laplace Transform Method.....                                  | 142 |
| Appendix I: Hamiltonian of the Nanoparticle II.....                            | 143 |
| Appendix J: Fehlberg Fourth-fifth Order Runge-Kutta Method (RK45) .....        | 143 |
| Appendix K: Switching Power .....  | 144 |

# Chapter 1

## 1 Introduction

Over the course of the last century, studies of quantum coherence and interference have garnered increasing interest in the fields of quantum optics and radiation physics. These phenomena are recognized as being essential for controlling and suppressing the occurrence of spontaneous emission, which is the primary source of undesirable noise in optical devices. This has great relevance in the contexts of quantum computation, teleportation and quantum information processing [1]. Many interesting effects have been predicted in these areas using the ideas of quantum coherence and a wide range of practical applications have been proposed.

This thesis presents our study of the phenomenon of coherent population trapping (CPT) and the ac Stark effect, which occur due to quantum coherence and interference effects in two important classes of materials – namely, photonic crystals and dispersive materials. These materials are doped with an ensemble of nanoparticles which interact with the electromagnetic excitations present in them. Furthermore, when the concentration of the doped nanoparticles is high, they interact with each other via dipole-dipole interaction (DDI). Consequently, we have also studied the effect of DDI on CPT and the ac Stark effect.

### 1.1 Photonic Crystals

Under the framework of quantum coherence, the past two decades have seen crystalline media such as photonic crystals come under intense research scrutiny. These materials have gaps in their photon energy spectra and are studied widely due to their unusual optical properties and great potential for novel applications.

Since their emergence at the end of the 1980s, there has been a growing push towards studying the properties of photonic crystals [2–4], which have wide-ranging applications in photonics and nanotechnology [5–9]. The most significant of these is the phenomenon of light localization, which was first predicted by Sajeev John [10].



A current major area of study involving photonic crystals focuses on the modifications of the radiative properties of nanoparticles doped within the crystal reservoir [11–29]. More specifically, these investigations consider how the optical properties of atoms and molecules embedded in these crystals are altered. Numerous experimental techniques have been developed for doping nanoparticles in photonic crystals and their optical properties have been studied [30–35]. These have important applications in quantum computing and cryptography.

The structure of a photonic crystal is achieved by a periodic arrangement of dielectric materials with differing dielectric constants [2–12]. The resulting periodicity in the dielectric constant function of the crystal leads to the formation of band gaps [2–4], analogous to the energy gaps in the electronic band structures of semiconductors. In other words, photonic crystals facilitate the micromanipulation of photons in much the same way semiconductors manipulate the flow of electrons [36, 37]. Due to the presence of the stop bands in the energy spectra of photonic crystals, photons with energies in the gap regions are not able to propagate in these systems.

The existence of band gaps in photonic crystals is due to multiple photon scattering by spatially correlated scatterers. These gaps may extend over the entire Brillouin zone, known as absolute (isotropic) band gaps, where wave propagation is forbidden irrespective of the direction. If the same is applicable over only a limited domain of wave vectors, the gap is classified as incomplete. The first absolute band gap in a three-dimensional crystalline structure possessing the symmetry of an fcc lattice was independently proposed by John [2] and Yablonovitch [3]. Recently one- [38], two- [39–41] and three- dimensional [42–45] photonic crystals have been fabricated by several groups in the world.

## 1.2 Dispersive Materials

In addition to photonic crystals, energy gaps also exist in dispersive materials. Examples of this type of materials include II–IV, III–V, IV–IV semiconductors (e.g. GaAs and SiC), oxide crystals (e.g. MgO), etc. The gaps in these materials are caused by photons coupling to elementary excitations of the media, i.e. excitons, optical phonons, etc. [46–

48]. When the external field and the excitation of the medium are approximately at resonance, the coupling between the photons (field) and phonons/excitons (medium) changes the character of the propagation and creates a forbidden energy band. We have only considered dielectric materials which have energy gaps in their polaritonic energy spectra confirmed by experiments.

It is important to note that the presence of the energy gap in a dispersive material is not related to any intrinsic periodicity [49]. It is, in fact, due to the phonon-photon coupling in these materials, whereby a quantum of the combined phonon-photon field is formed, known as a polariton. Consequently, materials of this kind are also known as dispersive polaritonic band-gap materials. The discoveries of new phenomena related to the polaritonic energy gap have opened up many new and exciting avenues of research in dispersive materials [20, 21, 50] and numerous potentially applicable effects have been investigated [2–4, 50–52].

For example, Rupasov and Singh have studied the quantum electrodynamics of a single [20, 50] or two identical [22] two-level atom(s) – i.e. nanoparticle(s) – placed within a dispersive material. For either system, due to the presence of the energy gap, only solitons containing an even number of polaritons are found to propagate within the gap, while a soliton with an odd number of polaritons is pinned to the atom and forms a many-polariton-atom bound state. As a result, a significant suppression of spontaneous emission is observed. Also, in the case of an identical pair of atoms separated by a relatively small distance, the polariton-atom bound state lying within the gap is shown to be split into a doublet due to an effective atom-atom interaction [21].

If the dopant is an ordered chain of identical two-level atoms instead, an impurity band is found within the energy gap when the resonance frequencies of the two-level atoms lie inside the gap [54]. It is also observed that, as the interatomic distances increase, the polariton energy bandwidth decreases, along with the effective mass of the polariton. Finally, if the dopant pair of two-level atoms are not identical, a pair of impurity states is formed within the gap [55]. They found that, for small interatomic distances, the

polariton-atom system exhibits superradiance while in the symmetric state, and subradiance (suppression of emission) while in the antisymmetric state.

Recently, Singh [56] has developed a theory of nonlinear two-photon absorption in dispersive materials doped with an ensemble of three-level nanoparticles. He has considered that the nanoparticles are interacting with the polaritonic material. An expression of two-photon absorption has been obtained by using the density matrix method. The DDI effect has also been included in the formulation, which leads to interesting phenomena. More specifically, it has been found that the phenomenon of two-photon absorption can be turned on and off when the resonance energies of the three-level nanoparticles are moved within the lower energy band. It has also been found that the inhibition effect can also be achieved by controlling the strength of the DDI.

### 1.3 Dipole-dipole Interaction

Another important focus of investigations in the field of quantum coherence is the role played by the interaction between the electric dipoles, in different optical properties of multi-level systems [57–61]. When the density of the particles in a system is very high, they interact with each other via DDI. For example, Dowling and Bowden [57, 58] have studied the effect of DDI in the presence of a single laser field on a three-level atomic gas. They found that the observed absorption peak changes from a symmetric shape to an asymmetric shape in the presence of DDI. They also found an enhancement of inversionless gain and absorptionless refractive index for certain values of the nanoparticle density.

Manka et al. [59] have used the theory of Dowling and Bowden [57, 58] to study the effect of atomic nonlinearities on an atomic gas system subject to a single laser field. They predicted a density-dependent switching between absorption and amplification. Calderón et al. [60], on the other hand, have studied DDI in the presence of both one and two laser fields in V-type nanoparticles. They found that the absorption profiles are deformed due to the presence of DDI. They also found that the system changes from absorption to gain due to the phase difference between the probe and the pump fields. In a similar set-up, Afansev et al. [61] have derived the expression for nonlinear

macroscopic polarization in V-type nanoparticles, in the presence of DDI and a bichromatic field.

More recently, Li et al. [62] have performed a theoretical study of the response of nonlinear absorption and population dynamics in optically dense media of four-level atoms driven by a single laser field, subject to near DDI. They found that, with increasing DDI, it is possible to achieve transient amplification with probe-field transparency and ground-state trapping in the steady-state limit. Zhang and Chen [63] have found that the sudden death of the entanglement between atoms in the non-degenerate two photons Travis-Cummings model can be weakened by introducing DDI. Also, Reboiro [64] and Civitarese et al. [65] have demonstrated the DDI dependence of the phenomenon of atomic squeezing in three-level atoms.

Very recently, Vlasov et al. [66] have shown that DDI has a significant effect on the resonance fluorescence spectra of multi-level atoms, in general, interacting with an external field of constant intensity. They have observed the dynamics of the ensemble as compared to that of a single atom and discovered new components in the fluorescence related to auto-oscillations of the level populations. And, most notably, Ablayev et al. [67] have proposed an effective system of elementary quantum gates based on multi-atomic coherent ensembles or quantum dots (QDs) featuring DDI. They showed the advantages of the system in accelerating quantum computation for these gates.

Some work has also been done to study the effect of DDI on photonic crystals and dispersive materials [13, 68–77]. For example, John and Quang [13] have studied self-induced transparency due to DDI in a photonic crystal doped with two-level nanoparticles. Singh and Haque [68, 69] have done some preliminary work on the effect of DDI on CPT. Also, Singh [70] has studied the effect of DDI on the enhancement of the refractive index in a photonic crystal doped with five-level nanoparticles, driven by one laser field.

Recently, Singh [71] has studied the effect of DDI on electromagnetically induced transparency (EIT) and spontaneous emission cancellation [72] in an ensemble of four-level nanoparticles doped in a photonic crystal driven by a probe and a pump laser field

and found that the particle density influences the absorption profile and can be used as a switching mechanism. He has also studied nonlinear two-photon absorption in a similar system [73, 74] and discovered the inhibition of two-photon absorption to be related to DDI strength. Also, Novitsky and Mikhnevich [75, 76] have studied the bistability of the optical response of a one-dimensional photonic crystal with a dense resonant medium as a defect, both theoretically and experimentally, and showed that the structure and spectral properties of the crystal determines the bistable response. Finally, Wang et al. [77] have studied the entangle dynamics of two atoms subject to DDI coupled to a common photonic band gap and showed that the detuning conditions and the DDI both play crucial roles in controlling entanglement in a two-qubit system.

DDI has also been studied in nonlinear photonic crystal systems doped with nanoparticles in recent years [78–80]. Such a crystal is made up of nonlinear dielectric spheres. The refractive indices of these spheres can be changed upon application of a strong pulsed laser (pump) field. The background material is taken as a linear dielectric material whose refractive index does not change. Singh [78] has observed that the absorption spectrum has two peaks and a minimum at zero detuning in the absence of DDI. However, in the presence of this interaction, the two peaks disappear and a single peak appears near zero detuning. When the pump field is applied, the peak near the zero detuning mark disappears and a new peak appears at a different detuning location. This happens because the refractive index of the system changes due to the pump field and, in turn, the location of the defect mode is altered. This means that the pump field and the DDI effect can be used, in tandem, to switch the location of the absorption peak.

In the present decade, notably, Singh et al. [79] have investigated the effect on the energy transfer and photoluminescence in donor and acceptor QDs, which interact via DDI, doped in a nonlinear photonic crystal. They have predicted a hybrid system than can be used to fabricate ultrafast switching and sensing nanodevices. Also, Cox et al. [80] have considered the DDI between a QD and a graphene nanodisk embedded in a similar crystal. They found that, in the presence of DDI, the power spectrum of the QD shows that that the energy transfer between the QD and the graphene nanodisk can be switched

on and off either through the application of the pump laser or by adjusting the strength of the DDI.

## 1.4 Coherent Population Trapping

Studies of coherence and interference effects in quantum systems have recently become very active research areas in optics, photonics, radiation and condensed matter physics, and even in many fields of chemistry. One phenomenon that has received significant attention is CPT [81]. Many other interesting phenomena have also been discovered using ideas derived from quantum coherence and interference including, lasing without inversion [82, 83], the Hanle effect [84], coherent Raman beats [84], photon echo [84], self-induced transparency [84], etc.

In the CPT effect, under certain conditions, the application of two continuous wave radiation fields to a nanoparticle leads to its preparation in a coherent superposition of states, which is stable against absorption from the radiation field. This phenomenon was first observed in 1976 by Alzetta et al. [85] as a decrease in the fluorescent emission in a laser optical pumping experiment on sodium atoms. The experiment involved a three-level system with two ground levels and one excited level. Almost concurrently, Whitley and Stroud [86] performed a theoretical investigation of the pumping and trapping originated by two laser fields resonant with the two coupled transitions in a three-level nanoparticle in cascade configuration.

Eventually, in 1978, Gray et al. [87] carried out extensive experimental studies of CPT in sodium atoms with two ground levels and one excited level. Subsequent theoretical analyses pointed out that the sodium atoms were pumped in a non-absorbing state due to quantum interference effects. The complete designation of CPT appeared for the first time in the abstract of a paper by Agrawal [88], dealing with the possibilities of using three-level systems for optical bistability [81].

Recently, the CPT phenomenon has been studied in atomic gases, semiconductor nanostructures and photonic crystals. It is of particular importance in lasing [89, 90], pulse propagation [91, 92] and quantum information processing [93, 94]. Generally, CPT

is studied in multi-level nanoparticles, which could be conventional atoms or artificial systems with quantized energy states such as QDs, wires, wells, etc.

The typical system used for CPT studies consists of an ensemble of multi-level nanoparticles doped in a host material. These nanoparticles have quantized energy levels and interact with the photons which are inside the host reservoir. The CPT effect arises due to the coherent superposition of two energy levels in a nanoparticle. The electrons in this coherent state are pumped by means of an external radiation field to an excited level, which initially has no electrons. During this process, two photons are absorbed which subsequently interfere with each other. Under certain conditions, this interference is destructive; leading to zero absorption and the electrons become trapped in the coherent state. Consequently, the CPT phenomenon is sometimes also referred to as photon trapping.

It is important to note that the study of CPT can involve more complicated systems, such as nonlinear condensates. For example, Ling et al. [47] have analyzed the collective excitation spectrum of the CPT state in a coupled atom-molecule condensate system. They found that collisions between particles can cause the CPT state to be dynamically unstable, which is a unique feature of the nonlinear system. They obtained a set of analytical criteria for determining the stability properties of the CPT state in the long-wavelength limit.

Another variation on CPT studies involves using non-optical radiation fields. Godone et al. [51] have examined the spectral characteristics of a CPT maser. They carried out a theoretical investigation of the coherent microwave emission associated with the trapping phenomenon by taking into account the impact of the various noise contributions on the physical principle of operation. They compared their theory with experimental results obtained with a laboratory prototype of Rb CPT maser.

Initial studies of the CPT effect almost invariably used two-level nanoparticles in vacuum. For example, Gateva et al. [95, 96] have studied CPT resonance on the degenerate two-level system of the  $^{87}\text{Rb}$   $D_1$  line by means of a Hanle effect configuration in an uncoated vacuum cell. They found that the measured fluorescence resonance has a

complex shape. They have also measured the dependence of the width and amplitude of the CPT resonance structures at different laser power densities in the fluorescence and transmission regimes. Also, they found that the shape of the resonances is different in different cells [97].

A bulk of the focus in the study of CPT has been centered on three-level nanoparticles. For example, Guo et al. [98] have studied CPT when  $\Lambda$ -type three-level nanoparticles are interacting with a two-mode cavity field. They found the CPT effect when the nanoparticles are initially in coherent superpositions of their lower states and the cavity field is in coherent superposition of photon numbers. Affolderbach et al. [99] have found the CPT effect in a thermal vapor of three-level nanoparticles irradiated by two co-propagating laser beams of suitable frequencies.

Recently, Obada et al. [100] and Morteza pour et al. [101] have studied the effects of cavity damping and coupling field on the entanglement dynamics for a three-level atomic system. Macovei et al. [102] considered a collection of V- and  $\Lambda$ -type three-level nanoparticles co-interacting with two strong coherent driving fields. They found that the trapping state of the ensemble can be rapidly populated or depopulated by changing the phase difference between the two fields.

More recently, Gao et al. [103] have investigated steady-state squeezing in the phase of the resonance fluorescence emitted from a three-level V-type atom driven by two coherent fields and damping in common vacuum and found that the squeezing of the observed driven transition between the excited state and the ground state is strongly affected by the decay rate of the controlling transition, detuning and intensity of the fields, and the phase quadrature of the fluorescent light.

Morigi [104] has studied the quantum dynamical effect of the centers of mass of trapped three-level nanoparticles on CPT. They considered that the internal degrees of the nanoparticles are driven in  $\Lambda$ -type configurations with the laser tuned at a two-photon resonance and found that transient CPT occurs when the motion of the wave packet is well-localized over the laser wavelength. Also, Arkhipkin and Timofeev [105] have studied the spatial and temporal evolution of two strong laser pulses interacting with



dense  $\Lambda$ -type three-level nanoparticles under the trapping regime. More recently, Hou et al. [106] and Yang et al. [107] have studied the effects of vacuum-induced coherence on dispersion and absorption properties in moving  $\Lambda$ -type atomic systems. The other effects of note which have been studied in relation to CPT in  $\Lambda$ -type three-level atomic systems include coherence induced by an incoherent pump field and vacuum decay [108] and spontaneous emission with the two transitions coupled to separate reservoirs [109].

CPT has also been studied in four-level [48, 110–126] and five-level [127–129] atomic systems. Hou et al. [48], for example, have considered the effects of vacuum-induced coherence on population trapping against single- and two-photon absorption in four-level Y-type nanoparticles. They found that the coherence can give probe gain without incoherent pumping and suppress two-photon transparency. They also showed that the absorption profiles are related to the relative phase between the probe and coupling lasers. Ladrón de Guevara and Orszag [115], in contrast, have investigated CPT and its effects on fluorescence in Y-type nanoparticles. They showed that the CPT effect produces fluorescence along the coupled transitions with an incoherent component at a frequency different than the driving frequency.

More recently, Sandhya [116] has studied the absorption profile of a four-level  $\Xi$ -type atomic system interacting with three driving fields analytically and found that the ground-state absorption is influenced by upper-level couplings. Entezar et al. [117] have investigated the effect of a modified reservoir on the nature of the quantum interference in the spontaneous emission of a driven double V-type four-level system where the transitions interact with a free vacuum and a modified reservoir, leading to two possible types of quantum interference. Their results show that the type of interference in the free vacuum reservoir depends on the type of and the absence or the presence of interference in the modified reservoir. In a similar atomic configuration, Yu et al. [118] have found that nonlinear optical behaviors in pulse propagation lead to double-dark resonances, which can be used to dynamically control light propagation. In a cold double  $\Lambda$ -type four-level system driven by two counter propagating laser fields, Xie and Yang [119] and Yang et al. [120] have studied decoherence and enhanced-coherence actions and the enhancement of population transfer efficiency, respectively. Ou et al. [121] have used a

laser-driven four-level closed-loop diamond-shape atomic system to investigate the phenomenon of spontaneously generated coherence. Experimentally, Mahmoudi et al. [122] have analyzed the behavior of optical bistability and CPT in a four-level mercury atomic system, whereas Aumiler [123] has demonstrated that the same can be achieved in room-temperature in four-level  $^{87}\text{Rb}$  atoms with up to 95% efficiency. Also, Shen [124] and Qi [125] have utilized the four-level Y-configuration double-control atomic system to study the potential application of the destructive (or constructive) quantum interference between the control transitions in designing logic gates for quantum computing. Finally, very recently, Fang and Gao [126] have employed the four-level N-type system to establish that the CPT effect can be used to overcome the limitation of two-photon absorption.

Using five-level systems, Doery et al. [127] have proposed a CPT scheme in under two-frequency laser excitations. They found that the trapped state has a time-dependent nature and its stability can be controlled by selective detuning of the laser beams. Kanokogi and Sakurai [128] have examined the position and resonance width of the CPT state in a symmetric five-level system with two lasers and two RF fields. They found that narrower trapped states due to the RF fields appear at positions that depend on the Rabi frequencies and the detuning of the fields. And, recently, Gu et al. [129] have studied the interaction of two pairs of near-resonant laser fields with a five-level M-type atom and found both EIT and CPT to occur under conditions of two two-photon resonances.

It should be noted that, in general, the physical make-up of the nanoparticle offers an additional level of latitude in the possible utilization of the CPT effect. For example, QDs, wires or well structures fabricated using semiconductor materials provide a convenient platform for CPT studies. Dynes et al. [130] have investigated the CPT effect in quantum wells, with each well having only three transitions which are all dipole allowed due to their asymmetrical nature. These artificial atomic systems are driven coherently by two infrared optical fields. One of these fields simultaneously couples with two of the three transitions which are nearly degenerate. The other field couples with the remaining transition. They found that the absorption strength of the weak probe field increases by a factor of over an order of magnitude as the coupling strength of the second

field is increased. The results are shown to be due to an optically mediated CPT effect. A similar study was performed by Sadeghi and Li [46] which dealt with the trapping of electron-hole excitons in  $\text{In}_{0.43}\text{Ga}_{0.57}\text{As}/\text{InP}$  quantum well structures interacting with a single infrared laser near resonance. Concurrently, Imamoğlu [131] has shown that CPT in a single hole charged QD could provide a powerful spectroscopic tool for understanding and controlling spin decoherence mechanisms. Also, Chua et al. [132] have studied two-mode photon-assisted transport through coupled non-identical QDs, modulating the shape and size of dots by applying electric field. They found that the CPT effect leads to the phenomenon of current antiresonance phenomenon.

In three-level  $\Lambda$ -type quantum well structures, Patnaik et al [133] have examined the role of ground-state coherence on the fluorescence from the excited state under continuous-wave excitation. They found that, when resonantly pumped, the fluorescence is strongly affected by any perturbation in the ground-state CPT. More recently, Maialle and Degani [134] have performed numerical simulations of the photocurrent generated by intersubband optical transitions in a double quantum well of a similar type coupled with a continuum of extended states. They found that the resonance between the exciting fields and the quantum states leads to coherent effects such as Rabi-dressed states, EIT and CPT. Litvinov et al. [135] have studied the phase sensitivity of CPT in tunneling-coupled quantum wells and found that the effect can be switched on or off depending on the algebraic sum of the phases of the exciting fields.

Some studies have used novel atomic schemes to obtain new interesting effects. For example, Araujo [136] considered the interaction of two matched ultra-short pulses with a  $\Lambda$ -type system in which the upper intermediate level is replaced by a collection of discrete energy levels. The scheme further assumed many of these levels being simultaneously accessed by the broad bandwidth of the two excitation pulses. It is predicted that, under appropriate conditions, this "multi- $\Lambda$ " system can exhibit coherence effects such as population trapping and electromagnetically induced transparency of one of the excitation pulses.

A considerable portion of the work that has been done on CPT involves various systems under the influence of magnetic fields. For example, Fu et al. [137] have investigated the CPT effect in high-purity n-type GaAs subject to a strong magnetic field. They isolated a  $\Lambda$ -type system composed of two Zeeman states of neutral donor-bound electrons and the lowest Zeeman state of bound excitons. As a result, they observed a pronounced dip in the excited-state photoluminescence coinciding with zero two-photon detuning of the system, which indicates the creation of a CPT state. Bevilacqua et al. [138] have reported on the effects induced by an alternating magnetic field on CPT resonances. They showed that the oscillating field produces sidebands of these resonances, which have very small linewidths. They also found that these bands are resolved even for very low field frequencies. Finally, Kolesov [139] has observed CPT at the ground-state Zeeman sublevels of the  $\text{Cr}^{3+}$  ion in  $^{87}\text{Rb}$  at room temperature. He has also investigated a mechanism of CPT in a situation when the optical pulse duration is shorter than the population decay time from the excited optical state.

Very recently, Margalit et al. [140] have studied CPT transients induced by an ac magnetic field for a realistic three-level  $\Lambda$  system in the  $D_1$  line of  $^{87}\text{Rb}$ . They have also analyzed the effect of a transverse magnetic field (TMF) on the absorption spectra of degenerate two-level systems in the  $D_2$  line of  $^{87}\text{Rb}$  [141]. In the latter case, they showed that the absorption spectra in both configurations are split in the presence of a TMF and that the splitting is proportional to its magnitude. The CPT dip in the pump-probe configuration is also shifted by the longitudinal magnetic field (LMF), so that the effects of the LMF and TMF can be distinguished from each other. Most recently, they have performed theoretical calculations of CPT transients induced by a modulated transverse magnetic field (TMF). They found that the application of a TMF causes the appearance of new  $\Lambda$  subsystems, creation of new dark states, and rearrangement of the population among the Zeeman sublevels.

There have also been many recent studies concerning the effects of bulk properties on CPT. For example, Post et al. [52] have investigated the effect of pressure on trapping both theoretically and experimentally. They found that the optimum waveforms produce strong CPT signals at low buffer-gas pressures, where the hyperfine structure (HFS)

splitting of the optical absorption lines is well resolved and at high buffer-gas pressures, where the HFS is not optically resolved due to pressure broadening. They also found that CPT resonances from frequency-modulated waves are severely degraded for high-pressure conditions.

Increasingly, practical applications of the CPT effect are being developed, particularly in the fabrication of novel optical devices. A prime example is the optical atomic clock scheme in  $^{88}\text{Sr}$  proposed by Santra et al. [53] using the idea of coherent trapping. The scheme uses two lasers to establish a coherent coupling between the  $5s^2\ ^1S_0$  ground state and the first excited state,  $5s5p\ ^3P_0$  of  $^{88}\text{Sr}$ . The coupling is mediated by the broad  $5s5p\ ^1P_1$  state. The effective linewidth of the clock can be controlled by adjusting the laser intensity. A clock accuracy of better than  $2 \times 10^{-17}$  seconds is predicted. Very recently, Yang et al. [143] have proposed and experimented with a scheme for a Ramsey-CPT atomic clock driven by a periodically microwave modulated current. Their experimental results suggest that the implementation of such a clock would have better frequency stability.

## 1.5 ac Stark Effect

Recent efforts in studying quantum coherence and interference in quantum optical systems have led to the discoveries of many interesting phenomena [82, 144–198]. These include lasing without inversion [82, 147–149], electromagnetically induced transparency [150–153], enhancement of nonlinear susceptibility [154–157], the ac Stark effect [158–183, 192–198], etc.

The ac Stark effect – also known as Autler–Townes (A–T) splitting – occurs due to nonlinear interactions between light and matter in the presence of one or more strong variable radiation field(s) [158–160]. Irradiation by a strong field leads to dynamic splitting of the energy levels of nanoparticles [161]. The split states are said to be dressed by the strong radiation field. The splitting phenomenon is particularly well resolved when the Rabi frequency of the strong field is larger than the decay rates of the energy levels [162].

In the past four decades, the ac Stark effect has been studied – theoretically and experimentally – in many different types of systems, such as atomic gases [163–176], laser-cooled atoms [177–189], ions [190–193], gas-phase molecules [194–200] and solid state materials [201–203], under both steady-state and transient [205, 206] conditions. In particular, there has been considerable interest in studying the effect in three-level nanoparticles [163–167, 207–210], which are taken in either of the  $\Lambda$ , V or  $\Xi$  (cascade or ladder) configurations.

Recently, investigations of the ac Stark effect have been extended to semiconductor nanostructures, such as QDs, wells, wires, etc. These nanostructures are essential for the fabrication of devices for quantum computing. QDs, in particular, have been widely studied in this regard, when doped in semiconductors [211–218]. Studies of the ac Stark effect in these structures have addressed both theoretical and experimental aspects. For example, a recent theoretical study has shown that the optical absorption spectra due to excitons in a QD superlattice embedded in a nanowire exhibit ac Stark splitting [219, 220]. On the experimental side, a similar splitting effect has been observed in the intersubband transitions in semiconductor quantum wells and it has been shown that the dephasing mechanisms associated with these transitions have characteristics which make the wells behave as artificial atoms [221].

Much of the existing work on the ac Stark effect involves gases consisting of three-level atomic systems. The nanoparticles are taken in either of the  $\Lambda$ , V or  $\Xi$  (cascade or ladder) configurations [163–167, 211–220]. Recently, these studies have encompassed four-level nanoparticles as well. Most notably, Wei et al. [222] have carried out an extensive analysis of this system and found that the resulting spectrum has up to three-peaks (dynamic splitting), which can be explained in terms of the dressed state formalism.

Other types of four-level systems that have been used in ac Stark effect studies include doubly-driven Rb and Ba atoms. For example, density matrix calculations of the fluorescence obtained from a four-level Rb atomic system have shown A–T split states and transparency effects, which have been confirmed experimentally [223, 224]. Further empirical evidence of the effect has been found in the two-photon resonant spectrum

obtained in the presence of a strong coupling field from the non-degenerate four-wave mixing in a four-level Ba system (dressed cascade configuration) [225]. It has also been shown theoretically that tuning of the power of a single pump field interacting with a four-level nanoparticle can induce mixing and crossing of A–T components of closely-spaced transitions [171, 223, and 224].

## 1.6 Recent Related Developments in Photonic Crystals and Dispersive Materials

Recently, Singh [226] has investigated the effect of DDI on absorption processes in photonic nanowires manufactured by embedding a photonic crystal into another. Using an ensemble of three-level QDs doped within the embedded crystal, he has calculated the absorption coefficient of a probe field after a control field has been applied to induce dipole moments, taking into account the DDI between the induced dipoles and the interaction of the QDs with the bound photon states of the nanowire via electron-photon interactions. He has found that, by changing the locations of the resonant energies in the QDs, the DDI can be controlled which, in turn, acts as a switching mechanism for the absorption coefficient.

Hatef and Singh [227] have developed a theory for the decay of a two-level QD doped in a two-dimensional metallic photonic crystal consisting of two different metallic columns periodically arranged in air. The photonic crystal has an isotropic band gap with suitable choices for the sizes of the metallic columns. The density of states and the optical properties of the crystal can be controlled by changing the plasma energies of the contrasting metals. They calculated the linewidth broadening and the spectral function of the spontaneous emission and showed that these can be controlled by changing the plasma energies of the metals.

Cox et al. [228] have investigated the acousto-optic effect in polaritonic nanofibers made by embedding a single cylindrical polaritonic doped nanowire, made of either a phonon-polaritonic or excitons-polaritonic material, within a photonic crystal. The dopants are noninteracting QDs, which only interact with the nanofiber via excitons-polariton interaction. They have found that, for certain acoustic strain intensity, the nanofiber has a

localized-to-delocalized polariton transition similar to metal-to-insulator transitions in doped semiconductors. Furthermore, the nanofiber can be rendered transparent to applied radiation fields due to the excitons-bound polariton couplings. The transparency can be switched on/off by the external acoustic strain intensity.

Goban et al. [229] have developed a “novel integrated optical circuit with a photonic crystal capable of both localizing and interfacing atoms with guided photons.” The optical bands of the photonic crystal waveguide are aligned with selected atomic transitions. From the measured reflection spectra, they were able to infer that atoms are localized within the waveguide by means of optical dipole forces. The importance of this work is amplified by the fact that it represents a first step towards surmounting the challenges in nanofabrication and atomic manipulation, which would ultimately bring about the integration of nanophotonics and atomic physics, including novel quantum transport and many-body phenomena with photon-mediated atomic interactions.

The most productive area of study involving photonic crystals over the last one and a half decade has focused on the modifications in the radiative properties of nanoparticles doped within the host environment of these materials, in relation to the coherent interaction between the particles and external laser fields.

Nihei and Okamoto [230] have investigated the spontaneous emissions from a singly-driven V-type three-level nanoparticle doped within an anisotropic photonic crystal which has a band-edge energy midway between the two upper levels of the particle.

Using a more elaborate setup, Zhang et al. [231, 232] have studied two distinct types of quantum interferences in the spontaneous emission spectra obtained from a double V-type four-level nanoparticle embedded in a double-band photonic crystal. Also of note are related earlier investigations by Zhu et al. [233] and Yang and Zhu [234].

The spontaneous emission from two-level [235–240], three-level [241–244], four-level [245–247] and five-level [248] atoms embedded in anisotropic photonic crystals have been studied extensively in both single- and double-band reservoir setups. Some interesting features such as narrowing, enhancement and suppression of spectral lines and the occurrence of dark lines in the spontaneous emission have been observed universally.



Most notably, Wu et al. [238] have investigated the spontaneous emission from a two-level atom embedded in an anisotropic photonic crystal using fractional calculus where the spectrum is obtained analytically by solving the fractional kinetic equations. They found that, unlike the spontaneous emission phenomenon obtained from atoms doped in isotropic photonic crystals, the emission near the band edge of an anisotropic reservoir does not feature a photon-atom bound state. The same mathematical technique has been used by Huang et al. [241] to study the spontaneous emission dynamics of a V-type three-level atom.

Other notable studies include that by Yang et al. [240] which focuses on studying the spontaneous emission of a two-level atom in an anisotropic photonic crystal without the limitations of the rotating wave approximation (RWA) and de Vega and Alonso [249] which uses a similar atomic system embedded in a general non-Markovian reservoir. Also, Entezar [250] has used a quantum entropy model to study the entanglement of a two-level atom and its radiation field near the edge of a photonic band gap. Finally, Takeda and John [251] have recently performed a theoretical study of the phenomenon of population switching in quantum dots doped in both one- and two-dimensional photonic crystals by solving the semi-classical Maxwell-Bloch equations self-consistently.

Similar studies have also been done in three-level [252–254], four-level [255 – 259] and five-level [260] atoms in isotropic photonic crystals. Most notably, Zhang et al. [260] have studied the spontaneous emission spectra of a five-level atom being driven by two external fields, doped in a photonic crystal. They found that the interference effects produced by the two fields lead to spectra with different characteristics compared to that obtained from the case of only one driving field.

In dispersive materials, Singh [261] has studied the optoelectronics of a polaritonic nanowire fabricated by embedding a polaritonic crystal into another, with the condition that the band gap of the embedded crystal lies within the band gap of the host. To satisfy this band-gap condition, GaP and MgO crystals can be used with MgO as the host crystal. He has calculated the bound states of the confined polaritons in the embedded crystal using the transfer-matrix method and evaluated the bound polariton energies for a GaP-

MgO nanowire. He showed that the number of bound states in the wire depends on its size, the depth of the potential well, and height of the potential barrier. He also calculated the absorption coefficient of the system using the time-dependent Schrödinger equation method and performed numerical simulations for the GaP-MgO nanowire showing that when the resonant energy of doped QD lies near the bound states, its absorption spectrum has several transparent states. As a result, the nanowire can be switched between transparent and absorbing states by tuning the resonant state of the QD.

Finally, Singh and Racknor [262] have studied the acousto-optic effect on photon transmission and spontaneous emission in a polaritonic photonic crystal fabricated from polaritonic materials such as GaP, MgO, LiNbO<sub>3</sub>, and LiTaO<sub>3</sub>. By doping a two-level QD in the polaritonic crystal, they calculated the decay rate of the spontaneous emission, the band structure, and the photon transmission coefficient. They found that the “band-gap width and the decay rate of QD depend strongly on the high-frequency dielectric constant of the polaritonic crystal while the photonic band edges vary inversely by the ratio of longitudinal- to transverse-optical phonon energies”. They also showed that the spontaneous decay rate of the QD can be controlled by the application of the external acoustic strain field and the system can be switched from a transmitting state to a reflecting state by the same means.

In both contrast and complement to these existing works, the theoretical developments presented in this thesis focus on the roles played by the decay rates of the energy levels of the nanoparticles and the DDI *between* the nanoparticles (in densely doped ensembles) in photon trapping (for both photonic crystal and dispersive material reservoirs) and the ac Stark effect (for photonic crystal reservoir only).

We show that the CPT effect is sensitive to the decay rates of the energy levels of the nanoparticles, allowing us to establish two distinct controls (via coherence and via manipulation of the decay rate) on the population densities of the upper levels of the doped nanoparticles.

In studying the ac Stark effect, we propose a new technique for obtaining transparency in quantum optical systems, making use of the unique properties of the band structures of

photonic crystals. Unlike comparable work in the literature, it is important to note that we do not consider the Stark splitting to be generated due to the coupling of the transitions between the energy levels of a nanoparticle to the density of states of the reservoir. Instead, the splitting in our proposed model occurs due to the external laser fields. This important distinction allows for greater control in achieving the desired transparency effect.

## 1.7 Outline of the Thesis

The aim of the thesis is to study the CPT phenomenon (in photonic crystals and dispersive materials) and the ac Stark effect (only in photonic crystals). We consider that an ensemble of nanoparticles is doped in these materials. These nanoparticles are taken to be interacting with either a photonic crystal or a dispersive material – both of which act as reservoirs – and are subject to probe and pump fields. We also consider cases where the nanoparticles interact with each other, as well, via DDI.

Chapter 2 details our investigation of the phenomenon of photon trapping in nanoparticles doped within photonic crystals. Primarily, we found that, in these materials, when the resonance energy lies within the lower and upper bands, one observes the CPT effect at certain values of the relative Rabi frequency for a given initial configuration of the energy levels of the nanoparticle. It is also found that the CPT effect can be controlled by moving the resonance energies of the nanoparticles within the lower and upper bands of the photonic crystal.

Chapter 3 presents our study of polariton trapping in a dispersive material doped with an ensemble of nanoparticles. These materials have band gaps, like photonic crystals, but the origin of the band gaps is very different comparatively. As a result, we obtain markedly different and interesting effects on photon trapping. Most usefully, we found that the steady-state atomic population in the upper level of a doped nanoparticle depends sensitively on the coherence conditions and the decay rate; increasing the decay rate can increase the fraction of population trapped in the system. In this way, the same population density in the upper level can be obtained for a range of values of the resonance energy simply by adjusting the intensity of the coupled field. It should be emphasized here that,

as photons and polaritons have different properties and the energy ranges for photonic and polaritonic band gaps are located in different regions, there are significant dissimilarities between photonic and polaritonic devices.

Chapter 4 deals with the effect of DDI on a photonic crystal and a dispersive material when the number density of the doped nanoparticles is very high. For both the photonic crystal and the dispersive material, we found that when the resonance energies lie away from the band edges and within the lower or upper bands, trapping is observed at certain values of the relative Rabi frequency, which vary depending on the strength of the DDI between the nanoparticles. Also, in both media, as DDI becomes stronger, the population density of the uppermost level increases. Moreover, the CPT effect can be switched on and off due to the effect of DDI. However, when the resonance energies lie in the upper band of the photonic crystal and the dispersive material, converse effects are observed. More specifically, in the dispersive material reservoir, the population density vanishes when the resonance energy lies near the lower band edge. But, this effect is not observed if the resonance energy lies near the upper band edge. In the case of the photonic crystal, the population density of the uppermost level is seen to vanish near both the upper and lower band edges. This is explained by the symmetric and asymmetric structures of the photonic crystal and dispersive material form factors, respectively, about the corresponding band gaps.

Chapter 5 details our study of the ac Stark effect, which occurs due to quantum coherence and interference, in photonic crystals. The photonic crystal is lightly doped with an ensemble of nanoparticles which are not interacting with each other. The ac Stark effect is a nonlinear quantum optical phenomenon where an intense pump field is applied. We found that the manipulation of the decay rates of the energy levels of a doped nanoparticle offers a new mechanism for switching the particle from an inverted to a non-inverted state (and vice versa), with regards to the population of the ground level of the nanoparticle. Our calculations have also shown that due to the role played by the band structure of the photonic crystal, the doped nanoparticle effectively becomes transparent to any radiation field tuned to the resonance energy of the probed transition.

Chapter 6 presents our study of the effect of DDI on dynamic Stark splitting in a photonic crystal doped with an ensemble of five-level nanoparticles. It is found that, when the concentration of the particles is high, the induced dipoles interacting with each other via DDI decreases the absorption in the system with increasing interaction strength. Also, the absorption peaks shift to new positions due to the DDI effect. In addition, the system can be switched from a three-peak spectral profile to that featuring two peaks, simply by changing the DDI parameter. This property can be used to make new types of photonic devices (such as switches).

The thesis is concluded by making a few closing remarks in Chapter 7 and briefly addressing the potential for future work in the areas discussed in Chapters 2 – 6.

## Chapter 2

### 2 Population Trapping in Photonic Crystals

For nearly a century, the phenomenon of photon trapping in atomic gases has been extensively studied. The aim of this chapter is to investigate this trapping effect in nanoparticles doped within photonic crystals<sup>1</sup>.

#### 2.1 Introduction

A major area of study involving photonic crystals is focused on the modifications in the radiative properties of nanoparticles doped within the host environment of these materials, in addition to the coherent interaction between the particles and external laser fields. Notably, prominent workers such as Quang et al. [14] and Woldeyohannes and John [15, 17] have studied the coherent control of spontaneous emission in a doubly-driven three-level nanoparticle located within a photonic crystal, with one resonant frequency near the band edge of the crystal.

The present chapter details our study of the phenomenon of coherent population trapping (CPT) in photonic crystals. First, we provide pertinent background information on photonic crystals (Section 2.2) and the CPT effect (Section 2.3). Next, we propose a theory of CPT for a photonic crystal lightly doped with an ensemble of identical five-level nanoparticles. These particles interact with the photonic crystal reservoir and two external photon fields. But, due to the light nature of doping, they do not interact with one another. The level scheme of the doped nanoparticles is shown in Fig. 2-1. The energy levels are labeled as  $|a\rangle$ ,  $|b\rangle$ ,  $|c\rangle$ ,  $|d\rangle$  and  $|e\rangle$ . The energy difference between levels  $|i\rangle$  and  $|j\rangle$  is denoted as  $\omega_{ij}$ . The interaction between the nanoparticles and the reservoir causes both levels  $|b\rangle$  and  $|c\rangle$  to spontaneously decay to level  $|e\rangle$ , with

---

<sup>1</sup> The work presented in this chapter has been published in: M. R. Singh and I. Haque, *J. Mod. Opt.* **52**, 1857 (2005).

corresponding decay rates  $\Gamma_b$  and  $\Gamma_c$ , respectively, and level  $|a\rangle$  to spontaneously decay to level  $|d\rangle$ , with decay rate  $\Gamma_a$ . The magnitudes of the Rabi frequencies corresponding to the two fields are denoted as  $\Omega_1$  and  $\Omega_2$ .

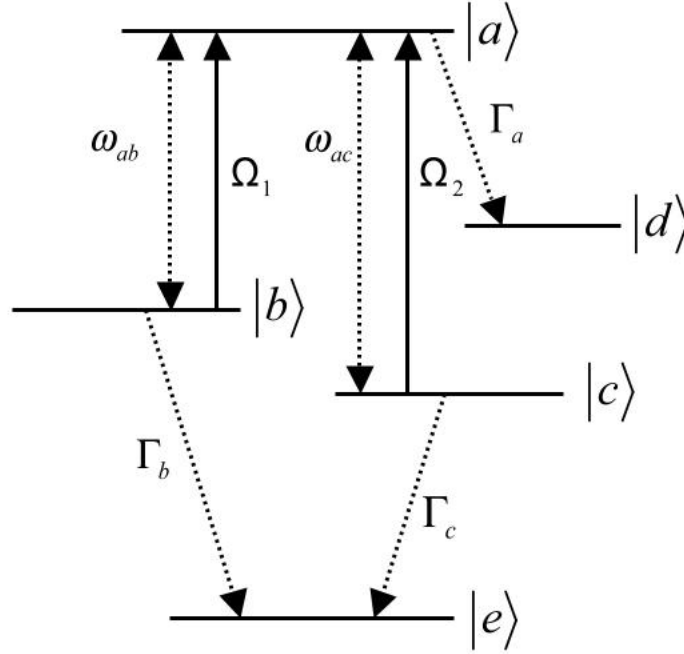


Figure 2-1: Level scheme of a five-level nanoparticle;  $\omega_{ij}$  is the energy difference between levels  $|i\rangle$  and  $|j\rangle$ . Here,  $|i\rangle$  and  $|j\rangle$  stand for  $|a\rangle$ ,  $|b\rangle$ ,  $|c\rangle$ ,  $|d\rangle$  and  $|e\rangle$ . Levels  $|b\rangle$  and  $|c\rangle$  both spontaneously decay to level  $|e\rangle$  and level  $|a\rangle$  spontaneously decays to level  $|d\rangle$ , due to nanoparticle-reservoir interaction.  $\Gamma_a$ ,  $\Gamma_b$  and  $\Gamma_c$  denote the linewidths of levels  $|a\rangle$ ,  $|b\rangle$  and  $|c\rangle$ , respectively.  $\Omega_1$  and  $\Omega_2$  are the magnitudes of the Rabi frequencies corresponding to the two fields.

Our calculations illustrate the role played by the decay rates of the energy levels of the nanoparticles in photon trapping. We use the Schrödinger equation and the Laplace transform method to calculate the expressions for the population densities of the energy levels. Numerical simulations are performed for a photonic crystal with a gap-midgap ratio of 5%. The results show that when the resonance energies lie within the propagation bands of the crystal, the population density of the uppermost level vanishes at a specific value of the intensity ratio of the two fields, indicating the occurrence of CPT. The initial

states of the nanoparticles are chosen such that this particular value of the intensity ratio is 1.

We proceed to show that the CPT effect is sensitive to the decay rates of the energy levels of the nanoparticles. More specifically, when one of the resonance energies lies near the lower band edge of the photonic crystal, the population density vanishes at all intensities of the fields. This is due to the very large values of the density of states near the lower band edges of these materials and is not an evidence of CPT. A similar result is found when the resonance energy lies near the upper band edge of the photonic crystal.

The study of CPT in photonic crystals has great potential for implementation in the design of novel optical devices such as low-threshold switches, all-optical transistors, quantum memory devices, etc., owing to the unusual properties of these crystals. The potential for applications of the newly predicted effect lies in the fact that it facilitates two distinct modes of control on the population densities of the uppermost levels of the doped nanoparticles.

This study is very timely as, very recently, Gozzini et al. [263] have reported the first experimental observation of CPT in thermal potassium vapour in a  $\Lambda$ -type three-level scheme. Potassium required a lower modulation frequency with a large resonance contrast which is an advantage over other alkalis, making it very promising for future CPT and EIT applications, in particular where optical pumping losses are limiting factors. Also, last year, Zhang and George [264] have shown that the CPT effect can occur in buckminsterfullerene ( $C_{60}$ ) radiated with a pair of coupling laser pulses which render the atom transparent to a weak probe field. The stability of the CPT state depends sensitively on the laser field amplitudes, pulse durations and the time delay between the coupling pulses.

## 2.2 Photonic Crystals

This section describes a few basic concepts pertaining to photonic crystals and provides a brief outline for the calculation of their dispersion relations.



A photonic crystal represents a class of nanomaterials in which two dielectric materials with differing dielectric constants or refractive indices are arranged in a periodic structure. The resulting periodicity in the dielectric constant function of the crystal leads to the formation of energy gaps, where linear electromagnetic wave propagation is forbidden [12]. This is analogous to the energy gaps observed between the valence and the conduction bands of an electronic (semiconductor) crystal. The primary distinction between these two types of crystals is the scale of the lattice constant. For electronic crystals, the lattice constant is on the sub-nanometer scale. In the case of photonic crystals, it is on the order of the wavelengths of the relevant electromagnetic waves.

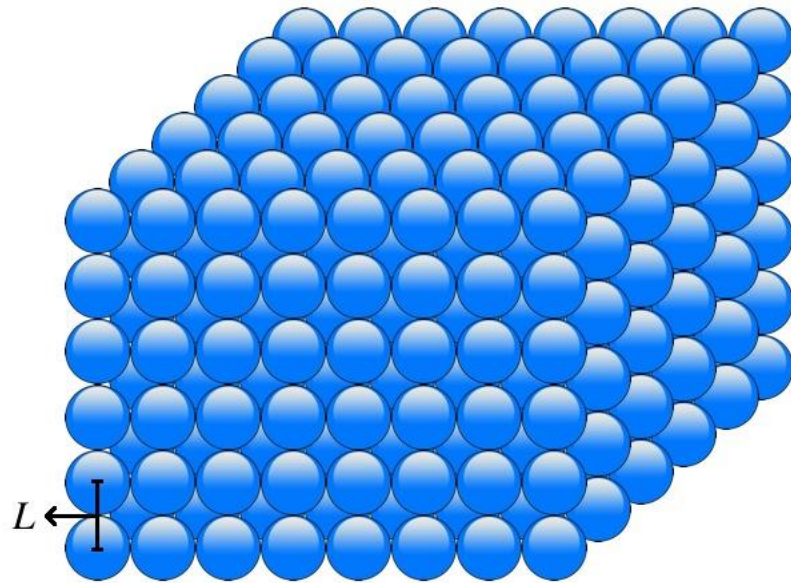


Figure 2-2: Schematic representation of a photonic crystal with three-dimensional periodicity. It consists of a periodic arrangement of dielectric spheres in air. The lattice constant is denoted as  $L$ .

Photonic crystals can have different spatial periodic arrangements of the regions of high and low refractive indices. The periodicity can be one-, two- or three-dimensional. A schematic representation of a three-dimensional photonic crystal is shown in Fig. 2-2. It consists of a periodic lattice of dielectric spheres in air, with lattice constant  $L$ . If the energy gap in a photonic crystal extends over the entire Brillouin zone, it is known as an absolute (isotropic) band gap. In this case, the band gap is not dependent on the direction of the wave vector. In an absolute band gap, the density of photon states goes to zero. In

contrast, if wave propagation is forbidden over only a limited domain of wave vectors, the gap is classified as partial or incomplete.

The band structure of a photonic crystal relates the energies of the photons to the wave vectors. It depends primarily on the dielectric contrast, the lattice constant and the structure of the crystal. It is possible to gain an intuitive understanding of the concept of the band structure by studying a three-dimensional isotropic photonic crystal [18, 19]. For simplicity, we consider a photonic crystal made up of dielectric spheres of radius  $a$  and refractive index  $n$ , periodically arranged in air with lattice constant  $L = 2a + b$ , where  $b$  is the spacing between the spheres [19]. Since the crystal is isotropic, the one-dimensional Maxwell equations can be used to calculate the dispersion relation, ignoring the vector nature of the electromagnetic field.

The one-dimensional scalar wave equation for the crystal can be written as (discussed in Appendix A):

$$-\nabla^2 \varphi - \frac{\omega^2}{c^2} \epsilon(x) \varphi = \frac{\omega^2}{c^2} \varphi \quad (2.1)$$

where  $\varphi$  represents a scalar wave function,  $\omega$  denotes frequency,  $c$  is the speed of light and  $\epsilon(x)$  is the dielectric constant function with periodicity:

$$\epsilon(x) = \epsilon(x + L)$$

As the scalar wave equation resembles the time-independent Schrödinger equation, it is possible to re-write the periodic dielectric constant function as:

$$\epsilon(x) = \sum_{m=-\infty}^{m=\infty} u(x - mL)$$

where

$$\begin{aligned} u(x) &= n^2 - 1, & \text{for } |x| < a \\ u(x) &= 0, & \text{otherwise} \end{aligned}$$

Eqn. (2.1) can, therefore, be solved analytically, giving the following energy dispersion relation for the photonic crystal [18, 19] (discussed in Appendix B):

$$4n \cos(kL) = \left( (1+n)^2 \cos \left[ \frac{\varepsilon_k (2na+b)}{ch} \right] - (1-n)^2 \cos \left[ \frac{\varepsilon_k (2na-b)}{ch} \right] \right) \quad (2.2)$$

where  $\varepsilon_k$  and  $k$  denote the energy and the wave vector of the photons, respectively. A schematic representation of this dispersion relation is shown in Fig. 2-3.

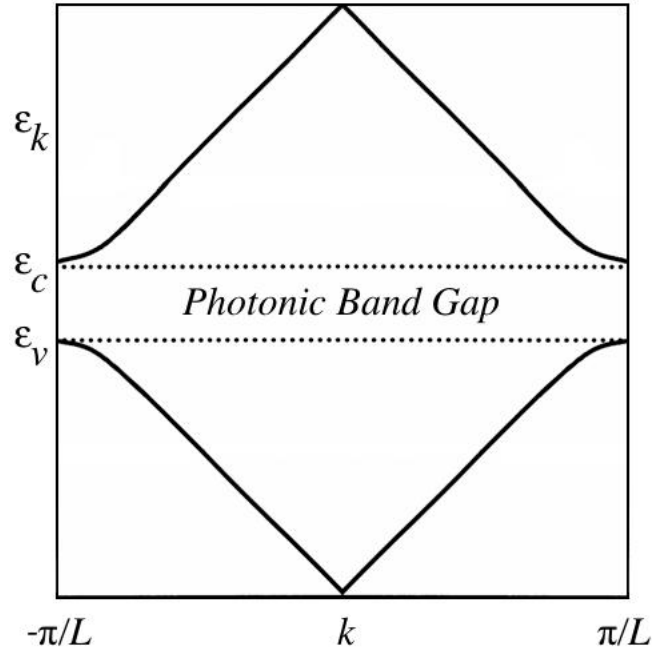


Figure 2-3: Plot of the photon energy  $\varepsilon_k$  as a function of the wave vector  $k$  for a photonic crystal. Note that there is an energy gap between  $\varepsilon_c$  and  $\varepsilon_v$ .

The photonic band gap is located at:

$$k = k_0 = \frac{\pi}{L}$$

Note that, as the wave vector  $k$  repeats itself outside the Brillouin zone, the dispersion curves fold back into the zone at reaching its edges.

## 2.3 Coherent Population Trapping

This section defines the CPT phenomenon, in the context of quantum coherence, and provides a brief description of the mechanism behind the trapping effect.

A process is said to be coherent if it is characterized by the existence of some well-defined deterministic phase relationship, independent of any phenomena which induce random noise [84]. In quantum mechanical systems, coherences between states are generated whenever an external interaction renders the system in a superposition of the energy eigenstates. In such circumstances, the presence of coherence produces quantum interference phenomena, which are widely exploited in spectroscopy and quantum optics [81].

Many interesting effects have been predicted using the ideas of quantum coherence and a wide range of practical applications have been proposed. In particular, it has been found that, under certain conditions, the application of two continuous wave radiation fields to a nanoparticle leads to its preparation in a coherent superposition of states, which is stable against absorption from the radiation field. This phenomenon has been designated as coherent population trapping owing to the presence of the coherent superposition of the energy states and the stability of the population.

Alternatively, CPT can also be described as the process of pumping the nanoparticle to a non-absorbing state. The exciting radiation creates a coherence such that the evolution of the nanoparticle is prepared exactly out of phase in relation to the incoming radiation, cancelling all absorption events.

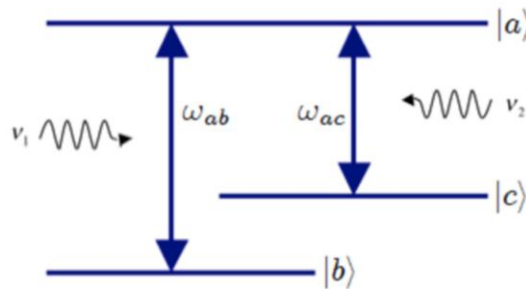


Figure 2-4: Level scheme of a  $\Lambda$ -type three-level nanoparticle. The energy difference between levels  $|i\rangle$  and  $|j\rangle$  is denoted as  $\omega_{ij}$ . Levels  $|a\rangle$  and  $|b\rangle$  are coupled by a field of frequency  $\nu_1$  and amplitude  $E_1$ ;  $|a\rangle$  and  $|c\rangle$  are coupled by a probe field of frequency  $\nu_2$  and amplitude  $E_2$ .

In order to understand the mechanism behind the CPT effect, we consider a  $\Lambda$ -type three-level system, in which there are two coherent routes for absorption that interfere destructively, leading to the cancellation of absorption [84]. A schematic representation of the system is shown in Fig. 2-4.

The upper level  $|a\rangle$  and level  $|b\rangle$  are coupled by a field of frequency  $\nu_1$  and amplitude  $E_1$  and levels  $|a\rangle$  and  $|c\rangle$  are coupled by a probe field of frequency  $\nu_2$  and amplitude  $E_2$ . Transitions between the lower doublet states are dipole forbidden. Due to selection rules produced by a proper choice of the polarizations, each laser field – considered to be perfectly monochromatic and coherent – acts only on one dipole transition [81].

The detunings of the radiation fields are defined as:

$$\begin{aligned}\delta_1 &= \nu_1 - \omega_{ab} \\ \delta_2 &= \nu_2 - \omega_{ac}\end{aligned}$$

The nanoparticle maintains a coherent phase relationship with the applied fields.

The coherence is preserved in terms of the Rabi frequencies:

$$\begin{aligned}\Omega_1 &= \mu_{ab} E_1 / \hbar \\ \Omega_2 &= \mu_{ac} E_2 / \hbar\end{aligned}$$

where  $\mu_{ab}$  and  $\mu_{ac}$  are the induced electric dipole moments between states  $|a\rangle$  and  $|b\rangle$ , and  $|a\rangle$  and  $|c\rangle$ , respectively.  $\Omega_1$  and  $\Omega_2$  are also characterized by complex phase factors  $e^{-i\varphi_1}$  and  $e^{-i\varphi_2}$ , respectively.

The initial state (coherent superposition) of the nanoparticle can be written as:

$$|\lambda, 0\rangle = \cos\left(\frac{\theta}{2}\right)|b\rangle + \sin\left(\frac{\theta}{2}\right)e^{-i\phi}|c\rangle$$

where  $\cos(\theta/2)$  and  $\sin(\theta/2)$  are the initial amplitudes of levels  $|b\rangle$  and  $|c\rangle$ , respectively, with a phase factor of  $e^{-i\psi}$ .

In the present system, CPT occurs under conditions of two-photon resonance, i.e.:

$$\delta_1 = \delta_2$$

which means that trapping can be achieved here by simply altering the laser frequencies, provided that:

$$\begin{aligned}\theta &= \pi / 2 \\ \varphi_1 - \varphi_2 - \phi &= \pm\pi\end{aligned}$$

When the condition for two-photon resonance is satisfied, corresponding to the formation of coherently trapped population in  $|b\rangle$  and  $|c\rangle$ , the population of  $|a\rangle$  becomes zero.

If the intensities of the two lasers are increased, one must tune increasingly further from resonance to obtain appreciable excitation to level  $|a\rangle$ . The CPT effect observed here is due to the destructive quantum interference between the two transitions.

## 2.4 Population Density and Photon Trapping

This section provides a detailed theoretical background of the system under scrutiny and describes the calculations performed in order to study the phenomenon of CPT. We consider that an ensemble of non-interacting five-level nanoparticles are doped within a photonic crystal. As shown in Fig. 2-1, the energy levels of a doped nanoparticle are denoted as  $|a\rangle$ ,  $|b\rangle$ ,  $|c\rangle$ ,  $|d\rangle$  and  $|e\rangle$ . The two lower levels  $|b\rangle$  and  $|c\rangle$  are coupled to the excited level  $|a\rangle$ . Levels  $|b\rangle$  and  $|a\rangle$  are coupled by a photon field of frequency  $\nu_1$  and amplitude  $E_1$  and levels  $|c\rangle$  and  $|a\rangle$  are coupled by that of frequency  $\nu_2$  and amplitude  $E_2$ . The transition from level  $|b\rangle$  to  $|c\rangle$  is dipole forbidden. Due to the interaction between the nanoparticle and the reservoir, levels  $|b\rangle$  and  $|c\rangle$  both decay spontaneously to level  $|e\rangle$  and level  $|a\rangle$  decays spontaneously to level  $|d\rangle$ .

For simplicity, the photonic crystal is taken to consist of an isotropic periodic arrangement of identical dielectric spheres, in a background dielectric medium which has a distinct dielectric constant. The background material in this case is taken as air which has a refractive index of 1.

Recently, John and co-workers have proposed a band structure theory for three-dimensional photonic crystals (see Section 2.1). According to this theory, the energy dispersion relation for the photonic crystal can be written as [18, 19]:

$$\cos(kL) = \frac{(1+n^2)}{4n} \cos\left[\frac{4na\varepsilon_k}{ch}\right] - \frac{(1-n)^2}{4n} \quad (2.3)$$

where, as before,  $k$  is the photon wave vector inside the crystal,  $\varepsilon_k$  is the photon energy corresponding to the wave vector  $k$ ,  $n$  is the refractive index of the dielectric spheres,  $a$  is the radius of each sphere and  $c$  is the speed of light.  $L$  is the lattice constant of the crystal and is defined as (taking the special case where  $b = 2na$ ):

$$L = 2a(n+1)$$

A plot of the dispersion relation is given in Fig. 2-5.

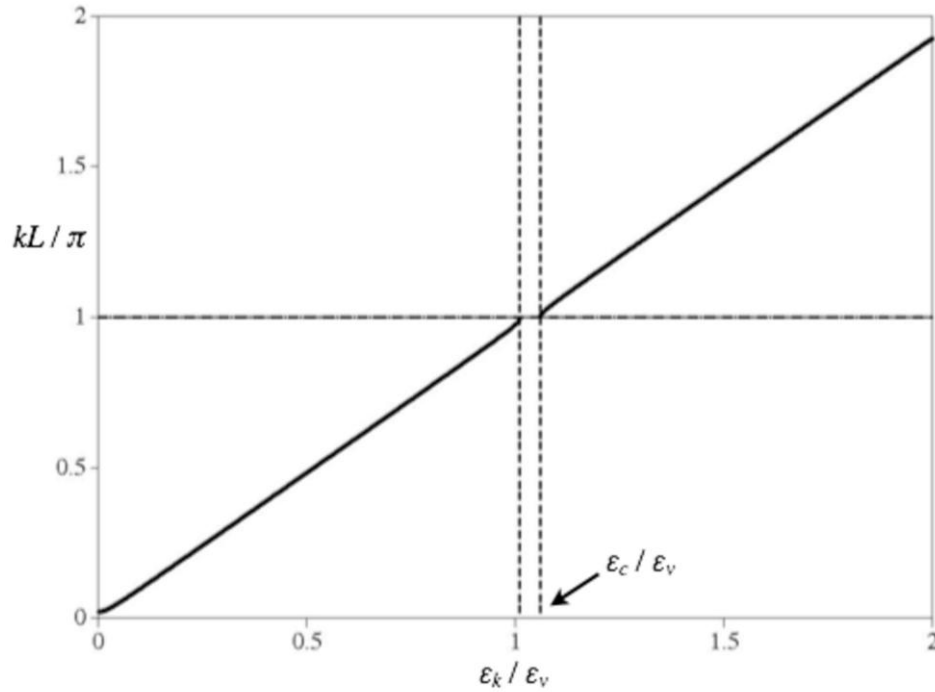


Figure 2-5: Plot of the dispersion relation of the photonic crystal with  $n = 1.082$ ,  $a/L = 0.24$  and  $L = 300$  nm. The quantities  $\varepsilon_v$  and  $\varepsilon_c$  are the maximum energy of the valence band and the minimum energy of the conduction band, respectively. The horizontal axis is the ratio of the energy  $\varepsilon_k$  to the maximum valence band energy  $\varepsilon_v$ . The band gap of the crystal lies between  $\varepsilon_k/\varepsilon_v = 1$  and  $\varepsilon_c/\varepsilon_v$ , shown by the vertical dashed lines.

The quantities  $\varepsilon_v$  and  $\varepsilon_c$  represent the maximum energy of the valence band and the minimum energy of the conduction band, respectively. The band gap of the crystal lies between these two energy values,  $\varepsilon_v = 1.94$  eV and  $\varepsilon_c = 2.04$  eV (approximately), and its gap-midgap ratio is 5%. This energy gap corresponds to the optical region of the electromagnetic spectrum.

The Hamiltonian for the system is written in energy space as (this equation is discussed in Appendix C):

$$H = H_A + H_R + H_{AF} + H_{AR} \quad (2.4)$$

where the first term is the Hamiltonian of the five-level nanoparticle and is given by (discussed in Appendix D):

$$H_A = \hbar\omega_{ab}\left(\sigma_{ab}^z + \frac{1}{2}\right) + \hbar\omega_{ac}\left(\sigma_{ac}^z + \frac{1}{2}\right) + \hbar\omega_{ad}\left(\sigma_{ad}^z + \frac{1}{2}\right) + \hbar\omega_{be}\left(\sigma_{be}^z + \frac{1}{2}\right) \quad (2.5)$$

The second term in Eqn. (2.4) represents the Hamiltonian of the reservoir. It can be written as:

$$H_R = \int_C \frac{d\varepsilon_q}{2\pi} \varepsilon_q p^+(\varepsilon_q) p(\varepsilon_q) \quad (2.6)$$

The integration contour  $C$  consists of two intervals:  $-\infty < \varepsilon_q \leq \varepsilon_v$  and  $\varepsilon_c \leq \varepsilon_q < \infty$  [20, 21, 50].

The third term in  $H$  denotes the interaction Hamiltonians between the nanoparticle and the two photon fields of frequencies  $\nu_1$  and  $\nu_2$ . It is given by:

$$H_{AF} = -\frac{\hbar}{2} \Omega_1 Z(\varepsilon_{ab}) [\sigma_{ab}^+ e^{i\Delta_{ab}t} + \sigma_{ab}^- e^{-i\Delta_{ab}t}] - \frac{\hbar}{2} \Omega_2 e^{i\varphi} Z(\varepsilon_{ac}) [\sigma_{ac}^+ e^{i\Delta_{ac}t} + \sigma_{ac}^- e^{-i\Delta_{ac}t}] \quad (2.7)$$

The final term in Eqn. (2.4) is the nanoparticle-reservoir interaction Hamiltonian and is responsible for the decays from level  $|a\rangle$  to  $|d\rangle$ ,  $|b\rangle$  to  $|e\rangle$  and  $|c\rangle$  to  $|e\rangle$ . It can be written as:



$$H_{AR} = \begin{bmatrix} -\int_C \frac{d\varepsilon_q}{2\pi} \sqrt{\gamma_{be}} Z(\varepsilon_q) [p(\varepsilon_q) \sigma_{be}^+ + \sigma_{be}^- p^+(\varepsilon_q)] \\ -\int_C \frac{d\varepsilon_{q'}}{2\pi} \sqrt{\gamma_{ce}} Z(\varepsilon_{q'}) [p(\varepsilon_{q'}) \sigma_{ce}^+ + \sigma_{ce}^- p^+(\varepsilon_{q'})] \\ -\int_C \frac{d\varepsilon_{q''}}{2\pi} \sqrt{\gamma_{ad}} Z(\varepsilon_{q''}) [p(\varepsilon_{q''}) \sigma_{ad}^+ + \sigma_{ad}^- p^+(\varepsilon_{q''})] \end{bmatrix} \quad (2.8)$$

where the terms  $p^+(\varepsilon_q)$  and  $p(\varepsilon_q)$  denote the photon creation and annihilation operators in energy space, respectively.

It is important to note that the interaction Hamiltonians given in Eqns. (2.7, 2.8) are obtained in the dipole and rotating-wave approximations [20, 21, and 50] (discussed in Appendix E and Appendix F, respectively).

The remaining terms in the expressions of the Hamiltonians given above are defined as:

$$\begin{aligned} \sigma_{ij}^z &= |i\rangle\langle i| - |j\rangle\langle j| \\ \sigma_{ij}^+ &= |i\rangle\langle j| \\ \sigma_{ij}^- &= |j\rangle\langle i| \\ \Delta_{ab} &= \omega_{ab} - \nu_1 \\ \Delta_{ac} &= \omega_{ac} - \nu_2 \\ \gamma_{ij} &= (4\mu_{ij}^2 \omega_{ij}^3 / 3) \end{aligned}$$

where  $\mu_{ij}$  and  $\omega_{ij}$  are the dipole matrix element and the energy difference, respectively, between levels  $|i\rangle$  and  $|j\rangle$ . Note that  $\varepsilon_{ij} = \hbar\omega_{ij}$ .

The magnitudes of the Rabi frequencies corresponding to the two fields are:

$$\begin{aligned} \Omega_1 &= \mu_{ab} E_1 / \hbar \\ \Omega_2 &= \mu_{ac} E_2 / \hbar \end{aligned}$$

where the phase factor between  $\Omega_1$  and  $\Omega_2$  is taken as  $e^{i\varphi}$ .

$Z(\varepsilon_{ij})$  is known as the form factor for the transition from  $|i\rangle$  to  $|j\rangle$ . For photonic crystals, the form factor has been calculated in Reference [20, 21] using the isotropic model proposed in Reference [19]. It is written as (discussed in Appendix G):

$$Z(\varepsilon_{ij}) = \left[ \frac{(a/L)(1+n)^2 \sin\left(\frac{4na\varepsilon_{ij}}{hc}\right)}{[1-\zeta^2(\varepsilon_{ij})]^{1/2}} \right]^{1/2} \quad (2.9)$$

where  $\zeta(\varepsilon_{ij})$  is defined as:

$$\zeta(\varepsilon_{ij}) = \frac{(1+n)^2 \cos\left(\frac{4na\varepsilon_{ij}}{hc}\right) - (1-n)^2}{4n}$$

A plot of the form factor is given in Fig. 2-6. As before, the band gap of the crystal lies between  $\varepsilon_k / \varepsilon_v = 1$  and  $\varepsilon_c / \varepsilon_v$ , shown by the vertical dashed lines.

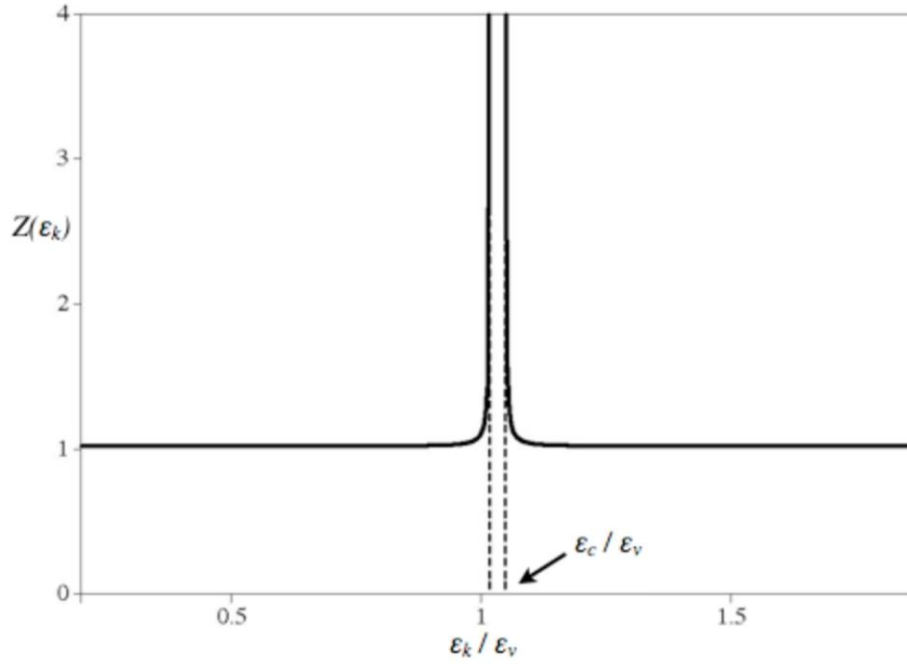


Figure 2-6: Plot of the form factor  $Z(\varepsilon_k)$  of the photonic crystal. The choices of the crystal parameters and the horizontal axis are identical to those for the dispersion relation in Fig. 2-5.

Initially, the five-level nanoparticle is prepared such that it is in coherent superposition of the two levels  $|b\rangle$  and  $|c\rangle$ :

$$|\lambda, 0\rangle = B(0)|b\rangle + C(0)e^{i\psi}|c\rangle \quad (2.10)$$

where  $B(0)$  and  $C(0)$  are the initial amplitudes of levels  $|b\rangle$  and  $|c\rangle$ , respectively. The phase factor between  $B(0)$  and  $C(0)$  is taken as  $e^{i\varphi}$ .

The state of the nanoparticle and the polariton field at a later time  $t$  is written as:

$$|\lambda, t\rangle = A(t)|a\rangle + B(t)|b\rangle + C(t)|c\rangle \quad (2.11)$$

Writing the Schrödinger equations for  $A(t)$ ,  $B(t)$  and  $C(t)$ , we get:

$$\frac{dA(t)}{dt} = \left(\frac{i}{2}\right) \left[ \Omega_1 Z(\varepsilon_{ab}) B(t) + \Omega_2 e^{i\varphi} Z(\varepsilon_{ac}) C(t) \right] - \frac{\Gamma_a}{2} A(t) \quad (2.12a)$$

$$\frac{dB(t)}{dt} = -\left(\frac{i}{2}\right) \left[ \Omega_1 Z(\varepsilon_{ab}) \right]^* A(t) - \frac{\Gamma_b}{2} B(t) \quad (2.12b)$$

$$\frac{dC(t)}{dt} = -\left(\frac{i}{2}\right) \left[ \Omega_2 e^{i\varphi} Z(\varepsilon_{ac}) \right]^* A(t) - \frac{\Gamma_c}{2} C(t) \quad (2.12c)$$

where  $\Gamma_a$ ,  $\Gamma_b$  and  $\Gamma_c$  are the decay rates for  $|a\rangle$ ,  $|b\rangle$  and  $|c\rangle$ , respectively, and are written as:

$$\Gamma_a = \frac{1}{2} \gamma_{ad} Z(\varepsilon_{ad})^2 \quad (2.13a)$$

$$\Gamma_b = \frac{1}{2} \gamma_{be} Z(\varepsilon_{be})^2 \quad (2.13b)$$

$$\Gamma_c = \frac{1}{2} \gamma_{ce} Z(\varepsilon_{ce})^2 \quad (2.13c)$$

In Eqns. (2.12a, 2.12b, 2.12c), we have neglected the real part of the self-energy associated with each of levels  $|a\rangle$ ,  $|b\rangle$  and  $|c\rangle$ . From here onwards, we will write  $Z(\varepsilon_{ij})$  as simply  $Z_{ij}$ , to avoid clutter.

It must be noted here that Eqns. (2.13a, 2.13b, 2.13c) are obtained when the resonance energies lie within the propagation bands of the photonic crystal. When the resonance energy lies within the band gap,  $\Gamma_i = 0$  [20, 21].

Applying the Laplace transform method (discussed in Appendix H) to Eqns. (2.12a, 2.12b, 2.12c), we can calculate  $A(t)$  as follows:

$$A(t) = \frac{e^{st} A_1}{(s-s_+)(s-s_-)} + \frac{e^{s_+t} A_2}{(s_+-s)(s_+-s_-)} + \frac{e^{s_-t} A_3}{(s_--s)(s_--s_+)} \quad (2.14)$$

In Eqn. (2.14),  $s$  is given by:

$$s = -\frac{\alpha}{3} + \frac{1}{6}\xi - \frac{2\zeta}{\xi}$$

and  $s_+$  and  $s_-$  are found to be:

$$s_{+,-} = \left( -\frac{\alpha}{3} - \frac{1}{12}\xi - \frac{\zeta}{\xi} \right) \pm \frac{i\sqrt{3}}{2} \left( \frac{1}{6}\xi + \frac{2\zeta}{\xi} \right)$$

where

$$\zeta = \beta - \frac{\alpha^2}{3}$$

$$\xi = \left( 36\alpha\beta - 108\delta - 8\alpha^3 + 12\sqrt{81\delta^2 + 12\alpha^3\delta - 54\alpha\beta\delta - 3\alpha^2\beta^2 + 12\beta^3} \right)^{1/3}$$

In the above,

$$\alpha = \frac{\Gamma_a + \Gamma_b + \Gamma_c}{2}$$

$$\beta = \frac{\Gamma_a\Gamma_b + \Gamma_b\Gamma_c + \Gamma_a\Gamma_c + |\Omega_1 Z_{ab}|^2 + |\Omega_2 Z_{ac}|^2}{4}$$

$$\delta = \frac{\Gamma_a\Gamma_b\Gamma_c + |\Omega_1 Z_{ab}|^2\Gamma_c + |\Omega_2 Z_{ac}|^2\Gamma_b}{8}$$

The variables  $A_1$ ,  $A_2$  and  $A_3$  appearing in Eqn. (2.14) are given by:

$$A_1 = (i/2) \left[ \Omega_2 Z_{ac} C(0) e^{i(\varphi+\psi)} (s + \Gamma_b/2) + \Omega_1 Z_{ab} B(0) (s + \Gamma_c/2) \right]$$

$$A_2 = (i/2) \left[ \Omega_2 Z_{ac} C(0) e^{i(\varphi+\psi)} (s_+ + \Gamma_b/2) + \Omega_1 Z_{ab} B(0) (s_+ + \Gamma_c/2) \right]$$

$$A_3 = (i/2) \left[ \Omega_2 Z_{ac} C(0) e^{i(\varphi+\psi)} (s_- + \Gamma_b/2) + \Omega_1 Z_{ab} B(0) (s_- + \Gamma_c/2) \right]$$

Similarly, the expressions for  $B(t)$  and  $C(t)$  are found as:

$$B(t) = e^{-\Gamma_b t/2} B(0) - \frac{1}{\left(s + \frac{\Gamma_b}{2}\right)} \left[ \frac{e^{-\Gamma_b t/2} B_1}{\left(s_+ + \frac{\Gamma_b}{2}\right) \left(s_- + \frac{\Gamma_b}{2}\right)} + \frac{e^{st} B_2}{(s-s_+)(s-s_-)} \right]$$

$$- \frac{e^{s_+t} B_3}{\left(s_+ + \frac{\Gamma_b}{2}\right) (s_+ - s) (s_+ - s_-)} - \frac{e^{s_-t} B_4}{\left(s_- + \frac{\Gamma_b}{2}\right) (s_- - s) (s_- - s_+)} \quad (2.15)$$

$$C(t) = e^{-\Gamma_c t/2} C(0) e^{i\psi} - \frac{1}{\left(s + \frac{\Gamma_c}{2}\right)} \left[ \frac{e^{-\Gamma_c t/2} C_1}{\left(s_+ + \frac{\Gamma_c}{2}\right) \left(s_- + \frac{\Gamma_c}{2}\right)} + \frac{e^{st} C_2}{(s - s_+)(s - s_-)} \right] \\ - \frac{e^{s_+ t} C_3}{\left(s_+ + \frac{\Gamma_c}{2}\right) (s_+ - s)(s_+ - s_-)} - \frac{e^{s_- t} C_4}{\left(s_- + \frac{\Gamma_c}{2}\right) (s_- - s)(s_- - s_+)} \quad (2.16)$$

where

$$B_1 = \frac{\left[ |\Omega_1|^2 Z_{ab}^2 B(0) (\Gamma_b - \Gamma_c) \right]}{8} \\ B_2 = \frac{\left[ \Omega_1 \Omega_2 Z_{ac} Z_{ab} C(0) e^{i(\varphi+\psi)} \left(s + \frac{\Gamma_b}{2}\right) + |\Omega_1|^2 Z_{ab}^2 B(0) \left(s + \frac{\Gamma_c}{2}\right) \right]}{4} \\ B_3 = \frac{\left[ \Omega_1 \Omega_2 Z_{ac} Z_{ab} C(0) e^{i(\varphi+\psi)} \left(s_+ + \frac{\Gamma_b}{2}\right) + |\Omega_1|^2 Z_{ab}^2 B(0) \left(s_+ + \frac{\Gamma_c}{2}\right) \right]}{4} \\ B_4 = \frac{\left[ \Omega_1 \Omega_2 Z_{ac} Z_{ab} C(0) e^{i(\varphi+\psi)} \left(s_- + \frac{\Gamma_b}{2}\right) + |\Omega_1|^2 Z_{ab}^2 B(0) \left(s_- + \frac{\Gamma_c}{2}\right) \right]}{4} \\ C_1 = \frac{\left[ |\Omega_2|^2 Z_{ac}^2 C(0) e^{i\psi} (\Gamma_c - \Gamma_b) \right]}{8} \\ C_2 = \frac{\left[ |\Omega_2|^2 Z_{ac}^2 C(0) e^{i\psi} \left(s + \frac{\Gamma_b}{2}\right) + \Omega_2 e^{-i\varphi} \Omega_1 Z_{ac} Z_{ab} B(0) \left(s + \frac{\Gamma_c}{2}\right) \right]}{4} \\ C_3 = \frac{\left[ |\Omega_2|^2 Z_{ac}^2 C(0) e^{i\psi} \left(s_+ + \frac{\Gamma_b}{2}\right) + \Omega_2 e^{-i\varphi} \Omega_1 Z_{ac} Z_{ab} B(0) \left(s_+ + \frac{\Gamma_c}{2}\right) \right]}{4} \\ C_4 = \frac{\left[ |\Omega_2|^2 Z_{ac}^2 C(0) e^{i\psi} \left(s_- + \frac{\Gamma_b}{2}\right) + \Omega_2 e^{-i\varphi} \Omega_1 Z_{ac} Z_{ab} B(0) \left(s_- + \frac{\Gamma_c}{2}\right) \right]}{4}$$

Without compromising any physical integrity of the problem, we consider the case when  $\Gamma_b = \Gamma_c$ . Under this simplification, we have found the following analytical expressions for  $A(t)$ ,  $B(t)$  and  $C(t)$ :

$$A(t) = \frac{ie^{-(\Gamma_a + \Gamma_b)t/4} \sin(\eta t) \left[ \Omega_1 Z_{ab} B(0) + \Omega_2 Z_{ac} C(0) e^{i(\varphi+\psi)} \right]}{\sqrt{\Omega_1^2 Z_{ab}^2 + \Omega_2^2 Z_{ac}^2 - \left(\frac{\Gamma_a - \Gamma_b}{2}\right)^2}} \quad (2.17)$$

where

$$\eta = \sqrt{\Omega_1^2 Z_{ab}^2 + \Omega_2^2 Z_{ac}^2 - \left(\frac{\Gamma_a - \Gamma_b}{2}\right)^2} = \frac{i\Omega}{2}$$

and

$$B(t) = \frac{e^{-\Gamma_b t/2} [B(0)G_1 + C(0)e^{i(\varphi+\psi)}G_2]}{\Omega^2 + \left(\frac{\Gamma_a - \Gamma_b}{2}\right)^2} \quad (2.18)$$

$$C(t) = \frac{e^{-\Gamma_b t/2} [B(0)H_1 + C(0)e^{i(\varphi+\psi)}H_2]}{\Omega^2 + \left(\frac{\Gamma_a - \Gamma_b}{2}\right)^2} \quad (2.19)$$

where

$$\begin{aligned} G_1 &= \Omega^2 + \left(\frac{\Gamma_a - \Gamma_b}{2}\right)^2 - |\Omega_1|^2 \frac{Z_{ab}^2}{\Omega} \left[ \Omega + e^{-(\Gamma_a - \Gamma_b)t/4} \Theta \right] \\ G_2 &= -\Omega_1 \Omega_2 Z_{ac} Z_{ab} - \frac{\Omega_1 \Omega_2 Z_{ac} Z_{ab} e^{-(\Gamma_a - \Gamma_b)t/4} \Theta}{\Omega} \\ H_1 &= \Omega^2 + \left(\frac{\Gamma_a - \Gamma_b}{2}\right)^2 + \frac{\Omega_2 e^{-i\varphi} \Omega_1 Z_{ab} Z_{ac}}{\Omega} \left[ \Omega + e^{-(\Gamma_a - \Gamma_b)t/4} \Theta \right] \\ H_2 &= |\Omega_2|^2 Z_{ac}^2 - \frac{|\Omega_2|^2 Z_{ac}^2 e^{-(\Gamma_a - \Gamma_b)t/4} \Theta}{\Omega} \end{aligned}$$

with

$$\Theta = \frac{(\Gamma_a - \Gamma_b)^2}{2} \sin\left(\frac{\Omega t}{2}\right) - \Omega \cos\left(\frac{\Omega t}{2}\right)$$

The physical interpretation of  $|A(t)|^2$  is that it gives the probability of finding two photons in level  $|a\rangle$ , when they are excited from levels  $|b\rangle$  and  $|c\rangle$  to  $|a\rangle$ . This leads to the trapping of the two photons in the system. The next section describes the calculation of the value of  $|A(t)|^2$ .

## 2.5 Results and Discussions

For all calculations in this section, we let  $B(0)$  and  $C(0)$  be  $\cos(\theta/2)$  and  $\sin(\theta/2)$ , respectively, with  $0 \leq \theta \leq \pi$ . We also let the combined phase factor  $\varphi + \psi = \pi$ . The numerical simulations are performed at a scaled arbitrary time  $\gamma_{ad}t = 0.6$ .

As in the cases of Figs. (2-5, 2-6), we choose a photonic crystal characterized by the following set of parameters [15, 17]:

$$\begin{aligned}
n &= 1.082 \\
L &= 300 \text{ nm} \\
(a / L) &= 0.24
\end{aligned}$$

It is important to note that the main findings of this section do not depend on the choice of the photonic crystal.

As in Reference [48], we assume that:

$$\gamma_{be} / \gamma_{ad} = \gamma_{ce} / \gamma_{ad} = 1/3$$

All frequencies are subsequently measured with respect to  $\gamma_{ad}$ .

It is important to note that, in the present calculations, we have only investigated the role of  $\Gamma_a$ . The decay rates of the energy levels of the nanoparticles depend on the location of the resonance energies  $\varepsilon_{ij}$  in relation to the band structure of the photonic crystal, as evident from Eqns. (2.13a, 2.13b, 2.13c). Whereas the value of  $\Gamma_a$  is calculated for different cases – e.g. resonance energy at mid-band, at band edge, etc. –  $\Gamma_b$  and  $\Gamma_c$  are calculated when the resonance energy lies near the middle of the band. Hence,  $\Gamma_b$  and  $\Gamma_c$  act as constants, as in other works. Consequently, the five-level system reduces to a four-level system.

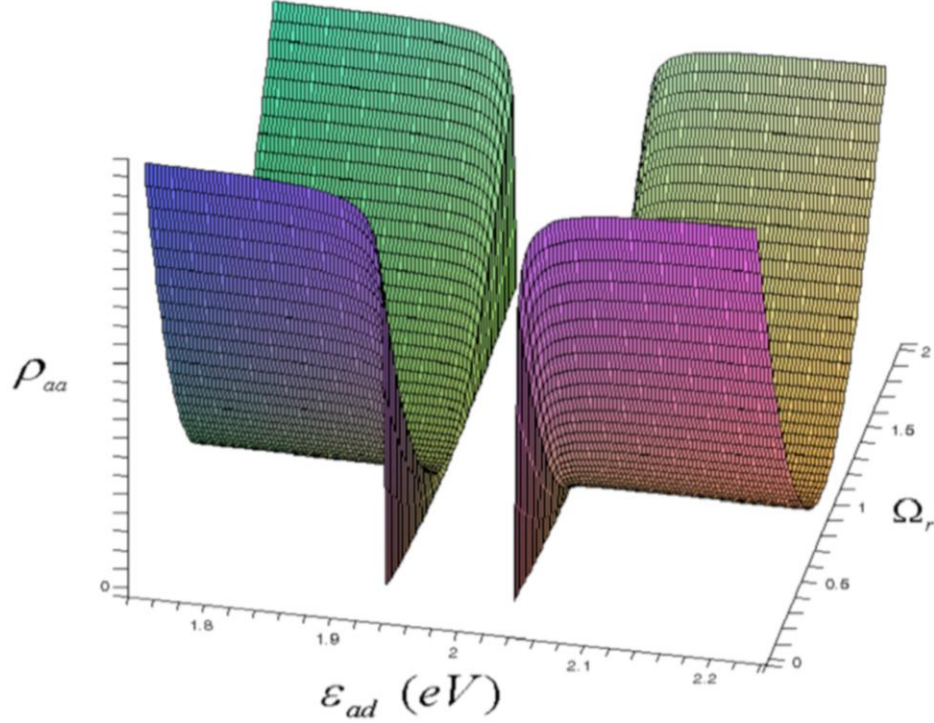


Figure 2-7: Plot of  $\rho_{aa}$  against varying  $\Omega_r$  and  $\varepsilon_{ad}$  for the photonic crystal – displays symmetric response about the band gap.

We calculate the population density of level  $|a\rangle$  ( $\rho_{aa} = |A(t)|^2$ ) when the resonance energies lie within the lower band of the crystal ( $\varepsilon_{ab} = \varepsilon_{ac} = \varepsilon_{be} = \varepsilon_{ce} = 0.97$  eV) and  $\theta = \pi/2$  (see Fig. 2-7). We define the magnitude of the relative Rabi frequency  $\Omega_r = \Omega_2 / \Omega_1$  and let  $\Omega_1 = 1.8$ . Numerical calculations for  $\rho_{aa}$  are plotted as a function of  $\Omega_r$  and  $\varepsilon_{ad}$ .

Note that the population density in Fig. 2-7 becomes zero for all values of the resonance energy  $\varepsilon_{ad}$  at  $\Omega_r = 1$ . This demonstrates the occurrence of the CPT effect in these materials. Similar results are also found when the resonance energies lie within the upper band of the crystal.

However, it is important to note that  $\rho_{aa}$  vanishes at all values of the relative Rabi frequency when  $\varepsilon_{ad}$  approaches either of the edges of the band gap. This is due to the fact that the decay rates of the energy levels of the nanoparticle depend on the density of



states of the photonic crystal and the energy difference between levels (i.e. the resonance energy). More precisely,  $\Gamma_a$  depends on the resonance energy  $\varepsilon_{ad}$ . As this energy goes from the mid-band regions to the band edges,  $\Gamma_a$  becomes large, as reflected in Fig. 2-7. This means, in this case,  $\rho_{aa} = 0$  is a consequence of the decay from level  $|a\rangle$  to  $|d\rangle$  and cannot be interpreted as an indicator of CPT.

The plot in Fig. 2-7 shows that the CPT effect can be observed by fixing  $\theta$  and changing  $\Omega_r$ . It is evident that the same result can be obtained by fixing  $\Omega_r$  and changing  $\theta$ .

However, in photonic crystals, the presence of the form factor – related to the band structure of the photonic crystal – generates a more interesting scenario. One can also get the CPT effect by fixing  $\theta$  and  $\Omega_r$  and varying  $\varepsilon_{ab}$  and  $\varepsilon_{ac}$ . Numerical calculations for this case have not been performed.

The study of CPT in photonic crystals has great potential for application in the design of novel optical devices such as low-threshold switches, all-optical transistors, quantum memory devices, etc., owing to the unusual properties of these crystals. The potential for applications of the newly predicted effect described in this chapter lies in the fact that it allows us to establish two distinct controls on the population densities of the upper levels of the doped nanoparticles:

1. Control via coherence i.e. by changing the relative intensity of the driving fields.
2. Control via manipulating the decay rate of the upper level by changing the relative position of level  $|d\rangle$ .

As the steady state population in the upper level is sensitive to the coherence conditions and the decay rate, increasing the latter can increase the fraction of population trapped in the system. In this way, the same population density in the upper level can be obtained for a range of values of the resonance energy  $\varepsilon_{ad}$  simply by adjusting the intensities of the coupled fields (see Fig. 2-7).

## 2.6 Summary and Conclusion

In summary, we found that, in a photonic crystal, when the resonance energy lies within the lower and upper propagation bands, one observes the CPT effect at certain values of the relative Rabi frequency for a given initial configuration of the energy levels of the doped nanoparticle. We also discussed the possibility of obtaining CPT by preparing the nanoparticles in a coherent superposition of states for a given ratio of the Rabi frequencies of the coupled fields. Particularly interesting results are found when one of the resonance energies lies near the upper or lower band edges. In this case, the population density of the excited level of the five-level system becomes zero for all values of the intensity ratio of the driving fields due to the effect of the form factor, which is related to the band structure of the material.

This concludes the description of our study of the CPT phenomenon in identical, non-interacting nanoparticles doped within a photonic crystal. The next chapter presents our investigation of this particular phenomenon in a similar ensemble of dopants within a dispersive material reservoir.

## Chapter 3

### 3 Population Trapping in Dispersive Materials

Chapter 2 details our study of the phenomenon of photon trapping in an ensemble of doped nanoparticles within a photonic crystal reservoir. The discussions in this chapter are focused on our study of polariton trapping in a dispersive material doped with an identical ensemble of five-level nanoparticles<sup>2</sup>. Polaritons are formed due to the coupling of phonons and photons. This means that they have markedly different properties compared to those of photons. Therefore, polaritons exhibit significantly different physics relative to photons.

#### 3.1 Introduction

In recent years, dispersive materials have come under scrutiny due to the presence of interesting features in their energy band structures, in the same vein as photonic crystals. For example, Rupasov and Singh [20–22] have shown that there is a suppression of spontaneous emission due to the decay of an energy level of an atom (or a nanoparticle) when it is coupled with a system of polaritons and placed within the reservoir of a dispersive material. They have also shown that, if the atomic resonance frequency lies near the energy gap of the dispersive material reservoir, the spectrum of the system contains a novel polariton-atom bound state with energy lying within the gap, with the radiation and medium polarization of the bound state localized in the vicinity of the atom [50]. Furthermore, the formation of this bound state leads to a significant suppression of spontaneous emission.

The aim of the present chapter is to study the phenomenon of coherent population trapping (CPT) in dispersive materials, in contrast with that in photonic crystals detailed in the previous chapter. As noted earlier, in dispersive materials [20, 21], the existence of energy gaps is due to photons coupling to elementary excitations of the media. First, we

---

<sup>2</sup> The work presented in this chapter has been published in: M. R. Singh and I. Haque, *J. Mod. Opt.* **52**, 1857 (2005).

provide a detailed primer on dispersive materials, concentrating mainly on developing the Hamiltonians of the medium and its interaction with external radiation fields, leading to the formulation of a dispersion relation.

Next, we consider that the dispersive material is doped with an ensemble of five-level nanoparticles. These particles do not interact with each other. Two external laser fields are applied and the population density is calculated for the uppermost level. The nanoparticles interact with the dispersive material and the two external photon fields. The schematic structure of the nanoparticle considered here and the configuration of the transitions and decay channels are shown in Fig. 3-1.

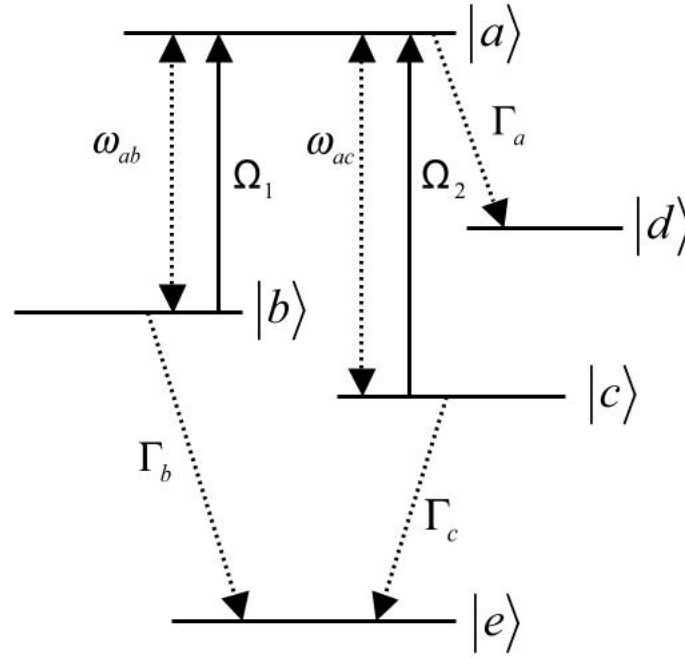


Figure 3-1: Level scheme of a five-level nanoparticle;  $\omega_{ij}$  is the energy difference between levels  $|i\rangle$  and  $|j\rangle$ . Here,  $|i\rangle$  and  $|j\rangle$  stand for  $|a\rangle$ ,  $|b\rangle$ ,  $|c\rangle$ ,  $|d\rangle$  and  $|e\rangle$ . Levels  $|b\rangle$  and  $|c\rangle$  both spontaneously decay to level  $|e\rangle$  and level  $|a\rangle$  spontaneously decays to level  $|d\rangle$ , due to nanoparticle-reservoir interaction.  $\Gamma_a$ ,  $\Gamma_b$  and  $\Gamma_c$  denote the linewidths of levels  $|a\rangle$ ,  $|b\rangle$  and  $|c\rangle$ , respectively.  $\Omega_1$  and  $\Omega_2$  are the magnitudes of the Rabi frequencies corresponding to the two fields.

The configuration is similar to that considered in the previous chapter. However, the energy scale is significantly different as the current chapter deals with polaritons instead of photons.

Using the mathematical techniques outlined in the previous chapter, we proceed to calculate the expression for the population densities of the energy levels of the nanoparticles. Numerical simulations are performed for a SiC reservoir. The occurrence of CPT is again observed, in agreement with the results found for photonic crystals. Also, when one of the resonance energies lies near the lower band edge, the population density vanishes at all intensities of the fields for the dispersive material, similar to the case for photonic crystals, with the same analyses applicable.

In Chapter 2, it can be seen that the density of states in a photonic crystal has singularities at the band edges. It also has a symmetrical shape. Therefore, the population of the upper level vanishes at all values of the relative Rabi frequency when the resonance energies of the nanoparticles lie at both the lower and upper band edges. This is a consequence of the symmetrical nature of the density of states.

However, the density of states in a dispersive material has an asymmetric shape. It features a singularity near the lower band edge and a zero value at the upper band edge. Therefore, the population of the upper level vanishes at all values of the relative Rabi frequency only when the relevant resonance energy of the nanoparticle lies at the lower band edge. This is because a dispersive material has different signatures in the lower and upper bands due to the nature of its density of states.

We conclude by noting that, in contrast to the case detailed in the previous chapter, for a dispersive material, the population density of the upper state does not become zero when one of the resonance energies lies near the upper band edge, except due to the CPT effect brought on by unit intensity ratio of the photon fields.

## 3.2 Dispersive Materials

This section provides an outline of the mathematical model of the Hamiltonian of a dispersive medium and describes the steps leading to the formulation of an appropriate dispersion relation, as detailed in Reference [265].

We consider that an electromagnetic field is interacting with a dispersive material. A model Hamiltonian of these materials has been derived in References [21, 41]. For notational convenience, in this section, it is assumed that  $\hbar = h/(2\pi) = 1$  and  $c = 1$ , where the quantities  $h$  and  $c$  represent Planck's constant and the speed of light, respectively.

A dispersive material consists of molecules or atoms, which can be considered as a continuous set of charged harmonic oscillators. Letting each molecule have a frequency  $\Omega$ , charge  $e$ , and mass  $m_0$ , the Hamiltonian of the material can be written as:

$$H_M = \frac{1}{2m_0} \int d\mathbf{r} [\mathbf{P}^2(\mathbf{r}) + m_0^2 \Omega^2 \mathbf{Q}^2(\mathbf{r})] \quad (3.1)$$

where  $\mathbf{Q}(\mathbf{r})$  and  $\mathbf{P}(\mathbf{r})$  are the displacement and the momentum of an oscillator, respectively, and are well-known to obey a specific set of commutation relations.

The Hamiltonian of the electromagnetic field propagating within the dispersive material can be written as:

$$H_F = \frac{1}{8\pi} \int d\mathbf{r} [\mathbf{E}^2(\mathbf{r}) + \mathbf{H}^2(\mathbf{r})] \quad (3.2)$$

where  $\mathbf{E}$  and  $\mathbf{H}$  denote the electric and magnetic components of the radiation field, respectively.

The molecules of the dispersive material possess electric dipoles. The electric dipole moment of a molecule at position  $\mathbf{r}$  can be written as  $e\mathbf{Q}(\mathbf{r})$ . The interaction Hamiltonian between the electric dipoles of the dispersive material and the electromagnetic field is written, in the dipole approximation, as:

$$V_{MF} = e\sqrt{n} \int d\mathbf{r} \mathbf{Q}(\mathbf{r}) \cdot \mathbf{E}(\mathbf{r}) \quad (3.3)$$

where  $n$  is the number density of the oscillators in the material. The total Hamiltonian of the system, then, is:

$$H_{MF} = H_F + H_M + V_{MF} \quad (3.4)$$

It is useful to write the above Hamiltonian in terms of the second quantized notation (i.e. raising and lowering operators). Following the method of References [21, 41], the Hamiltonian of the electromagnetic field can be written as:

$$H_F = \int_0^\infty \frac{dk}{2\pi} k c^+(k) c(k) \quad (3.5)$$

where  $k$  is the wave vector of the electromagnetic field. The operators  $c^+(k)$  and  $c(k)$  are called the photon creation and annihilation operators, respectively, and obey the commutation relations for boson operators.

Similarly, Eqn. (3.1) can be written in the second quantized notation as:

$$H_M = \Omega \int_0^\infty \frac{dk}{2\pi} b^+(k) b(k) \quad (3.6)$$

where  $b^+(k)$  and  $b(k)$  are the phonon creation and annihilation operators, respectively, and also obey the well-known commutation relations applicable for boson operators.

Finally, the interaction Hamiltonian can also be converted to the second quantized form (in the rotating wave approximation):

$$V_{MF} = \int_0^\infty \frac{dk}{2\pi} \sqrt{k\Delta} [c^+(k) b(k) + b^+(k) c(k)] \quad (3.7)$$

where

$$\Delta = \frac{\pi e^2 n}{m_0 \Omega}$$

The total Hamiltonian of the system can then be written as:

$$\begin{aligned} H_{MF} = & \int_0^\infty \frac{dk}{2\pi} k c^+(k) c(k) + \Omega \int_0^\infty \frac{dk}{2\pi} b^+(k) b(k) \\ & + \int_0^\infty \frac{dk}{2\pi} \sqrt{k\Delta} [c^+(k) b(k) + b^+(k) c(k)] \end{aligned} \quad (3.8)$$

At this stage, it is useful to introduce the polariton operators  $p_\alpha(k)$  and  $p_\alpha^+(k)$  ( $\alpha=1$  and  $\alpha=2$  correspond to the lower and upper branches of the polariton spectrum, respectively). These are written as follows:

$$p_1(k) = \left( \frac{\Omega - \varepsilon_1(k)}{\varepsilon_2(k) - \varepsilon_1(k)} \right)^{1/2} c(k) - \left( \frac{\varepsilon_2(k) - \Omega}{\varepsilon_2(k) - \varepsilon_1(k)} \right)^{1/2} b(k) \quad (3.9a)$$

$$p_2(k) = \left( \frac{\varepsilon_2(k) - \Omega}{\varepsilon_2(k) - \varepsilon_1(k)} \right)^{1/2} c(k) + \left( \frac{\Omega - \varepsilon_1(k)}{\varepsilon_2(k) - \varepsilon_1(k)} \right)^{1/2} b(k) \quad (3.9b)$$

$$p_1^+(k) = \left( \frac{\Omega - \varepsilon_1(k)}{\varepsilon_2(k) - \varepsilon_1(k)} \right)^{1/2} c^+(k) - \left( \frac{\varepsilon_2(k) - \Omega}{\varepsilon_2(k) - \varepsilon_1(k)} \right)^{1/2} b^+(k) \quad (3.10a)$$

$$p_2^+(k) = \left( \frac{\varepsilon_2(k) - \Omega}{\varepsilon_2(k) - \varepsilon_1(k)} \right)^{1/2} c^+(k) + \left( \frac{\Omega - \varepsilon_1(k)}{\varepsilon_2(k) - \varepsilon_1(k)} \right)^{1/2} b^+(k) \quad (3.10b)$$

3The polariton operators are seen to be combinations of phonon and photon operators.

The expression for the operator  $p_\alpha^+(k)$  is obtained from that for  $p_\alpha(k)$  by taking the Hermitian conjugate. These operators can be shown to obey the following commutation relations:

$$[p_\alpha(k), p_\alpha^+(k')] = 2\pi\delta_{\alpha\alpha'}\delta(k - k')$$

$$[p_\alpha(k), p_\alpha(k')] = 0$$

$$[p_\alpha^+(k), p_\alpha^+(k')] = 0$$

The total Hamiltonian given in Eqn. (3.8) can be diagonalized in terms of the polariton operators. To this end, the photon and phonon operators are first expressed in terms of these new operators by using Eqns. (3.9, 3.10). Substituting the results in Eqn. (3.8), the following Hamiltonian is obtained:

$$H_{MF} = \sum_\alpha \int_0^\infty \frac{dk}{2\pi} \varepsilon_\alpha(k) p_\alpha^+(k) p_\alpha(k) \quad (3.11)$$

where  $\varepsilon_\alpha(k)$  is the energy of the polariton spectrum, given by:

$$\varepsilon_1(k) = \frac{1}{2} \left[ (\Omega + k) - \sqrt{(\Omega - k)^2 + 4k\Delta} \right] \quad (3.12a)$$

$$\varepsilon_2(k) = \frac{1}{2} \left[ (\Omega + k) + \sqrt{(\Omega - k)^2 + 4k\Delta} \right] \quad (3.12b)$$

The polariton spectrum is seen to have two branches  $\varepsilon_1(k)$  and  $\varepsilon_2(k)$ .



Defining

$$\varepsilon_v = \Omega - \Delta$$

$$\varepsilon_c = \Omega$$

$$\Delta = \varepsilon_c - \varepsilon_v$$

Eqns. (3.12a, 3.12b) can be re-written as:

$$\varepsilon_1(k) = \frac{1}{2} \left[ (\varepsilon_c + \hbar ck) - \sqrt{(\varepsilon_c - \hbar ck)^2 + 4\hbar ck (\varepsilon_c - \varepsilon_v)} \right] \quad (3.13a)$$

$$\varepsilon_2(k) = \frac{1}{2} \left[ (\varepsilon_c + \hbar ck) + \sqrt{(\varepsilon_c - \hbar ck)^2 + 4\hbar ck (\varepsilon_c - \varepsilon_v)} \right] \quad (3.13b)$$

where  $\varepsilon_v$  and  $\varepsilon_c$  denote the maximum energy corresponding to the lower polariton branch and the minimum energy corresponding to the upper polariton branch, respectively. The above expressions give the dispersion relation for polaritons in a dispersive material. Note that, in Eqns. (3.13a, 3.13b),  $\hbar$  and  $c$  have been re-inserted.

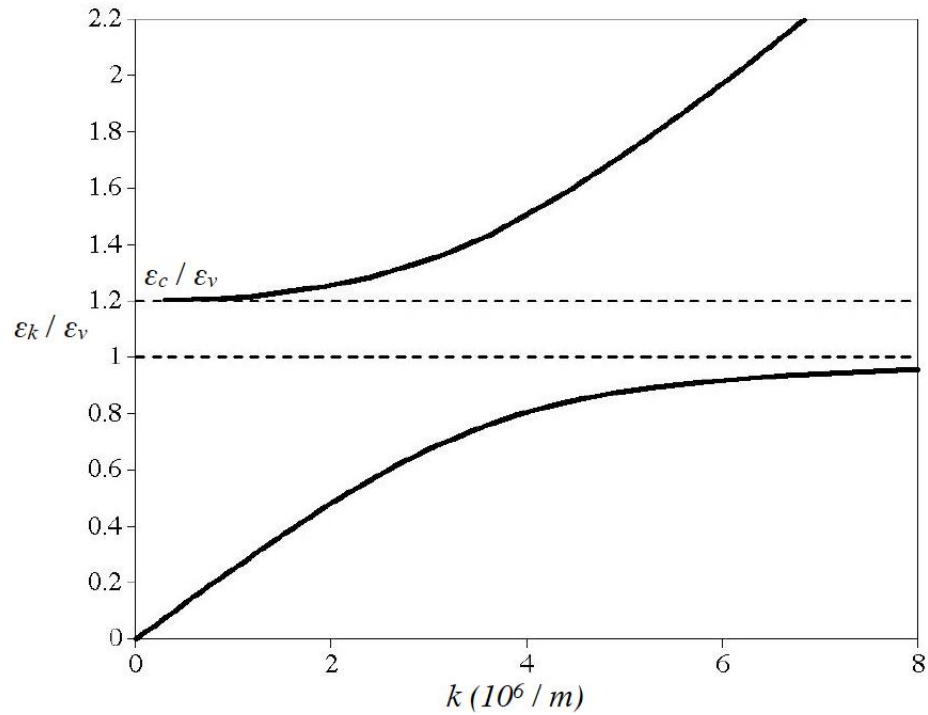


Figure 3-2: Plot of the dispersion relation for SiC. The parameters used are  $\varepsilon_v = 0.098$  eV,  $\varepsilon_c = 0.118$  eV and  $\kappa = 10^{-5}$  eV.

We have calculated the dispersion relation for SiC, which is a dispersive material. The results are plotted in Fig. 3-2.

The parameters chosen are  $\varepsilon_v = 0.098$  eV and  $\varepsilon_c = 0.118$  eV. The relaxation parameter  $\kappa = 10^{-5}$  eV. Note that the band gap lies between  $\varepsilon_v$  and  $\varepsilon_c$ .

The dispersion relation given in Eqn. (3.13) can be re-written in combination as:

$$k = \frac{\varepsilon(\varepsilon_c - \varepsilon)}{(\varepsilon_v - \varepsilon)} \quad (3.14)$$

It is mathematically more convenient to transform the expression of the polariton Hamiltonian from  $k$ -space to energy space by using Eqn. (3.14). To this end, the polariton operators in energy space are first expressed in terms of their corresponding representations in  $k$ -space:

$$p(\varepsilon_1) = \left( \frac{\varepsilon_2(k) - \varepsilon_1(k)}{\varepsilon_v - \varepsilon_1(k)} \right)^{1/2} p_1(k), \quad 0 \leq \varepsilon < \varepsilon_v \quad (3.15a)$$

$$p(\varepsilon_2) = \left( \frac{\varepsilon_2(k) - \varepsilon_1(k)}{\varepsilon_2(k) - \varepsilon_v} \right)^{1/2} p_2(k), \quad \varepsilon_c \leq \varepsilon < \infty \quad (3.15b)$$

$$p^+(\varepsilon_1) = \left( \frac{\varepsilon_2(k) - \varepsilon_1(k)}{\varepsilon_v - \varepsilon_1(k)} \right)^{1/2} p_1^+(k), \quad 0 \leq \varepsilon < \varepsilon_v \quad (3.16a)$$

$$p^+(\varepsilon_2) = \left( \frac{\varepsilon_2(k) - \varepsilon_1(k)}{\varepsilon_2(k) - \varepsilon_v} \right)^{1/2} p_2^+(k), \quad \varepsilon_c \leq \varepsilon < \infty \quad (3.16b)$$

Using the commutation relations for the polariton operators, they can be shown to satisfy the following new set of relations:

$$[p(\varepsilon), p^+(\varepsilon')] = 2\pi\delta(\varepsilon - \varepsilon')$$

$$[p^+(\varepsilon), p^+(\varepsilon')] = 0$$

$$[p(\varepsilon), p(\varepsilon')] = 0$$

Putting Eqns. (3.15, 3.16) into Eqn. (3.11) and changing the integration from  $k$ -space to energy space, the polariton Hamiltonian can finally be written as:

$$H_{MF} = \int_0^{\varepsilon_v} \frac{d\varepsilon_1}{2\pi} \varepsilon_1 p^+(\varepsilon_1) p(\varepsilon_1) + \int_{\varepsilon_c}^{\infty} \frac{d\varepsilon_2}{2\pi} \varepsilon_2 p^+(\varepsilon_2) p(\varepsilon_2)$$

This can be further simplified as follows:

$$H_{MF} = \int_C \frac{d\varepsilon}{2\pi} \varepsilon p^+(\varepsilon) p(\varepsilon) \quad (3.17)$$

where the integration contour  $C$  consists of the two allowed polariton branches,

$$0 \leq \varepsilon < \varepsilon_v \text{ and } \varepsilon_c \leq \varepsilon < \infty.$$

There is a gap between energies  $\varepsilon_v$  and  $\varepsilon_c$  with size  $(\varepsilon_c - \varepsilon_v)$ . The polaritons propagate in the medium when their energies lie within the lower and upper bands. Within the gap, the propagation of polaritons is forbidden.

### 3.3 Dispersive Materials as Reservoirs

In our model, we consider that the doped nanoparticles are interacting with the dispersive material, which acts as a reservoir. This interaction is responsible for the decays from levels  $|a\rangle$  to  $|d\rangle$ , and  $|b\rangle$  and  $|c\rangle$  to  $|e\rangle$ . The transition from level  $|b\rangle$  to  $|c\rangle$  is dipole forbidden. Due to the interaction between the nanoparticle and the reservoir, levels  $|b\rangle$  and  $|c\rangle$  both decay spontaneously to level  $|e\rangle$  and level  $|a\rangle$  decays spontaneously to level  $|d\rangle$ . The interaction Hamiltonian between the nanoparticles and the polaritons is written as:

$$H_{AR} = - \sum_{i=b,c} \int_C \frac{d\varepsilon_q}{2\pi} \sqrt{\gamma_{be}} Z(\varepsilon_{ie}) [p(\varepsilon_q) \sigma_{ie}^+] - \int_C \frac{d\varepsilon_q}{2\pi} \sqrt{\gamma_{ad}} Z(\varepsilon_{ad}) [p(\varepsilon_q) \sigma_{ad}^+] + c.c. \quad (3.18)$$

where c.c. denotes the complex conjugate.

Note that, in the lower branch, the polariton energy varies from zero to  $\varepsilon_v$ , whereas in the upper branch, the energy ranges from  $\varepsilon_c$  to  $+\infty$ . Here,  $p(\varepsilon_q)$  and  $p^+(\varepsilon_q)$  are the polariton annihilation and creation operators, respectively.

The form factor for the dispersive material can be obtained from its dispersion relation. This is done in Reference [49] and is given as:

$$Z(\varepsilon) = \frac{(\varepsilon_c - \varepsilon)^2}{(\varepsilon_v - \varepsilon)^2 + \kappa^2} \quad (3.19)$$

where  $\kappa$  accounts for relaxation processes in the medium.

We have calculated the form factor for SiC. The results are plotted in Fig. 3-3. The parameters chosen are  $\varepsilon_v = 0.098$  eV and  $\varepsilon_c = 0.118$  eV. The relaxation parameter  $\kappa = 10^{-5}$  eV. It is interesting to note that the polaritonic band-gap energy for the SiC crystal corresponds to the infrared region of the electromagnetic spectrum.

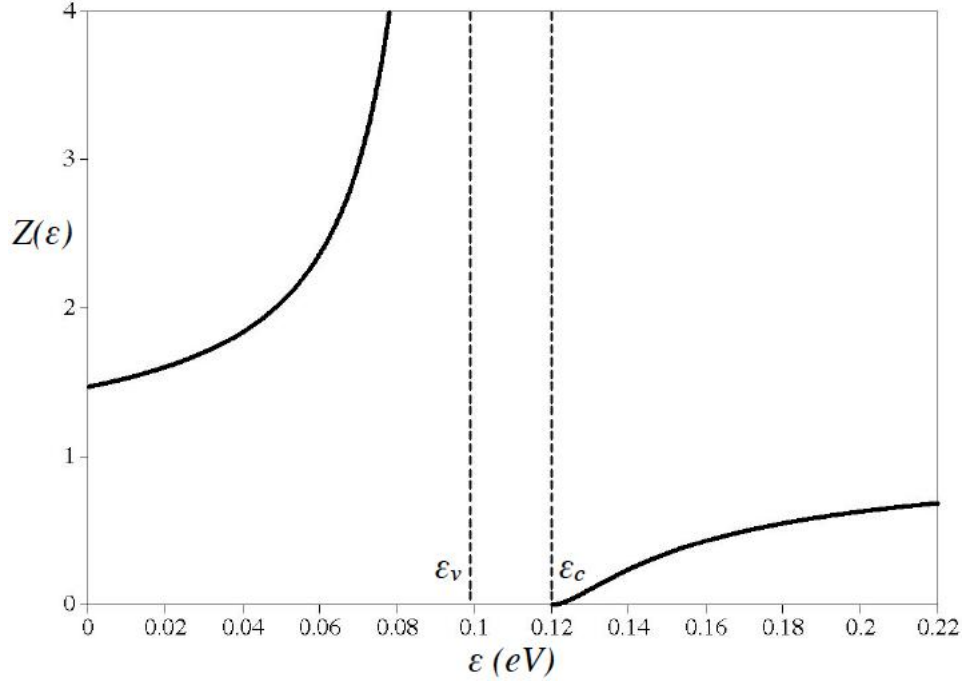


Figure 3-3: Plot of the form factor  $Z(\varepsilon)$  of the dispersive material reservoir. The choices of parameters are identical to those for the dispersion relation shown in Fig. 3-2.

It is important to observe that the form factor has a singularity near the lower band edge, identical to the case for photonic crystals. However, it does not have a singularity at the edge of the upper band. In contrast, photonic crystals have singularities near both band edges.

### 3.4 Population Density and Polariton Trapping

The theory of photon trapping has been developed in Chapter 2. We consider that, initially, the five-level nanoparticle is prepared such that it is in coherent superposition of the two levels  $|b\rangle$  and  $|c\rangle$ :

$$|\lambda, 0\rangle = B(0)|b\rangle + C(0)e^{i\psi}|c\rangle \quad (3.20)$$

where  $B(0)$  and  $C(0)$  are the initial amplitudes of levels  $|b\rangle$  and  $|c\rangle$ , respectively. The phase factor between  $B(0)$  and  $C(0)$  is taken as  $e^{i\psi}$ .

Following the method of the preceding chapter and Eqns. (3.17, 3.18, and 3.19), we get the following expression for the population density  $\rho_{aa}$  for energy level  $|a\rangle$ :

$$\rho_{aa} = \left| \frac{ie^{-(\Gamma_a + \Gamma_b)t/4} \sin(\eta t) \left[ \frac{\Omega_1(\varepsilon_c - \varepsilon_{ab})^2 B(0)}{(\varepsilon_v - \varepsilon_{ab})^2 + \kappa^2} + \frac{\Omega_2(\varepsilon_c - \varepsilon_{ac})^2 C(0)e^{i(\varphi + \psi)}}{(\varepsilon_v - \varepsilon_{ac})^2 + \kappa^2} \right]}{\sqrt{\frac{\Omega_1^2(\varepsilon_c - \varepsilon_{ab})^4}{((\varepsilon_v - \varepsilon_{ab})^2 + \kappa^2)^2} + \frac{\Omega_2^2(\varepsilon_c - \varepsilon_{ac})^4}{((\varepsilon_v - \varepsilon_{ac})^2 + \kappa^2)^2} - \left(\frac{\Gamma_a - \Gamma_b}{2}\right)^2}} \right|^2 \quad (3.21)$$

where

$$\eta = \sqrt{\frac{\Omega_1^2(\varepsilon_c - \varepsilon_{ab})^4}{((\varepsilon_v - \varepsilon_{ab})^2 + \kappa^2)^2} + \frac{\Omega_2^2(\varepsilon_c - \varepsilon_{ac})^4}{((\varepsilon_v - \varepsilon_{ac})^2 + \kappa^2)^2} - \left(\frac{\Gamma_a - \Gamma_b}{2}\right)^2} = \frac{i\Omega}{2} \quad (.)$$

Note that the above expression depends on the form factor of the dispersive material.

### 3.5 Results and Discussions

As for the case of the photonic crystal reservoir, we again let  $B(0)$  and  $C(0)$  be  $\cos(\theta/2)$  and  $\sin(\theta/2)$ , respectively, with  $0 \leq \theta \leq \pi$ , for all calculations in this section. We also let the combined phase factor  $\varphi + \psi = \pi$ . The numerical simulations are again performed at a scaled arbitrary time  $\gamma_{ad}t = 0.6$ .

It is important to note that, in the present calculations, we have only investigated the role of  $\Gamma_a$ . Whereas the value of  $\Gamma_a$  is calculated for different cases – e.g. resonance energy at mid-band, at band edge, etc. –  $\Gamma_b$  and  $\Gamma_c$  are calculated only for the case when the resonance energy lies near the middle of the band. Hence,  $\Gamma_b$  and  $\Gamma_c$  act as constants, as in other works. Because of this, the five-level system reduces to a four-level system.

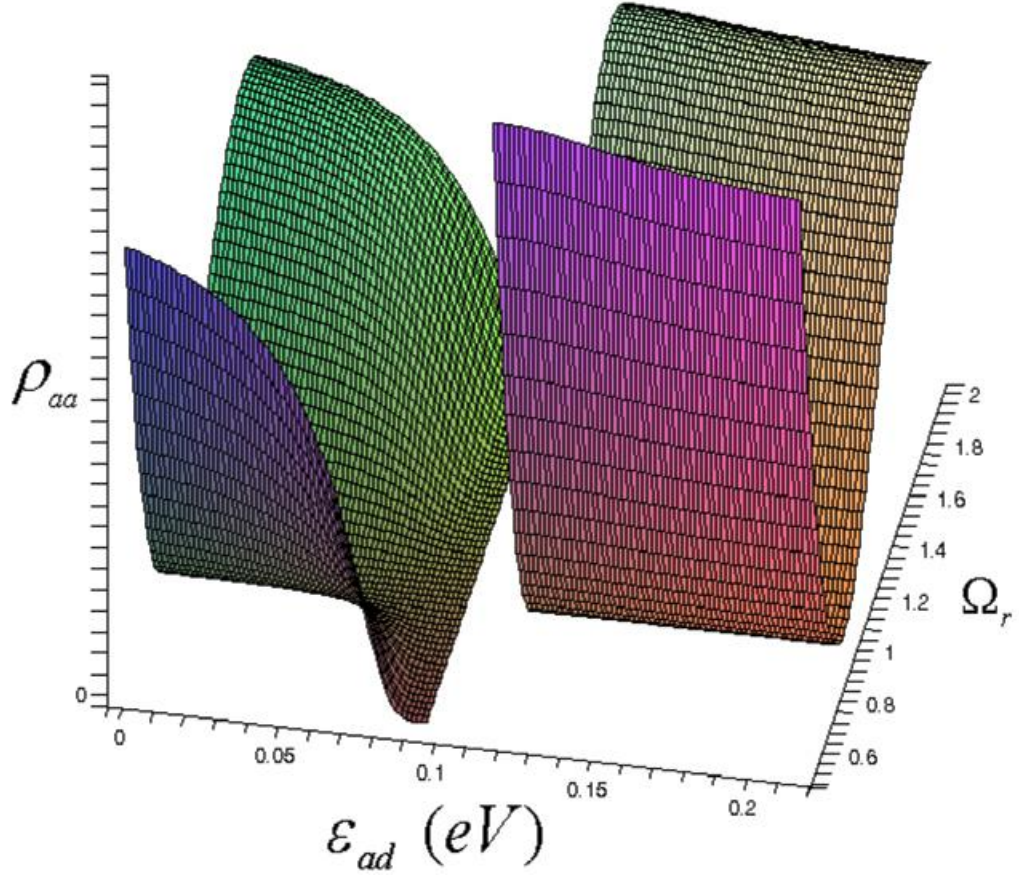


Figure 3-4: Plot of  $\rho_{aa}$  against  $\Omega_r$  and  $\varepsilon_{ad}$  for the dispersive material – shows different behaviors at the two band edges.

First, we calculate  $\rho_{aa}$  for SiC – a dispersive material. The values of the parameters are taken from References [2–4, 232] as  $\varepsilon_v = 0.098$  eV,  $\varepsilon_c = 0.118$  eV and  $\kappa = 10^{-5}$  eV. The gap energy corresponds to the infrared region of the electromagnetic spectrum.

Numerical values of  $\rho_{aa}$  are plotted as a function of  $\Omega_r$  and  $\varepsilon_{ad}$  in Fig. 3-4, when the remaining resonance energies lie within the lower propagation band ( $\varepsilon_{ab} = \varepsilon_{ac} = \varepsilon_{be} = \varepsilon_{ce} = 0.049$  eV) and  $\theta = \pi/2$ . In this case, across the lower band, the population density becomes zero for all values of the resonance energy  $\varepsilon_{ad}$  at  $\Omega_r = 1$ , giving evidence of the CPT effect in these materials. This is also true for the upper band, at the same value of the relative Rabi frequency. Moreover, these findings are similar to those for the photonic crystal, described in Chapter 2.

Note that the nature of the curves in the lower and upper bands are asymmetric and display very different behaviours. This is because the form factor has an asymmetric nature in the upper and lower bands of the dispersive material (plotted in Fig. 3-3). In contrast, in photonic crystals, the curves are symmetric both in the lower and upper bands. This is due to the fact that the form factor for a photonic crystal is symmetric about the band gap.

A closer look at the band edges in Fig. 3-4 reveals that, although  $\rho_{aa}$  vanishes at all values of the relative Rabi frequency when  $\varepsilon_{ad}$  approaches the lower band edge, the same does not apply to the case when it gets close to the upper band edge. This can be understood by considering that the form factors for both the photonic crystal and the dispersive material have the same physical behavior when energy values lie within the lower propagation band (both have very large values near the band edge). But, for energies close to the upper band edge, the form factor for the dispersive material has small values. This means that, across the upper energy band of the dispersive material (both close to and away from the band edge),  $\rho_{aa}$  vanishes only at  $\Omega_r = 1$ , due exclusively to the CPT effect.

### 3.6 Summary and Conclusion

The study of CPT in dispersive materials has great potential in the design of novel polaritonic devices such as low-threshold switches, all-optical transistors, quantum memory devices, etc., owing to the unusual properties of these materials. The potential for applications of the newly predicted effect lies in the fact that it allows us to establish controls on the population densities of the upper levels of the doped nanoparticles either by changing the relative intensity of the driving fields, or by manipulating the decay rate of the upper level by changing the relative position of level  $|d\rangle$ . As the steady-state atomic population on the upper level depends sensitively on the coherence conditions and the decay rate, increasing the latter can increase the fraction of population trapped in the system. In this way, the same population density in the upper level can be obtained for a

range of values of the resonance energy  $\varepsilon_{ad}$ , simply by adjusting the intensities of the coupled fields, as seen in Fig. 3-4.

The work described in this chapter establishes that the nature of the population density curves in a dispersive material reservoir is asymmetric. This is because the form factor has an asymmetric form in the upper and lower bands of the dispersive material. In photonic crystals, however, the curves are symmetric in nature owing to a symmetric form factor. This particular contrast leads to distinct trapping behaviours in dispersive materials compared to those observed for photonic crystals.

This concludes the discussion of our study of CPT in an ensemble of nanoparticles doped within a dispersive material. The next chapter details the extension of our investigations of the CPT phenomenon to include the effect of dipole-dipole interaction between the nanoparticles in the doped ensemble for both photonic crystal and dispersive material reservoirs.



## Chapter 4

### 4 Dipole-dipole Interaction and Coherent Trapping in Photonic Crystals and Dispersive Materials

The phenomenon of coherent population trapping (CPT) in multi-level nanoparticles doped within photonic crystals and dispersive materials has been dealt with extensively in Chapters 2 and 3, respectively. In the discussions in these two chapters, the concentration of the doped nanoparticles is assumed to be very low so that they do not interact with each other. In this chapter<sup>3</sup>, however, the concentration of the nanoparticles is assumed to be high and they interact with each other via dipole-dipole interaction (DDI).

#### 4.1 Introduction

The literature reviews and the discussions in the preceding chapters make it evident that the discoveries of photonic crystals and dispersive materials have re-invigorated the study of quantum coherence and correlation in condensed matter physics [14, 235]. Similar investigations in quantum optics and radiation physics have led to many interesting and unexpected consequences such as the Hanle effect, lasing without inversion, coherent Raman beats, photon echo and self-induced transparency [58, 266–269].

Continuing with this theme, this chapter presents our theory of the trapping of photons and polaritons in photonic crystals and dispersive materials, respectively, in the presence of DDI, taken in the mean field approximation. The nanoparticles are prepared as coherent linear combinations of the two lower levels. We consider the interaction between the nanoparticles to be due to their intrinsic dipole moments. This is known as dipole-dipole interaction. The absorption of photons from these lower levels to the uppermost level is allowed and other transitions are dipole forbidden.

---

<sup>3</sup> The work presented in this chapter has been published in: i) M. R. Singh and I. Haque, *Phys. Stat. Sol. (c)* **2**, 2998 (2005), ii) I. Haque and M. R. Singh, *AIP Conf. Proc.* **772**, 1246 (2005), and iii) I. Haque and M. R. Singh, *Photonics 2004, Cochin, SPIE Elec. Conf. Proc.* (2004).

First, we calculate the population density of the uppermost level by using the Schrödinger equation and the Laplace transform method. It is found that, the DDI between the nanoparticles plays a very important role in determining the conditions required for CPT. It is also observed that this interaction directly influences the population densities of the excited levels of the nanoparticles. More precisely, under certain conditions, the electron population is trapped in the lower levels and there is no absorption even in the presence of external resonant photon fields.

We have also found that the photon and polariton trapping effects undergo shifts in locations due to the DDI effect. This is a very interesting result and can be used to make photonic and polariton switching devices. In addition, we have established that the trapping of photons and polaritons disappear in certain situations in both photonic crystals and dispersive materials, due to the influence of DDI. This happens when the resonance energies of the nanoparticles are located in the lower bands of these materials.

However, when the resonance energies lie in the upper bands of the photonic crystal and the dispersive material, converse effects are observed. More specifically, in the dispersive material reservoir, the population density vanishes when the resonance energy lies near the lower band edge. But, this effect is not observed if the resonance energy lies near the upper band edge. This is in contrast with the case for the photonic crystal, where the population density of the uppermost level is seen to vanish near both the upper and lower band edges. This interesting phenomenon is explained by the symmetric and asymmetric structures of the photonic crystal and dispersive material form factors, respectively, about the corresponding band gaps.

Finally, we have also observed in general that, for both the photonic crystal and dispersive material reservoirs, as the number density of the doped nanoparticles increases, the population densities of the uppermost energy levels also increase, when the photon fields are held constant. This is a direct consequence of the increasing strength of the DDI between the nanoparticles.

## 4.2 Dipole-dipole Interaction

This section describes the theoretical framework behind the DDI effect. The presence of the electromagnetic fields induces electric dipole moments in the doped nanoparticles. These dipole moments interact with each other. The DDI in our model is calculated using mean field theory. The details of the relevant formulation can be found in Reference [270].

The energy levels of a doped nanoparticle are denoted by  $|a\rangle$ ,  $|b\rangle$ ,  $|c\rangle$ ,  $|d\rangle$  and  $|e\rangle$ . The atomic scheme is shown in Fig. 4-1.

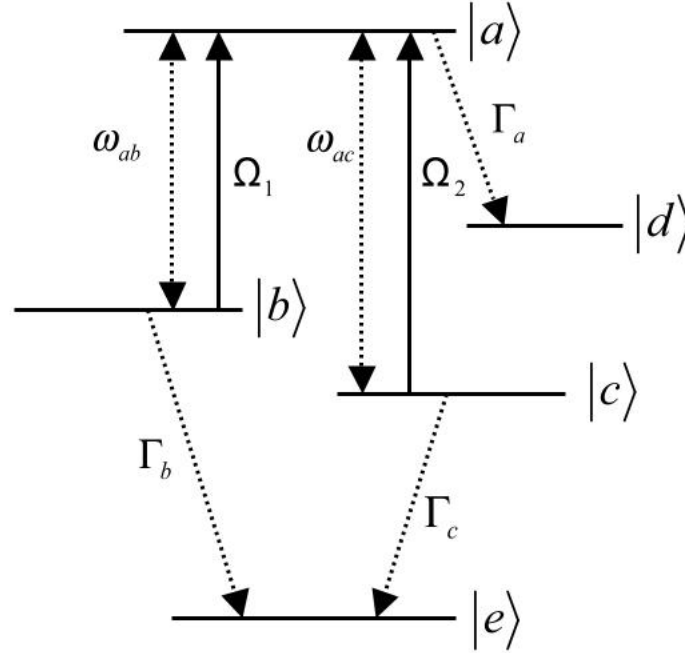


Figure 4-1: Level scheme of a five-level nanoparticle.  $\omega_{ij}$  is the energy difference between the levels  $|i\rangle$  and  $|j\rangle$ . Here  $|i\rangle$  and  $|j\rangle$  stand for  $|a\rangle$ ,  $|b\rangle$ ,  $|c\rangle$ ,  $|d\rangle$  and  $|e\rangle$ . The levels  $|b\rangle$  and  $|c\rangle$  both spontaneously decay to level  $|e\rangle$  and level  $|a\rangle$  spontaneously decays to level  $|d\rangle$ .

We consider that a probe field with amplitude  $E_0$  and energy  $\varepsilon_p$  is applied between levels  $|a\rangle$  and  $|b\rangle$ . The electric field for the probe laser can be written as:

$$E(t) = E_0 \cos(\varepsilon_p t / \hbar) \quad (4.1)$$

The probe laser field excites a transition between levels  $|a\rangle$  and  $|b\rangle$  and it induces a dipole moment in each nanoparticle. These dipoles are interacting with each other via DDI. The polarization due to the induced dipoles can be written as [271]:

$$P(t) = P_0 \cos(\varepsilon_p t / \hbar) \quad (4.2)$$

where  $P_0$  is the polarization amplitude.

We assume that there are  $N$  nanoparticles per unit volume and the induced dipole moment in the  $i^{th}$  particle is denoted by the operator  $\mu_i$ . The DDI Hamiltonian can be written as [272]:

$$H_{dd}^T = -\frac{1}{2} \sum_{i \neq j} J_{ij} \mu_i \mu_j \quad (4.3)$$

where  $J_{ij}$  is the DDI coupling constant.

According to mean field theory, the  $i^{th}$  dipole sees the mean electric field  $E_M$  created by all other dipoles. In other words, the electric field does not depend on the positions of the particles. The field, then, can be written as:

$$E_M = \left\langle \frac{1}{2} \sum_j J_{ij}(\mathbf{r}) \mu_j \right\rangle \quad (4.4)$$

where  $\langle \dots \rangle$  denotes the ensemble average. Generally, in the mean field approximation,  $E_M$  is written as [272]:

$$E_M(t) = \frac{P(t)}{3 \epsilon_0} \quad (4.5)$$

where  $\epsilon_0$  denotes the vacuum permittivity.

Putting the expression for  $P(t)$  from Eqn. (4.2) into  $E_M(t)$ , we get:

$$E_M(t) = \frac{P_0 \cos(\varepsilon_p t / \hbar)}{3 \epsilon_0} \quad (4.6)$$

For identical nanoparticles, we consider the case where  $\mu_i = \mu$ . Combining Eqns. (4.3, 4.4, and 4.6), we get:

$$H_{dd}^T = -N \left( \frac{P_0 \cos(\varepsilon_p t / \hbar)}{3 \epsilon_0} \right) \mu \quad (4.7)$$

The above expression can be written in quantized form as follows:

$$H_{dd}^T = - \left( \frac{N \mu P_0}{3 \epsilon_0} \right) (\sigma_{ab}^+ + \sigma_{ab}^-) \quad (4.8)$$

where  $\sigma_{ab}^+ = |a\rangle\langle b|$  and  $\sigma_{ab}^- = |b\rangle\langle a|$  are the raising and lowering operators, respectively.

The quantities  $\mu_{ab} = \langle a | \mu | b \rangle$  and  $\mu_{ab}^* = \langle b | \mu | a \rangle$  are the matrix elements of the dipole operator between levels  $|a\rangle$  and  $|b\rangle$ .

The expression for  $P_0$  is given by:

$$P_0 = \mu (\rho_{ab} + \rho_{ba}) \quad (4.9)$$

Finally, we get the following expression for the DDI Hamiltonian:

$$H_{dd}^T = - \left( \frac{N \mu^2}{3 \epsilon_0} \right) (\sigma_{ab}^+ \rho_{ab} + \rho_{ba} \sigma_{ab}^-) \cos(\varepsilon_p t / \hbar) \quad (4.10)$$

Note that the DDI effect depends on the number density  $N$  and the coherence matrix element  $\rho_{ab}$ .

### 4.3 Population Density and Coherent Population Trapping

This section describes the theoretical framework of our study of CPT in a doped five-level atomic ensemble in photonic crystals and dispersive materials, in the presence of DDI.

The nanoparticles are prepared in coherent superpositions of levels  $|b\rangle$  and  $|c\rangle$ :

$$|\lambda, 0\rangle = B(0)|b\rangle + C(0)e^{i\varphi}|c\rangle \quad (4.11)$$

where  $B(0)$  and  $C(0)$  are the initial amplitudes of the lower doublet  $|b\rangle$  and  $|c\rangle$ , respectively. The phase factor between  $B(0)$  and  $C(0)$  is taken as  $e^{i\psi}$ . Level  $|b\rangle$  and the upper level  $|a\rangle$  are coupled by a coupling field of frequency  $\nu_1$  and amplitude  $E_1$  and levels  $|c\rangle$  and  $|a\rangle$  are coupled by a weak probe field of frequency  $\nu_2$  and amplitude  $E_2$  (see Fig. 4-1). The transition from level  $|b\rangle$  to  $|c\rangle$  is dipole forbidden. Due to the interaction between the nanoparticle and the reservoir, levels  $|b\rangle$  and  $|c\rangle$  both decay spontaneously to level  $|e\rangle$  and level  $|a\rangle$  decays spontaneously to level  $|d\rangle$ . It is assumed that the decay rates of levels  $|b\rangle$  and  $|c\rangle$  are identical.

It is important to note that the dopants can be any of quantum dots, quantum wells, etc. Recently, semiconductor quantum dots and quantum wells have been used as multi-level nanoparticles to study Stark splitting, quantum coherence and electromagnetically induced transparency [273]. Furthermore, quantum dots have also been used to study electron-hole DDI [274].

The nanoparticles in the doped ensemble are taken to interact with each other via DDI. The interaction Hamiltonian has been derived in the previous section (see Eqn. (4.10)). The nanoparticles also interact with the reservoir. Under the dipole and rotating-wave approximations, the Hamiltonian for this interaction is given in Eqn. (2.8) in Chapter 2 for photonic crystals, and in Eqn. (3.17) in Chapter 3 for dispersive materials.

The state of the system at a later time  $t$  can be written as:

$$|\lambda, t\rangle = A(t)|a\rangle + B(t)|b\rangle + C(t)|c\rangle \quad (4.12)$$

Using the Schrödinger equation and the Laplace transform method (discussed in Appendix H), we obtained the following expressions for the amplitudes, in the mean field approximation:

$$A(t) = ie^{-(\Gamma_a + \Gamma_b)t/4} \frac{\sin(\eta t)}{\eta} \left[ (\Omega_m + \Omega_1) Z_{ab} B(0) + \Omega_2 Z_{ac} C(0) e^{i(\varphi + \psi)} \right] \quad (4.13)$$

$$B(t) = \frac{e^{-\Gamma_b t/2} \left[ B(0)\Theta_1 + C(0)e^{i(\varphi+\psi)}\Theta_2 \right]}{\Omega^2 + \left( \frac{\Gamma_a - \Gamma_b}{2} \right)^2} \quad (4.14)$$

where

$$\eta = \sqrt{(\Omega_m + \Omega_1)^2 Z_{ab}^2 + (\Omega_2)^2 Z_{ac}^2 - \left( \frac{\Gamma_a - \Gamma_b}{2} \right)^2} \quad (4.15)$$

$$\Omega_m = \left( \frac{2N\lambda\mu_{ab}^2 A(t)B^*(t)}{\hbar} \right) \quad (4.16)$$

and

$$\Theta_1 = \Omega^2 + \left( \frac{\Gamma_a - \Gamma_b}{2} \right)^2 - |\Omega_m + \Omega_1|^2 \frac{Z_{ab}^2}{\Omega} \left[ \Omega + e^{-(\Gamma_a - \Gamma_b)t/4} \Phi \right] \quad (4.17)$$

$$\Theta_2 = -(\Omega_m + \Omega_1)\Omega_2 Z_{ac} Z_{ab} - \frac{(\Omega_m + \Omega_1)\Omega_2 Z_{ac} Z_{ab} e^{-(\Gamma_a - \Gamma_b)t/4} \Phi}{\Omega} \quad (4.18)$$

with

$$\Phi = \frac{(\Gamma_a - \Gamma_b)^2}{2} \sin\left(\frac{\Omega t}{2}\right) - \Omega \cos\left(\frac{\Omega t}{2}\right) \quad (4.19)$$

In the above,  $N$  and  $\lambda$  are the number density of the nanoparticles and the mean-field parameter related to the coupling parameter  $J_{ij}$ , respectively.  $\Gamma_a$  and  $\Gamma_b$  are the decay rates for  $|a\rangle$  and  $|b\rangle$ , respectively, and are written as:

$$\Gamma_a = 1/2\gamma_{ad}Z_{ad}^2(\varepsilon_{ad}) \quad (4.20a)$$

$$\Gamma_b = 1/2\gamma_{be}Z_{be}^2(\varepsilon_{be}) \quad (4.20b)$$

The expression for the form factor for the photonic crystal has been derived in Chapter 2 and is given by (see Fig. 4-2, discussed in Appendix G):

$$Z(\varepsilon_{ij}) = \left[ \frac{(a/L)(1+n)^2 \sin\left(\frac{4na\varepsilon_{ij}}{\hbar c}\right)}{\left[1 - \varsigma^2(\varepsilon_{ij})\right]^{1/2}} \right]^{1/2} \quad (4.21)$$

$$\varsigma(\varepsilon_{ij}) = \frac{(1+n)^2 \cos\left(\frac{4na\varepsilon_{ij}}{\hbar c}\right) - (1-n)^2}{4n} \quad (4.22)$$

In plotting Fig. (4.2), we choose a photonic crystal with  $n = 1.082$ ,  $L = 300$  nm,  $(a/L) = 0.24$  and a gap-midgap ratio of 5% [24].

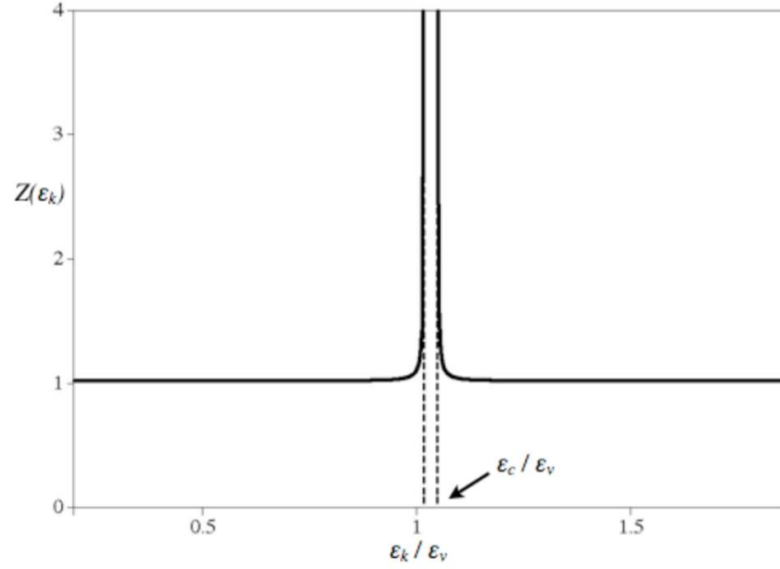


Figure 4-2: Plot of the form factor  $Z(\varepsilon_k)$  of the photonic crystal. The choices of the crystal parameters and the horizontal axis are identical to those for the dispersion relation in Fig. 2-5.

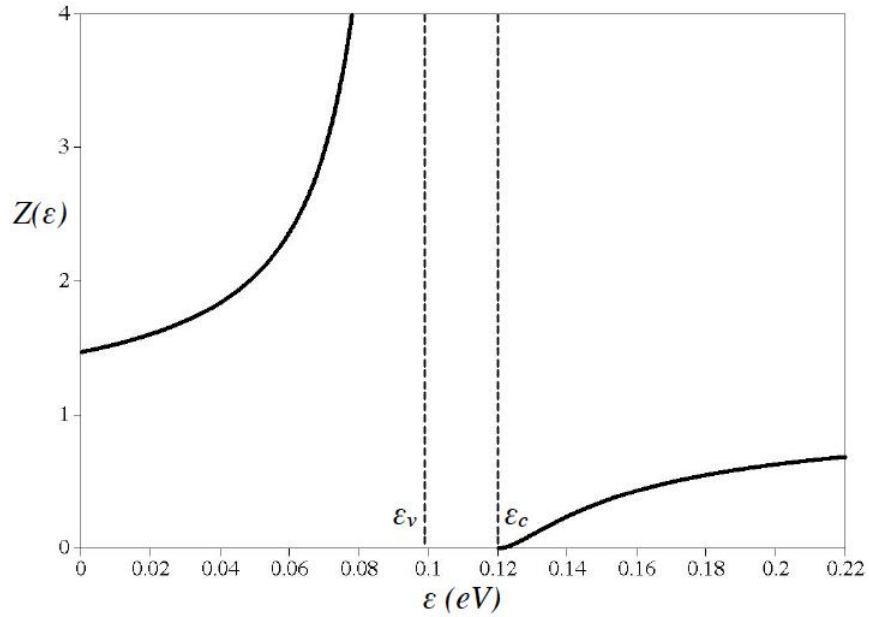


Figure 4-3: Plot of the form factor  $Z(\varepsilon)$  of the dispersive material reservoir. The choices of parameters are identical to those for the dispersion relation shown in Fig. 3-2.



Similarly, the expression for the form factor for the dispersive material is given in Chapter 3 and is written as (see Fig. 4-3):

$$Z(\varepsilon) = \frac{(\varepsilon_c - \varepsilon)^2}{(\varepsilon_v - \varepsilon)^2 + \kappa^2} \quad (4.23)$$

For Fig. (4.3), we choose a SiC crystal with  $\varepsilon_v = 0.098$  eV and  $\varepsilon_c = 0.118$  eV and a gap-midgap ratio of around 18%.

Note that Eqns. (4.13, 4.14) have the term  $A(t)B^*(t)$  on their right hand sides. Therefore, in order to calculate the population densities of the energy levels, these two equations have to be solved self-consistently.

Finally, the population density of level  $|a\rangle$  can be obtained as:

$$\rho_{aa} = |A(t)|^2 \quad (4.24)$$

$$\rho_{aa} = e^{-(\Gamma_a + \Gamma_b)t/2} \left( \frac{\sin(\eta t)}{\eta} \right)^2 \left[ \left( (\Omega_m + \Omega_1) Z_{ab} B(0) + \Omega_2 Z_{ac} C(0) e^{i(\varphi + \psi)} \right)^2 \right] \quad (4.25)$$

## 4.4 Results and Discussions

This section presents the results of our numerical calculations of CPT in photonic crystals and dispersive materials doped with ensembles of five-level nanoparticles. A major focus of these calculations is to study the effect of the DDI between the nanoparticles in the ensemble on the population densities of the energy levels of the nanoparticles and, hence, the trapping phenomenon.

### 4.4.1 Photonic Crystals

First, for photonic crystals, numerical calculations for  $\rho_{aa}$  are shown in Figs. (4-4, 4-5).

As before,  $B(0) = \cos(\theta/2)$  and  $C(0) = \sin(\theta/2)$ , respectively, where  $0 \leq \theta \leq \pi$ . We also let  $\varphi + \psi = \pi$ .

The numerical simulations are performed at a scaled arbitrary time  $\gamma_{ad}t = 0.6$ . We choose a photonic crystal with  $n = 1.082$ ,  $L = 300$  nm,  $(a/L) = 0.24$  and a gap-midgap ratio of

5% [24]. It is important to note that the main findings of this section do not depend on the choice of photonic crystal. We also assume that  $\gamma_{be} / \gamma_{ad} = \gamma_{ce} / \gamma_{ad} = 1/3$  and measure all other frequencies with respect to  $\gamma_{ad}$ .

We calculate the population density ( $\rho_{aa}$ ) when the resonance energies lie near the middle of the lower band of the photonic crystal, taking  $\theta = 2\pi/3$  and  $\Omega_1 / \gamma_{ad} = 10^{-5}$ .

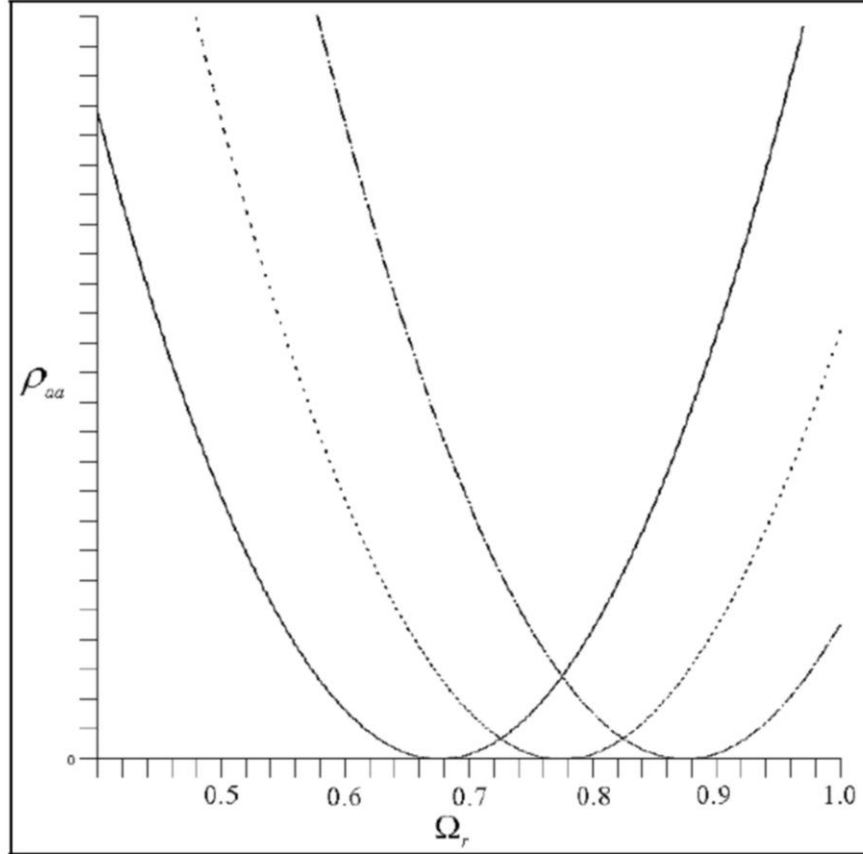


Figure 4-4: Plot of  $\rho_{aa}$  against  $\Omega_r$  for  $N = 10^{18}$  (dash-dotted curve),  $N = 2 \times 10^{18}$  (dotted curve) and  $N = 3 \times 10^{18}$  (solid curve), for a photonic crystal reservoir.

In Fig. 4-4,  $\rho_{aa}$  is plotted against the relative Rabi frequency ( $\Omega_r$ ) for three different values of  $N$ . For each case,  $\rho_{aa}$  becomes zero at a different value of  $\Omega_r$ . This shows the CPT effect in these materials. More interestingly, as  $N$  increases, the value of  $\Omega_r$  at which trapping occurs decreases. This means that the phenomenon of photon trapping

switches from one position to another due to the effect of the DDI. This is a very interesting result and can be used to make photonic switching devices.

Also, in Fig. 4-4, the intensity of the weak probe field required for the occurrence of CPT increases with increasing number density of the doped nanoparticles. This is because a large value of  $N$  implies strong DDI between the nanoparticles, which intensifies the coupling between levels  $|b\rangle$  and  $|a\rangle$ . This, in turn, means that a large probe intensity is required for destructive interference between the two transitions. Similar results are also found when the resonance energies lie within the upper band.

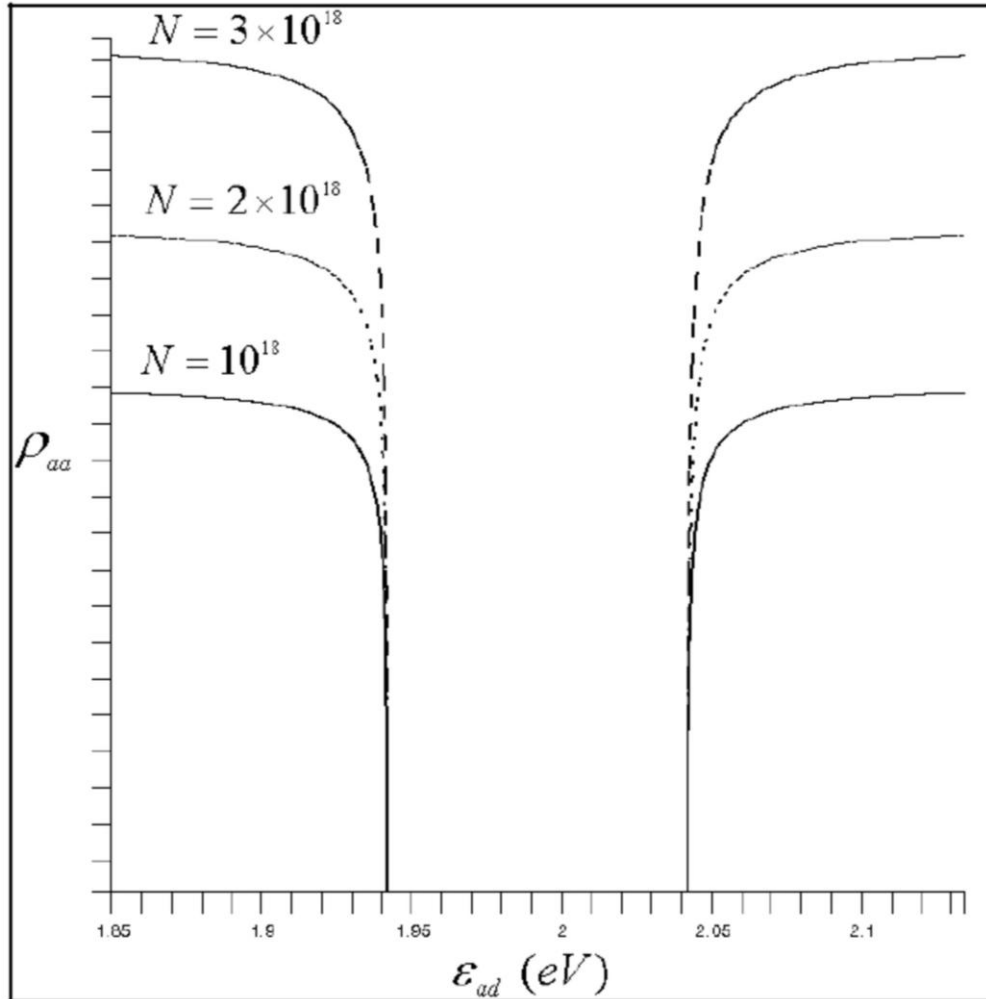


Figure 4-5: Plot of  $\rho_{aa}$  against  $\epsilon_{ad}$  for the values of  $N$  as in Fig 4.4, for a photonic crystal reservoir.

Next, we plot  $\rho_{aa}$  against  $\varepsilon_{ad}$  in Fig. 4-5 for  $\Omega_1 / \gamma_{ad} = 10^{-5}$  and  $\Omega_2 / \gamma_{ad} = 10^{-6}$ . The other parameters are kept the same, as in Fig. 4-4. It is found that  $\rho_{aa}$  becomes zero as  $\varepsilon_{ad}$  approaches either of the edges of the band gap of the photonic crystal. This is due to the effect of the form factor, given in Fig. 4-2, which becomes very large near the band edges and, in turn, broadens the level width substantially (see Eqn. (4.20)). Hence, the population density of the upper level becoming zero in this case cannot be interpreted as a signature of CPT.

The plot shows further that, as the number density of the doped nanoparticles increases, the population density of level  $|a\rangle$  also increases, when the photon fields are held constant. This is a consequence of the DDI between the nanoparticles.

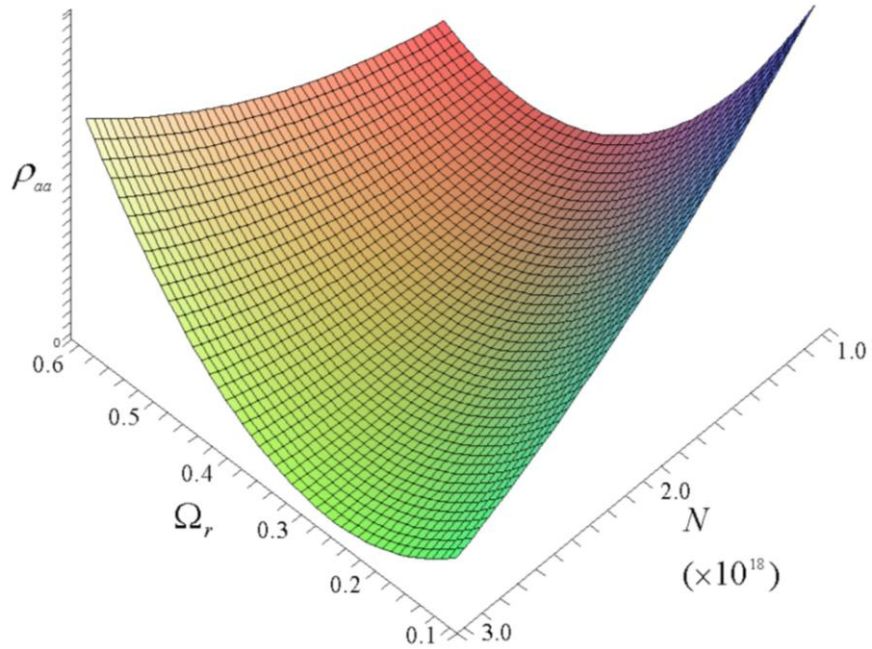


Figure 4-6: Three-dimensional plot of  $\rho_{aa}$  against  $\Omega_r$  (relative Rabi frequency) and  $N$  (number density of doped nanoparticles), for a photonic crystal reservoir.

Figs. (4-6, 4-7) show the above plots in three dimensions. In Fig. 4-6, it is found that, as  $N$  increases, the value of  $\Omega_r$  at which the trapping occurs decreases. This is because a large value of  $N$  implies strong DDI, thus requiring only a small relative frequency for destructive interference between the two transitions (see Eqn. (4.25)). Results are similar

irrespective of whether the resonance energies lie within the lower or upper band of the photonic crystal.

In Fig. 4-7, we observe that  $\rho_{aa}$  becomes zero as the resonance energy ( $\varepsilon_{ad}$ ) approaches either of the edges of the band gap. This is due to the effect of the form factor (see Fig. 4-2) – which becomes very large at the band edges – and cannot be interpreted as CPT.

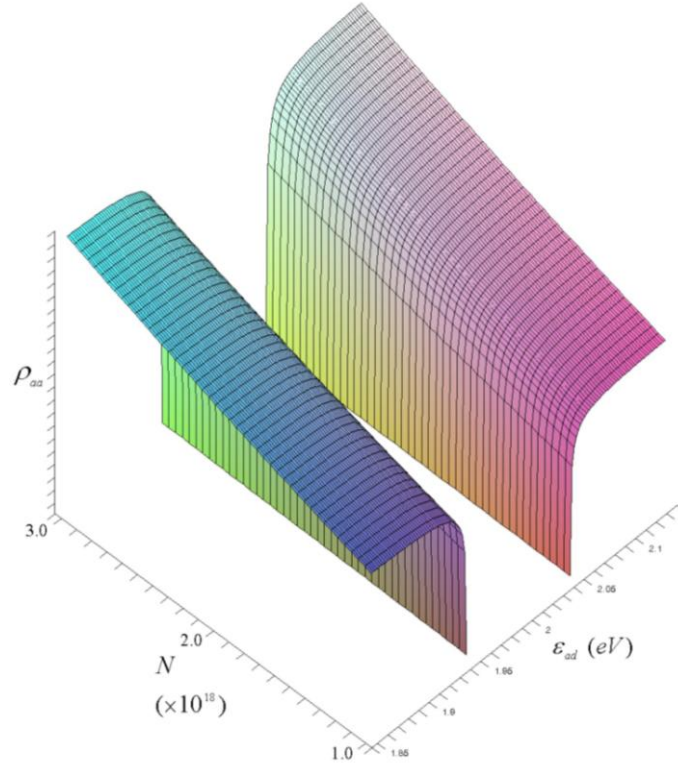


Figure 4-7: Three-dimensional plot of  $\rho_{aa}$  against  $\varepsilon_{ad}$  (energy) and  $N$  (number density of doped nanoparticles), for a photonic crystal reservoir.

Fig. 4-7 shows further that as the number density of the doped nanoparticles increases, the population density of level  $|a\rangle$  also increases, when the photon fields are held constant. This is a direct consequence of the DDI between the nanoparticles.

#### 4.4.2 Dispersive Materials

Next, we calculate the DDI effect in dispersive materials. For our simulations, we choose a SiC crystal with  $\varepsilon_v = 0.098\text{eV}$  and  $\varepsilon_c = 0.118\text{eV}$  and a gap-midgap ratio of around

18%. It is important to note that the main findings of this section do not depend on the choice of dispersive material.

First, we evaluate  $\rho_{aa}$  when the resonance energies lie near the middle of the lower band, taking  $\theta = (4/5)\pi$  and  $\Omega_1 / \gamma_{ad} = 1.9 \times 10^{-5}$ . In Fig. 4-8,  $\rho_{aa}$  is plotted against the relative Rabi frequency ( $\Omega_r$ ) for three different values of the nanoparticle density.

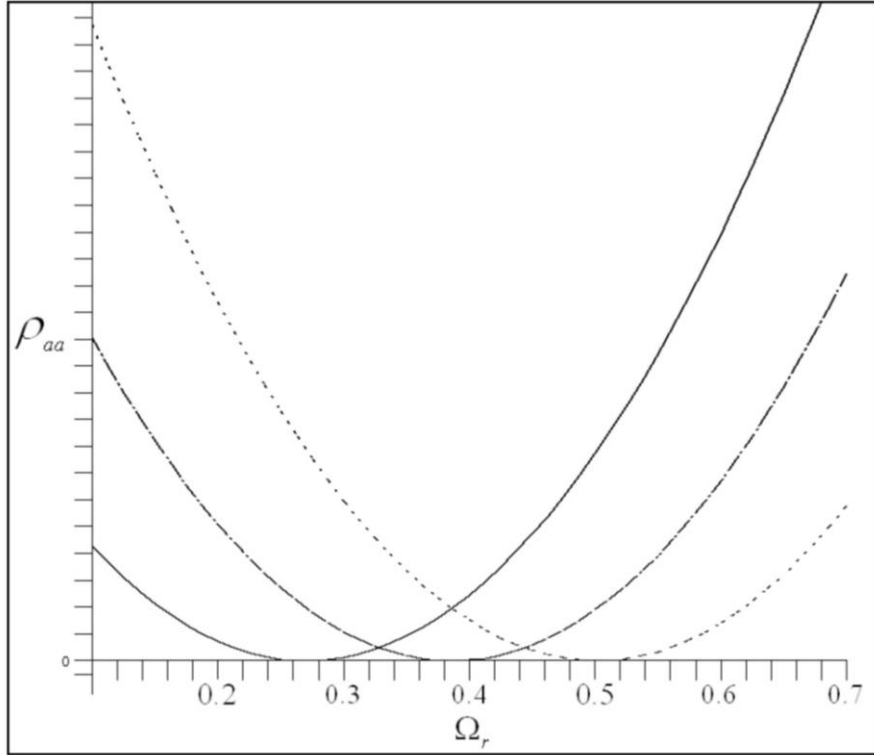


Figure 4-8: Plot of  $\rho_{aa}$  against  $\Omega_r$  for  $N = 10^{18}$  (dotted curve),  $N = 2 \times 10^{18}$  (dash-dotted curve) and  $N = 3 \times 10^{18}$  (solid curve), for a dispersive material reservoir.

In Fig. 4-8, for each curve,  $\rho_{aa}$  vanishes at a different value of  $\Omega_r$ . This demonstrates the CPT effect in these materials. We also note that, as  $N$  increases, the value of  $\Omega_r$  at which the trapping occurs decreases. This is because a larger value of  $N$  implies a higher DDI strength, thus requiring only a small relative frequency for the destructive interference effect between the two transitions. Results are similar irrespective of whether the resonance energies lie within the lower or upper band of the dispersive material.

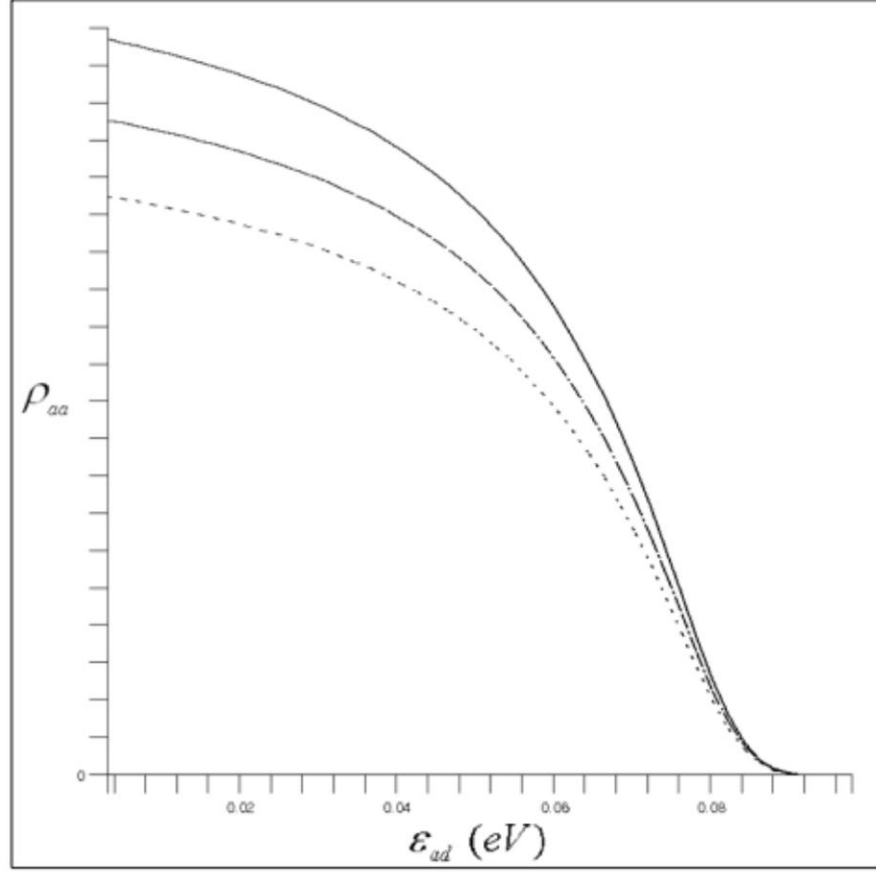


Figure 4-9: Plots of  $\rho_{aa}$  against  $\epsilon_{ad}$  for  $N = 2.8 \times 10^{18}$  (dotted curve),  $N = 2.9 \times 10^{18}$  (dash-dotted curve) and  $N = 3.0 \times 10^{18}$  (solid curve) showing the lower energy band, for a dispersive material reservoir.

Note that this behavior is similar to that for the photonic crystal, when the resonance energies lie within both its upper and lower bands.

Next, we evaluate  $\rho_{aa}$  against  $\epsilon_{ad}$  in Figs. (4-9, 4-10) for  $\Omega_r / \gamma_{ad} = 1/4$ . The other parameters are kept the same as in the simulation presented in Fig. 4-8.

In Fig. 4-9, it can be seen that  $\rho_{aa}$  becomes zero as  $\epsilon_{ad}$  approaches the lower edge of the band gap. This is due to the effect of the form factor for the dispersive material (see Fig. 4-3), which becomes very large near the lower band edge and, in turn, broadens the level width substantially. This becomes obvious from the nature of Eqns. (4.20a, 4.20b).

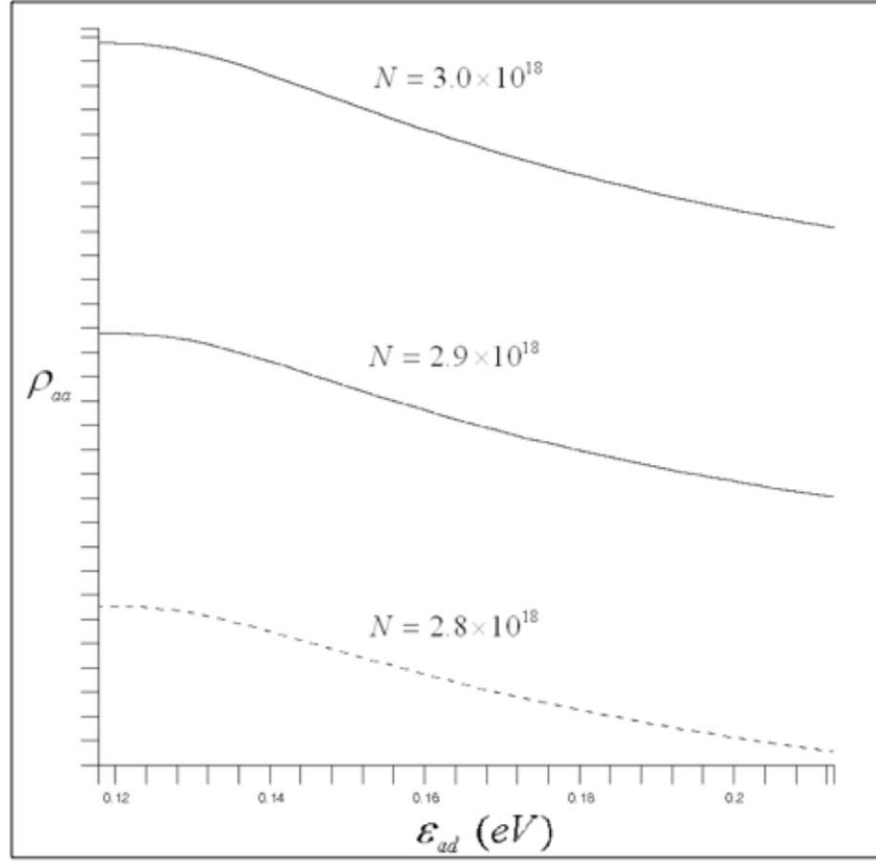


Figure 4-10: Plots of  $\rho_{aa}$  against  $\varepsilon_{ad}$  for  $N = 2.8 \times 10^{18}$  (dotted curve),  $N = 2.9 \times 10^{18}$  (dash-dotted curve) and  $N = 3.0 \times 10^{18}$  (solid curve) showing the upper energy band, for a dispersive material reservoir. The band gap is not shown.

Consequently, the vanishing population density of the upper level, in this case, cannot be interpreted as CPT. This finding is similar to that for the photonic crystal, whose form factor (see Fig. 4-2) displays similar behaviours in the lower band and near the lower band edge.

However, interestingly, the situation is quite distinct when  $\varepsilon_{ad}$  gets close to the upper band edge (see Fig. 4-10) of the dispersive material. In this case, the population density does not become zero, as in the case near the upper band edge of the photonic crystal.

This can be understood by considering that the form factor for the dispersive material has small values for energies close to the upper band edge. This means that, across the upper energy band of the dispersive material (both close to and away from the band edge), the



population of the upper level vanishes exclusively due to the CPT effect and is not a signature of the band structure. These results are very different compared to those found for photonic crystals.

This is explained by the symmetric and asymmetric structures of the photonic crystal and dispersive material form factors, about the corresponding band gaps (see Figs. (4-2, 4-3)), respectively. For the photonic crystal, the form factor has large values as the relevant resonance energy approaches either the lower or the upper band edge. But, for the dispersive material, this only happens when the relevant resonance energy approaches the lower band edge. At the upper band edge of the dispersive material, the form factor has relatively small values. These contrasting behaviours near the upper and lower band edges in the dispersive material, can be utilized in the fabrication of novel switching devices.

Figs. (4-9, 4-10) show further that, as the number density of the dopants increases, the population density of the uppermost energy level also increases, when the photon fields are held constant. This is a direct consequence of the increasing strength of the DDI between the nanoparticles.

However, the behavior is seen to be asymmetric, as opposed to the case for the photonic crystal. More specifically, the population density of the uppermost level vanishes when the resonance energy is near the lower band edge of the dispersive material; but, both in the upper band and near the upper band edge of this material, the population density does not become zero. This is a very interesting phenomenon and can, again, be understood by considering the asymmetric nature of the form factor of the dispersive material, about the band gap, as given in Fig. 4-3 and discussed above. This case is markedly different compared to that for the photonic crystal as, in the latter case, the form factor is symmetric about the band gap (see Fig. 4-2).

## 4.5 Summary and Conclusion

The discussion in this chapter detailed our study of one-photon absorption due to quantum coherence and interference in a photonic crystal and a dispersive material, when

they are doped with an ensemble of five-level nanoparticles. The nanoparticles are considered to interact with the pump and probe laser fields and a reservoir. The photon absorptions produce induced dipole moments in the nanoparticle systems and they interact with each other via DDI.

We consider the interaction between these induced dipole moments in the mean field approximation and utilize a self-consistent density matrix approach to calculate the population density of the uppermost level of the doped nanoparticle. The nanoparticles are prepared in coherent superpositions of the two lower levels and interact with a reservoir and two photon fields. The Schrödinger equation and the Laplace transform method are used to calculate the expressions for the population densities of the energy levels of the nanoparticle.

Numerical simulations for a photonic crystal reveal that when the resonance energies lie away from the band edges and within the lower or upper bands, trapping is observed at certain values of the relative Rabi frequency, which vary depending on the strength of the DDI between the nanoparticles. Also, if the photon fields are held constant, the population densities of the uppermost levels of the nanoparticles increase with increasing DDI.

For the dispersive material, when the resonance energy lies within the lower and the upper bands, one observes the CPT effect at certain values of the relative Rabi frequency, which vary depending on the strength of the DDI between the nanoparticles, as in the case for the photonic crystal. Also, as this interaction becomes stronger, the population density of the uppermost level increases.

This concludes the discussion of our study of the CPT phenomenon in photonic crystals and dispersive materials doped with ensembles of identical nanoparticles, both with and without the presence of DDI. The phenomenon of CPT has great potential for applications in engineering and optical computing. For example, interacting impurities in dispersive media can be used to coherently manipulate multi-atom collective states. The entangled superpositions of such states can be used to implement quantum logic gates using optically excited nanoparticles [274]. Another useful application would be to

exploit the effect of the relative phase of the driving laser fields on the coherently trapped state of the nanoparticle ensemble. This way, the ensemble can be used as a fast phase-controlled optical switching device [102].

## Chapter 5

### 5 The ac Stark Effect in Photonic Crystals

Discussion in Chapters 2 and 4 have focused the interaction between nanoparticles doped within photonic crystals and external radiation fields in the linear regime. Principally, we have investigated the phenomenon of photon trapping in these particles, both in the absence (Chapter 2) and presence (Chapter 4) of dipole-dipole interaction (DDI).

This chapter details our study of the phenomenon of ac Stark effect due to quantum coherence and interference in a photonic crystal, in the absence of DDI<sup>4</sup>. This means that we consider the crystal to be lightly doped with an ensemble of identical nanoparticles.

#### 5.1 Introduction

In the literature, along with other similar phenomena such as lasing without inversion [147–149], electromagnetically induced transparency [150–153], enhancement of nonlinear susceptibilities [154–157], etc., the ac Stark effect has primarily been studied in the contexts of quantum superposition and life-time broadening in atomic gases in the presence of multiple fields [158–208, 219–225]. Furthermore, much of the existing work on the ac Stark effect involves gases consisting of three-level systems. The nanoparticles are taken in either of the  $\Lambda$ ,  $V$  or  $\Xi$  (cascade or ladder) configurations [163–167, 211–220]. Recent studies in this area, however, have included four-level atomic gases [222–225].

A four-level system that has been found to be remarkably advantageous for the investigation of the diverse features of the ac Stark effect features the nanoparticle being driven by two pump fields and a weak probe field. At the core of this configuration is a  $\Xi$ -type three-level sub-system. The weak field can be configured to probe the transition to the level external to the cascade from either the ground or the intermediate level. Wei

---

<sup>4</sup> The work presented in this chapter has been published in: I. Haque and M. R. Singh, *J. Phys.: Condens. Matter* **19**, 156229 (2007).

et al. [222] have carried out an extensive analysis of this system and found that the resulting spectrum has up to three peaks (dynamic splitting), which can be explained in terms of the dressed state formalism. They also found that the positions and relative intensities of the spectral components are affected strongly by the intensities of the pump fields and the detuning of the pump and probe fields.

The present chapter deals with the study of the ac Stark effect in a three-dimensional photonic crystal doped with an ensemble of five-level nanoparticles, which leads to several new phenomena with great potential for applications. The crystal is taken to possess isotropic geometry and the nanoparticles in the doped ensemble are considered to be identical and non-interacting. However, these particles are assumed to interact with the photonic crystal, which plays the role of a reservoir.

First, we provide a brief description of the fundamental mechanism behind the ac Stark effect. Then, we construct our theoretical framework based on two distinct configurations of five-level nanoparticles, driven by two strong pump fields and a weak probe field (see Fig. 5-1). Due to the interaction between the particles and the reservoir, the excited levels decay spontaneously to the lower levels.

Next, we calculate the expressions for the susceptibility associated with the probed transitions using the master equation method. Numerical simulations for the level populations and the imaginary part of the susceptibility are performed for a photonic crystal with a gap-midgap ratio of around 20%. It is found that, by manipulating the decay rate with resonance tuning, the nanoparticle can be switched between an inverted and a non-inverted state, with regards to the population of the ground level of the cascade.

Furthermore, the band structure of the photonic crystal is found to have a major influence on the ac Stark effect observed in the doped nanoparticles. In particular, the probed transition of a doped nanoparticle could be rendered transparent to any resonant radiation field i.e. the nanoparticle can be switched between an absorption and a non-absorption state, simply by manipulating the location of the resonance energy.

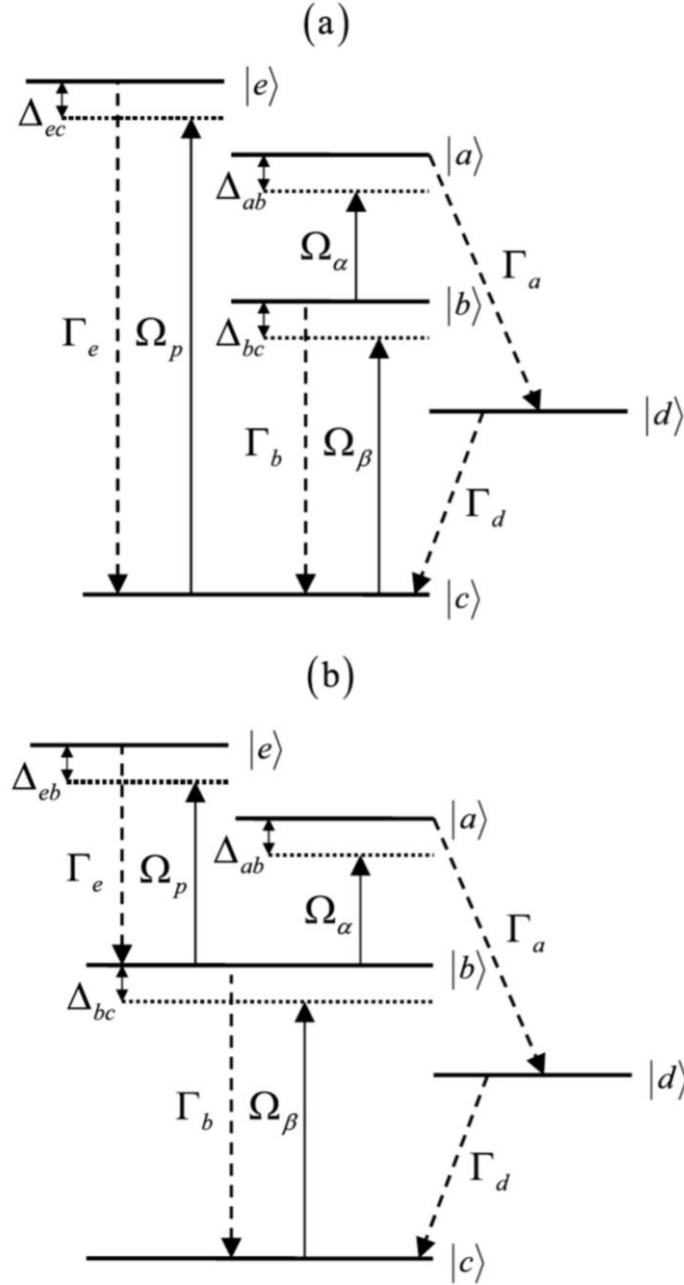


Figure 5-1: Schematic diagrams for the five-level atom, driven by two pump laser fields with Rabi frequencies  $\Omega_\alpha$  and  $\Omega_\beta$ . The levels are denoted as  $|a\rangle$ ,  $|b\rangle$ ,  $|c\rangle$ ,  $|d\rangle$  and  $|e\rangle$ . The probe field with Rabi frequency  $\Omega_p$  drives the (a)  $|c\rangle \rightarrow |e\rangle$  or (b)  $|b\rangle \rightarrow |e\rangle$  transition. The detuning of the two pump fields and the probe field are denoted as  $\Delta_{ab}$ ,  $\Delta_{bc}$  and (a)  $\Delta_{ec}$  or (b)  $\Delta_{eb}$ , respectively. The dashed arrows represent the decay channels and  $\Gamma_i$  denotes the decay rate of level  $|i\rangle$ .

Finally, we briefly discuss the distinct features of the work presented in this chapter in comparison to other studies of transparency and splitting of energy levels in doped photonic crystals found in the literature and address its potential for applications. The findings of our calculations indicate that it is possible to switch between an absorption state and a non-absorption state of a nanoparticle doped within a photonic crystal reservoir, by controlling the resonance energy. This provides a new technique of rendering material systems transparent to resonant laser radiation, which is very desirable in the fabrication of novel optical and photonic devices.

## 5.2 The ac Stark Effect

This section provides some brief background information on the ac Stark effect and describes the basic mechanism behind this particular phenomenon.

The shifting and splitting of atomic energy levels in a static electric field is known as the dc Stark effect, discovered by Johannes Stark in 1913 [160]. In 1955, Autler and Townes [158] proposed a theory of the Stark effect in rapidly varying fields. In the 1960s, the advent of lasers initiated extensive work on the shifting and splitting effects of atomic energy levels subject to variable electromagnetic fields. When the shifting and splitting of levels occur due to a variable monochromatic electric field, the phenomenon is known as the ac Stark effect (also known as Autler–Townes (A–T) splitting) [160].

The mechanism behind the ac Stark effect is best understood in the *dressed-state formalism* [275]. We consider the simplest case of a two-level nanoparticle and denote the ground and excited levels as  $|g\rangle$  and  $|e\rangle$ , respectively. In the presence of a radiation field consisting of a single mode, the *bare state* of this system is characterized by a photon number and the state of the nanoparticle, which can be either in its ground or excited state (see Fig. 5-2). This leads to the formation of a degenerate pair of states  $|g, N\rangle$  and  $|e, N-1\rangle$ , where  $N$  and  $N-1$  are photon numbers. By adding an extra photon, we get another pair of degenerate states – namely,  $|g, N+1\rangle$  and  $|e, N\rangle$ . Each pair of these degenerate states leads to the formation of a pair of *dressed states*, as shown

in Fig. 5-2. Therefore, four transitions are now allowed between the dressed states, indicated by the dashed, solid and dash-dotted arrows.

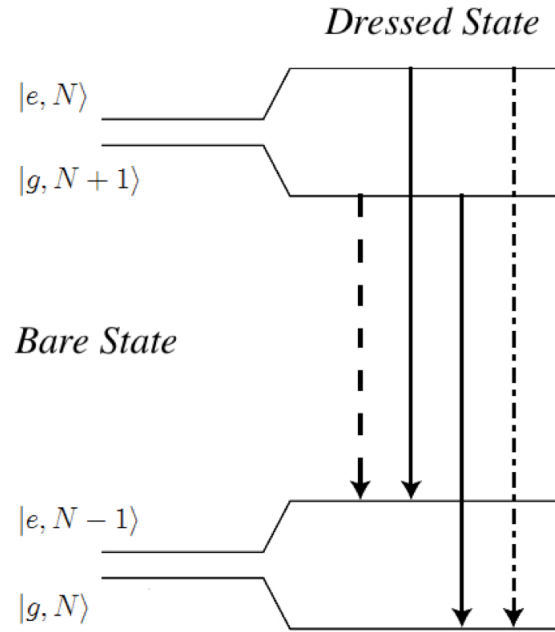


Figure 5-2: Schematic representation of the two-level nanoparticle, with ground level  $|g\rangle$  and excited level  $|e\rangle$ , showing the bare and dressed states. The dashed, solid and dash-dotted arrows indicate transitions between the dressed states.

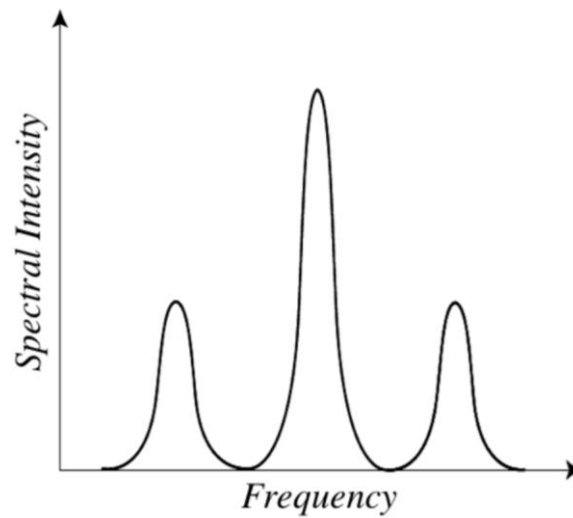


Figure 5-3: Plot of the spectral intensity against the frequency, obtained by application of the probe beam, showing the Mollow triplet.



The splitting effect described above can be monitored via obtaining a spectral profile produced by the application of a probe field connecting the ground level to an additional (third) level. This is shown in Fig. 5-3. From Fig. 5-2, it can be seen that the two transitions indicated by the solid arrows are degenerate. Therefore, the spectral signature consists of three peaks, known as the Mollow triplet [276].

In Fig. 5-3, the left and right side-peaks correspond to the transitions represented by the dashed and dash-dotted arrows, respectively, in Fig. 5-2. Note that the central peak is more intense as it originates from two transitions [277], as indicated by the two solid arrows in the figure.

### 5.3 Formulation of Susceptibility

This section describes the theoretical framework of our investigations and details our calculations of the susceptibility for both nanoparticle schemes.

The photonic crystal is considered to be doped with an ensemble of identical, non-interacting five-level nanoparticles. The crystal structure consists of a three-dimensional isotropic arrangement of dielectric spheres of radius  $a$ . The refractive index of the dielectric material  $n = 1.4$ . The lattice constant of the crystal  $L = 300$  nm and the ratio  $a/L = 0.2$ . The band structure equation for this particular type of photonic crystal has been calculated [18, 19] and is given by Eqn. (2.3) in Chapter 2. The energy dispersion relation given by this equation is plotted in Fig. 5-4 (top panel).

For the given crystal parameters, the gap energy corresponds to the near infrared and the optical regions of the electromagnetic spectrum. Photonic crystals are commonly characterized by their gap-midgap ratio, which is defined as  $2(\varepsilon_c - \varepsilon_v)/(\varepsilon_c + \varepsilon_v)$ . For this particular crystal, this ratio is around 20%. The parameters have been chosen to emulate the gap-midgap ratio obtained in Yablonovite crystals [4]. It is important to emphasize that the findings in the present chapter are independent of the choice of the photonic crystal.

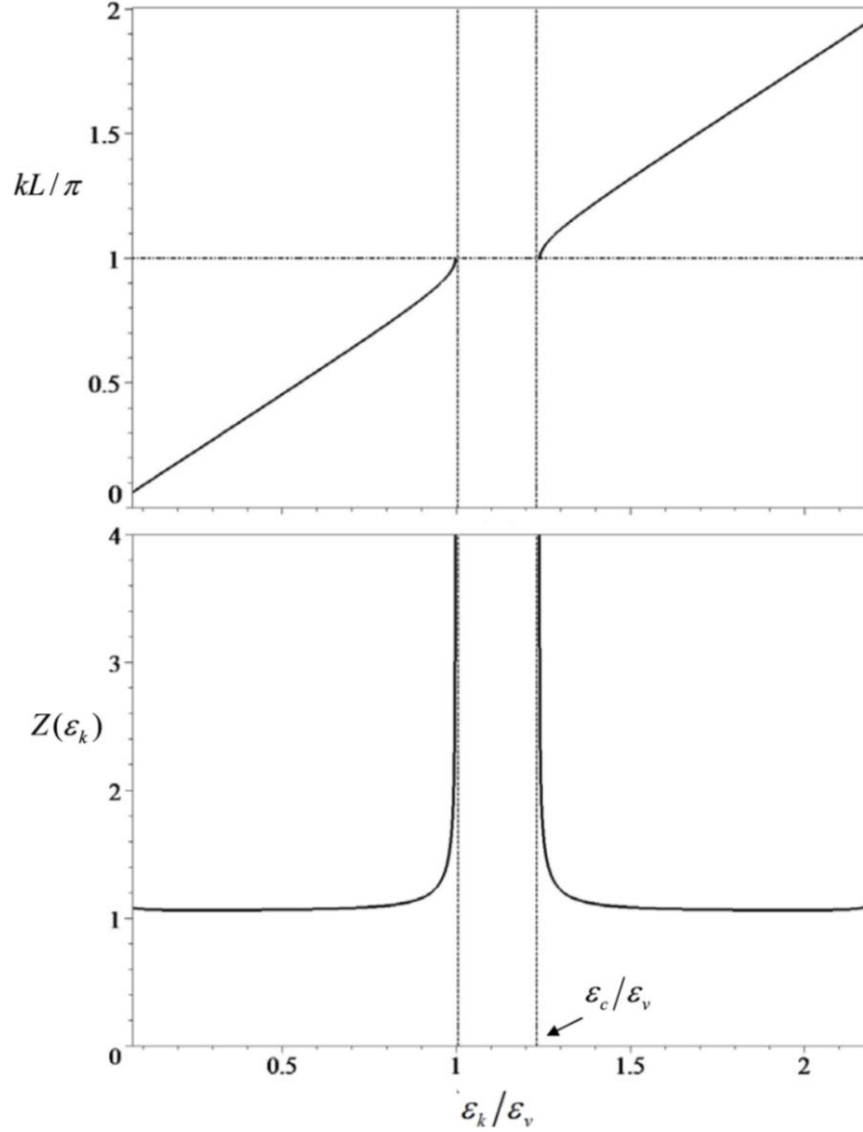


Figure 5-4: Plots of the dispersion relation (top panel) and the form factor  $Z(\varepsilon_k)$  (bottom panel) of the photonic crystal with  $n=1.4$ ,  $a/L=0.2$  and  $L=300$  nm, where  $k$  denotes the wave vector. The quantities  $\varepsilon_v$  and  $\varepsilon_c$  are the maximum energy of the valence band and the minimum energy of the conduction band, respectively. The horizontal axis is the ratio of the energy  $\varepsilon_k$  to the maximum valence band energy  $\varepsilon_v$ . The band gap of the crystal lies between  $\varepsilon_k/\varepsilon_v=1$  and  $\varepsilon_c/\varepsilon_v$ , shown by the vertical dashed lines.

The energy levels of a nanoparticle in the doped ensemble are denoted by  $|a\rangle$ ,  $|b\rangle$ ,  $|c\rangle$ ,  $|d\rangle$  and  $|e\rangle$ . The quantities  $\varepsilon_{ab}$ ,  $\varepsilon_{bc}$  and  $\varepsilon_{ec}$  (or  $\varepsilon_{eb}$ ) are the transition energies

corresponding to the  $|b\rangle \rightarrow |a\rangle$ ,  $|c\rangle \rightarrow |b\rangle$  and  $|c\rangle \rightarrow |e\rangle$  (or  $|b\rangle \rightarrow |e\rangle$ ) transitions, respectively (see Fig. 5-1). The energy difference between levels  $|a\rangle$  and  $|d\rangle$  is denoted as  $\varepsilon_{ad}$ . For our calculations and numerical simulations, it is considered that the transition energies  $\varepsilon_{ab}$ ,  $\varepsilon_{bc}$  and  $\varepsilon_{ec}$  (or  $\varepsilon_{eb}$ ) lie in a region away from the band gap of the photonic crystal, where its density of states is constant and does not influence the coupling of the laser fields with the doped nanoparticles.

We consider that the nanoparticles in the ensemble interact with the photonic crystal reservoir. Due to this interaction, level  $|a\rangle$  decays to level  $|d\rangle$  and levels  $|b\rangle$  and  $|d\rangle$  decay to level  $|c\rangle$ . Level  $|e\rangle$  decays to level  $|c\rangle$  (in Fig. 5-1(a)) or level  $|b\rangle$  (in Fig. 5-1(b)). It is important to note that the arrangement described above is similar to the experimental double resonance scheme used in Reference [278], with the exception that the present configuration has an extra level  $|e\rangle$  which is used to study the absorption spectrum.

The pair of excited levels  $|a\rangle$  and  $|b\rangle$  and the ground level  $|c\rangle$  are taken in  $\Xi$  configuration, as shown in Fig. 5-1. The transition  $|b\rangle \rightarrow |a\rangle$  is driven by a strong pump laser field of energy  $\varepsilon_\alpha$  and Rabi frequency  $\Omega_\alpha$ . Similarly, the transition  $|c\rangle \rightarrow |b\rangle$  is driven by a second strong pump laser field of energy  $\varepsilon_\beta$  and Rabi frequency  $\Omega_\beta$ . A weak tunable probe field of energy  $\varepsilon_p$  and electric field amplitude  $E_p$  is applied between the ground level  $|c\rangle$  (or the middle level  $|b\rangle$ ) and another excited level  $|e\rangle$ , as seen in Fig. 5-1(a) (or Fig. 5-1(b)). This weak field facilitates the study of the absorption spectrum of the nanoparticle. Other transitions are dipole forbidden.

It is important to note that this type of atomic configuration has been previously used in Reference [222]. A significant difference is that our model has a fifth level  $|d\rangle$  which acts as the base level in the decay channel originating from the excited level  $|a\rangle$ . The

addition of this extra level produces very interesting results which are used to propose new switching techniques. These are discussed in the next section.

The Hamiltonian of the system, for the configuration in Fig. 5-1(a), is written in energy space as (discussed in Appendix B):

$$H = H_A + H_R + V_{A-F} + V_{A-R} \quad (5.1)$$

where (discussed in Appendix I)

$$H_A = \varepsilon_a \sigma_{aa} + \varepsilon_b \sigma_{bb} + \varepsilon_c \sigma_{cc} + \varepsilon_d \sigma_{dd} + \varepsilon_e \sigma_{ee} \quad (5.2)$$

is the Hamiltonian of the five-level nanoparticle,

$$H_R = \int_C \frac{d\varepsilon_k}{2\pi} \varepsilon_k p^\dagger(\varepsilon_k) p(\varepsilon_k) \quad (5.3)$$

is the Hamiltonian of the crystal reservoir,

$$V_{A-F} = -(\hbar/2) \left( \Omega_\alpha \sigma_{ab}^+ e^{-i(\varepsilon_\alpha - \varepsilon_{ab})t/\hbar} + \Omega_\beta \sigma_{bc}^+ e^{-i(\varepsilon_\beta - \varepsilon_{bc})t/\hbar} + \Omega_p \sigma_{ec}^+ e^{-i(\varepsilon_p - \varepsilon_{ec})t/\hbar} \right) + h.c. \quad (5.4)$$

represents the nanoparticle-field interactions, and

$$\begin{aligned} V_{A-R} = & - \int_C \frac{d\varepsilon_k}{2\pi} \sqrt{\gamma_0} Z(\varepsilon_k) p(\varepsilon_k) \sigma_{ad}^+ e^{-i(\varepsilon_k - \varepsilon_{ad})t/\hbar} \\ & - \sum_{i=b,d} \int_C \frac{d\varepsilon_{k'}}{2\pi} \sqrt{\gamma_0} Z(\varepsilon_{k'}) p(\varepsilon_{k'}) \sigma_{ic}^+ e^{-i(\varepsilon_{k'} - \varepsilon_{ic})t/\hbar} \\ & - \int_C \frac{d\varepsilon_{k''}}{2\pi} \sqrt{\gamma_0} Z(\varepsilon_{k''}) p(\varepsilon_{k''}) \sigma_{ec}^+ e^{-i(\varepsilon_{k''} - \varepsilon_{ec})t/\hbar} + h.c. \end{aligned} \quad (5.5)$$

denotes the nanoparticle-reservoir interaction.

In the above equations,  $\varepsilon_i$  denotes the energy of level  $|i\rangle$  and  $\varepsilon_{ij} = \varepsilon_i - \varepsilon_j$ . Also,

$\sigma_{ii} = |i\rangle\langle i|$  and  $\sigma_{ij}^+ = |i\rangle\langle j|$ , where  $|i\rangle$  and  $|j\rangle$  denote levels  $|a\rangle$ ,  $|b\rangle$ ,  $|c\rangle$ ,  $|d\rangle$  and  $|e\rangle$ .

The interaction Hamiltonians  $V_{A-F}$  and  $V_{A-R}$  given in Eqn. (5.4) and Eqn. (5.5), respectively, are obtained under the electric dipole and rotating wave approximations [18, 19]. The  $p(\varepsilon_k)$  and  $p^\dagger(\varepsilon_k)$  operators denote the annihilation and creation of photons, respectively, where  $\varepsilon_k$  is the photon energy seen in Eqn. (2.3) in Chapter 2. The

integration contour  $C$  consists of two intervals:  $-\infty < \varepsilon_k \leq \varepsilon_v$  and  $\varepsilon_c \leq \varepsilon_k < \infty$ . The quantity  $\gamma_0$  is the vacuum decay rate, as defined in References [22–24]. All frequencies discussed in this chapter are measured with respect to  $\gamma_0$ .

Note that the Hamiltonian for the nanoparticle in Fig. 5-1(b) can be written as in Eqns. (5.1–5.5) with  $\sigma_{ec}^+$  in Eqns. (5.4, 5.5) replaced by  $\sigma_{eb}^+$ .

$Z(\varepsilon_k)$  is the form factor which is derived from Eqn. (2.3) and is written as [20–21] (discussed in Appendix G):

$$Z(\varepsilon_k) = \frac{\left[4n(a/L)(1+n)^2 \sin(4na\varepsilon_k / ch)\right]^{1/2}}{\left[16n^2 - \left[(1+n)^2 \cos(4na\varepsilon_k / ch) - (1-n)^2\right]^2\right]^{1/4}} \quad (5.6)$$

Note that the form factor, plotted in the bottom panel of Fig. 5-4, depends on the refractive index  $n$  and the ratio  $a/L$ . Also of note is the fact that it has a constant value of almost unity when  $\varepsilon_k$  is away from the band gap; it has a very large value when  $\varepsilon_k$  lies near either of the band edges.

The form factor in Fig. 5-4 has the same overall shape and characterizes the same behavior as that shown in Fig. 2-6 in Chapter 2. More specifically, it reflects the band structure of the photonic crystal through its asymptotic nature near the edges of the band gap and has a value close to unity away from the gap region. Any difference in the visual appearances of the two form factors is entirely due to the different sets of parameters used for the respective plots.

It is important to emphasize that, in the present chapter, we have considered an isotropic photonic crystal. The difference between an isotropic and an anisotropic crystal is that the former has a band gap which is identical in all directions, whereas the latter's band gap is direction-dependent. The band structure of an anisotropic photonic crystal, as seen from the point of view of a doped particle, varies with its location.

The form factor given in Eqn. (5.6) depends on the density of states which is determined by the energy gap of the crystal. As a result, the form factor for an anisotropic crystal has anisotropic values in different crystal directions. The predictions made in the present chapter using the band structure of an isotropic crystal are valid for all types of photonic crystals which have energy gaps in their dispersion relations.

As stated before, the primary aim of this section is to obtain an expression for the susceptibility due to the weak probe field. For the case of the nanoparticle in Fig. 5-1(a), the susceptibility can be written as [84]:

$$\chi_1 = \frac{2\mu_{ec}\rho_{ec}}{\epsilon_0 E_p} \quad (5.7)$$

where  $\rho_{ij}$  and  $\mu_{ij}$  denote the elements of the density matrix and the dipole operator associated with the transition  $|j\rangle \rightarrow |i\rangle$ , respectively, and  $\epsilon_0$  is the dielectric constant of the medium. The density matrix elements can be calculated using the master equation method.

The system is prepared in such a way that initially the nanoparticles are in ground level  $|c\rangle$ . As the pump fields are switched on, the excited levels become populated. Using Eqns. (5.1–5.5) and following the method used in References [70, 84, 222, 273, and 279], the equations of motion for the density matrix elements can be written as follows:

$$\rho_{aa} = -\Gamma_a \rho_{aa} - i\Omega_\alpha (\rho_{ab} - \rho_{ba}) / 2 \quad (5.8a)$$

$$\rho_{bb} = -\Gamma_b \rho_{bb} + i[\Omega_\alpha (\rho_{ab} - \rho_{ba}) - \Omega_\beta (\rho_{bc} - \rho_{cb})] / 2 \quad (5.8b)$$

$$\rho_{cc} = \Gamma_b \rho_{bb} + \Gamma_d \rho_{dd} + \Gamma_e \rho_{ee} + i[\Omega_\beta (\rho_{bc} - \rho_{cb}) + \Omega_p (\rho_{ec} - \rho_{ce})] / 2 \quad (5.8c)$$

$$\rho_{dd} = \Gamma_a \rho_{aa} - \Gamma_d \rho_{dd} \quad (5.8d)$$

$$\rho_{ee} = -\Gamma_e \rho_{ee} - i\Omega_p (\rho_{ec} - \rho_{ce}) / 2 \quad (5.8e)$$

$$\rho_{ab} = [i\Delta_{ab} - \Gamma_{ab}] \rho_{ab} - i[\Omega_\alpha (\rho_{aa} - \rho_{bb}) + \Omega_\beta \rho_{ac}] / 2 \quad (5.8f)$$

$$\rho_{ac} = [i(\Delta_{ab} + \Delta_{bc}) - \Gamma_a / 2] \rho_{ac} + i[\Omega_\alpha \rho_{bc} - \Omega_\beta \rho_{ab} - \Omega_p \rho_{ae}] / 2 \quad (5.8g)$$

$$\rho_{ad} = [i(\Delta_{ab} + \Delta_{bc}) - \Gamma_{ad}] \rho_{ad} + i\Omega_\alpha \rho_{bd} / 2 \quad (5.8h)$$

$$\rho_{bc} = [i\Delta_{bc} - \Gamma_b / 2] \rho_{bc} + i[\Omega_\alpha \rho_{ac} - \Omega_\beta (\rho_{bb} - \rho_{cc}) + \Omega_p \rho_{be}] / 2 \quad (5.8i)$$

$$\rho_{bd} = [i\Delta_{bc} - \Gamma_{bd}] \rho_{bd} + i[\Omega_\alpha \rho_{ad} + \Omega_\beta \rho_{cd}] / 2 \quad (5.8j)$$

$$\rho_{dc} = -\Gamma_d \rho_{dc} / 2 - i [\Omega_\beta \rho_{db} + \Omega_p \rho_{de}] / 2 \quad (5.8k)$$

$$\rho_{ea} = [i(\Delta_{ec} - \Delta_{ab} - \Delta_{bc}) - \Gamma_{ae}] \rho_{ea} - i [\Omega_\alpha \rho_{eb} - \Omega_p \rho_{ca}] / 2 \quad (5.8l)$$

$$\rho_{eb} = [i(\Delta_{ec} - \Delta_{bc}) - \Gamma_{be}] \rho_{eb} - i [\Omega_\alpha \rho_{ea} + \Omega_\beta \rho_{ec} - \Omega_p \rho_{cb}] / 2 \quad (5.8m)$$

$$\rho_{ec} = [i\Delta_{ec} - \Gamma_e / 2] \rho_{ec} - i [\Omega_\beta \rho_{eb} - \Omega_p (\rho_{cc} - \rho_{ee})] / 2 \quad (5.8n)$$

$$\rho_{ed} = [i\Delta_{ec} - \Gamma_{de}] \rho_{ed} + i\Omega_p \rho_{cd} / 2 \quad (5.8o)$$

where

$$\Gamma_{ij} = (\Gamma_i + \Gamma_j) / 2$$

and the Rabi frequency

$$\Omega_p = \mu_{ec} E_p / \hbar$$

The real detuning terms appearing in the differential equations in Eqn. (5.8) are given by:

$$\Delta_{ab} = (\varepsilon_\alpha - \varepsilon_{ab}) / \hbar$$

$$\Delta_{bc} = (\varepsilon_\beta - \varepsilon_{bc}) / \hbar$$

$$\Delta_{ec} = (\varepsilon_p - \varepsilon_{ec}) / \hbar$$

The  $\Gamma_i$  terms in the density matrix equations are the reservoir-mediated decay rates.

These are obtained, assuming that the resonance energies lie within the bands of the photonic crystal ( $\Gamma_i = 0$  otherwise), as follows [22–24]:

$$\Gamma_a = \gamma_0 Z(\varepsilon_{ad})^2 \quad (5.9a)$$

$$\Gamma_b = \gamma_0 Z(\varepsilon_{bc})^2 \quad (5.9b)$$

$$\Gamma_d = \gamma_0 Z(\varepsilon_{dc})^2 \quad (5.10a)$$

$$\Gamma_e = \gamma_0 Z(\varepsilon_{ec})^2 \quad (5.10b)$$

The density matrix element  $\rho_{ec}$  has been calculated, under the steady state approximation in the first order of the Rabi frequency  $\Omega_p$ , using the method in Reference [222]. The calculation includes all orders of the pump field Rabi frequencies  $\Omega_\alpha$  and  $\Omega_\beta$ . The susceptibility, which is a complex quantity, is written as

$$\chi_1 = \chi_1' + i\chi_1''$$

with  $\chi_1'$  and  $\chi_1''$  denoting the real and imaginary parts, respectively. The real part of the susceptibility corresponds to the refractive index of the material. The imaginary part corresponds to the absorption coefficient.

Using the definition in Eqn. (5.7),  $\chi_1'$  and  $\chi_1''$  can be expressed as follows:

$$\chi_1' = \frac{\chi_0 (G_1' H_1' + G_1'' H_1'')}{(H_1')^2 + (H_1'')^2} \quad (5.11a)$$

$$\chi_1'' = \frac{\chi_0 (G_1'' H_1' - G_1' H_1'')}{(H_1')^2 + (H_1'')^2} \quad (5.11b)$$

where

$$\chi_0 = \mu_{ec}^2 / (\epsilon_0 \hbar \gamma_0)$$

The terms  $G_1'$ ,  $G_1''$ ,  $H_1'$ , and  $H_1''$  appearing in Eqn. (5.11) are real-valued and are given by:

$$G_1' = -\Omega_\beta (\Delta_{ea} P_{cb}' + \Gamma_{ae} P_{cb}'' + \Omega_\alpha P_{ca}'' / 2) / 2 - \rho_{cc}^{(0)} (\Gamma_{be} \Delta_{ea} + \Gamma_{ae} \Delta_{eb}) \quad (5.12a)$$

$$G_1'' = \Omega_\beta (\Delta_{ea} P_{cb}'' - \Gamma_{ae} P_{cb}' + \Omega_\alpha P_{ca}' / 2) / 2 - \rho_{cc}^{(0)} (\Gamma_{ae} \Gamma_{be} + \Omega_\alpha^2 / 4 - \Delta_{ea} \Delta_{eb}) \quad (5.12b)$$

$$H_1' = \Delta_{ec} (\Gamma_{be} \Delta_{ea} + \Gamma_{ae} \Delta_{eb}) - \Gamma_e (\Gamma_{ae} \Gamma_{be} - \Delta_{ea} \Delta_{eb}) / 2 - (\Gamma_{ae} \Omega_\beta^2 + 2\Gamma_e \Omega_\alpha^2) / 4 \quad (5.12c)$$

$$H_1'' = \Delta_{ec} (\Gamma_{ae} \Gamma_{be} - \Delta_{ea} \Delta_{eb}) + \Gamma_e (\Gamma_{be} \Delta_{ea} + \Gamma_{ae} \Delta_{eb}) / 2 + (\Delta_{ea} \Omega_\beta^2 + 2\Gamma_e \Omega_\alpha^2) / 4 \quad (5.12d)$$

where the detuning terms are defined as:

$$\Delta_{ea} = \Delta_{ec} - \Delta_{ab} - \Delta_{bc}$$

$$\Delta_{eb} = \Delta_{ec} - \Delta_{bc}$$

The  $P_{cb}'$ ,  $P_{cb}''$ ,  $P_{ca}'$  and  $P_{ca}''$  terms in Eqns. (5.12a, 5.12b) have been derived as follows:

$$P_{cb}' = X_{cb}' \rho_{bb}^{(0)} + Y_{cb}' \rho_{aa}^{(0)} + S_{cb}' \rho_{dd}^{(0)} + Z_{cb}' \quad (5.13a)$$

$$P_{cb}'' = X_{cb}'' \rho_{bb}^{(0)} + Y_{cb}'' \rho_{aa}^{(0)} + S_{cb}'' \rho_{dd}^{(0)} + Z_{cb}'' \quad (5.13b)$$

$$P_{ca}' = X_{ca}' \rho_{bb}^{(0)} + Y_{ca}' \rho_{aa}^{(0)} + S_{ca}' \rho_{dd}^{(0)} + Z_{ca}' \quad (5.13c)$$

$$P_{ca}'' = X_{ca}'' \rho_{bb}^{(0)} + Y_{ca}'' \rho_{aa}^{(0)} + S_{ca}'' \rho_{dd}^{(0)} + Z_{ca}'' \quad (5.13d)$$

where the zeroth-order density matrix elements  $\rho_{aa}^{(0)}$ ,  $\rho_{bb}^{(0)}$  and  $\rho_{dd}^{(0)}$  appearing in Eqns.

(5.12, 5.13) are written as:



$$\rho_{aa}^{(0)} = \Omega_\alpha^2 (X_{aa}\rho_{bb}^{(0)} + Z_{aa}) / 2 \quad (5.14a)$$

$$\rho_{dd}^{(0)} = [\Gamma_a \Omega_\alpha^2 (X_{aa}\rho_{bb}^{(0)} + Z_{aa})] / 2\Gamma_d \quad (5.14b)$$

$$\rho_{bb}^{(0)} = \frac{\Omega_\alpha^2 Z_{aa} \zeta / 2 + \Omega_\beta^2 \Gamma_d \Re(Z_{bc}) / 2}{\Gamma_d [\Gamma_b - \Omega_\beta^2 \Re(X_{bc}) / 2] - \Omega_\alpha^2 X_{aa} \zeta / 2} \quad (5.14c)$$

with

$$X_{aa} = \frac{\Gamma_d X'_{ab}}{\Gamma_d \Gamma_a - \Omega_\alpha^2 [\Gamma_d Y'_{ab} + \Gamma_a S'_{ab}] / 2} \quad (5.15a)$$

$$Z_{aa} = \frac{\Gamma_d Z'_{ab}}{\Gamma_d \Gamma_a - \Omega_\alpha^2 [\Gamma_d Y'_{ab} + \Gamma_a S'_{ab}] / 2} \quad (5.15b)$$

$$\zeta = \Omega_\beta^2 (\Gamma_d \Re(Y_{bc}) + \Gamma_a \Re(S_{bc})) / 2 - \Gamma_a \quad (5.15c)$$

The density matrix element  $\rho_{cc}^{(0)}$  is obtained from:

$$\rho_{cc}^{(0)} = 1 - \rho_{aa}^{(0)} - \rho_{bb}^{(0)} - \rho_{dd}^{(0)}$$

The complex-valued terms  $X_{ij} = X'_{ij} + iX''_{ij}$ ,  $Y_{ij} = Y'_{ij} + iY''_{ij}$ ,  $Z_{ij} = Z'_{ij} + iZ''_{ij}$  and  $S_{ij} = S'_{ij} + iS''_{ij}$

appearing in Eqns. (5.13, 5.14, and 5.15) are derived as:

$$X_{ab} = \frac{-d_{bc}d_{ac} + \Omega_\beta^2 / 2 - \Omega_\alpha^2 / 4}{D}$$

$$X_{ca} = \frac{2d_{ba} + d_{cb}}{D}$$

$$X_{cb} = \frac{2d_{ca}d_{ba} + \Omega_\beta^2 / 2 - \Omega_\alpha^2 / 4}{D}$$

$$Y_{ab} = \frac{d_{bc}d_{ac} + \Omega_\alpha^2 / 4 + \Omega_\beta^2 / 4}{D}$$

$$Y_{ca} = \frac{d_{ba} - d_{cb}}{D}$$

$$Y_{cb} = \frac{d_{ca}d_{ba} + \Omega_\alpha^2 / 4 + \Omega_\beta^2 / 4}{D}$$

$$Z_{ab} = -\frac{\Omega_\beta^2}{4D} = -S_{ab}$$

$$Z_{cb} = \frac{-d_{ca}d_{ba} + \Omega_\beta^2 / 4}{D} = -S_{cb}$$

$$Z_{ca} = -\frac{d_{ba}}{D} = -S_{ca}$$

with

$$D = d_{cb}d_{ba}d_{ca} + d_{ba}\Omega_\alpha^2/4 + d_{cb}\Omega_\beta^2/4 \quad (.)$$

where  $d_{ij} = i\Delta_{ij} - \Gamma_{ij}$ , which denotes the complex detuning of the laser field coupled to the transition  $|i\rangle \rightarrow |j\rangle$ .

Similar calculations have also been performed for the nanoparticle in Fig. 5-1(b), where the weak field probes the  $|b\rangle \rightarrow |e\rangle$  transition. The corresponding equations of motion of the density matrix elements are written as:

$$\rho_{aa} = -\Gamma_a \rho_{aa} - i\Omega_\alpha (\rho_{ab} - \rho_{ba}) / 2 \quad (5.16a)$$

$$\rho_{bb} = -\Gamma_b \rho_{bb} + \Gamma_e \rho_{ee} + i \left[ \frac{\Omega_\alpha (\rho_{ab} - \rho_{ba}) - \Omega_\beta (\rho_{bc} - \rho_{cb}) + \Omega_p (\rho_{eb} - \rho_{be})}{2} \right] \quad (5.16b)$$

$$\rho_{cc} = \Gamma_b \rho_{bb} + \Gamma_d \rho_{dd} + i\Omega_\beta (\rho_{bc} - \rho_{cb}) / 2 \quad (5.16c)$$

$$\rho_{dd} = \Gamma_a \rho_{aa} - \Gamma_d \rho_{dd} \quad (5.16d)$$

$$\rho_{ee} = -\Gamma_e \rho_{ee} - i\Omega_p (\rho_{eb} - \rho_{be}) / 2 \quad (5.16e)$$

$$\rho_{ab} = [i\Delta_{ab} - \Gamma_{ab}] \rho_{ab} - i [\Omega_\alpha (\rho_{aa} - \rho_{bb}) - \Omega_\beta \rho_{ac} - \Omega_p \rho_{ae}] / 2 \quad (5.16f)$$

$$\rho_{ac} = [i(\Delta_{ab} + \Delta_{bc}) - \Gamma_a / 2] \rho_{ac} + i [\Omega_\alpha \rho_{bc} - \Omega_\beta \rho_{ab}] / 2 \quad (5.16g)$$

$$\rho_{ad} = [i(\Delta_{ab} + \Delta_{bc}) - \Gamma_{ad}] \rho_{ad} + i\Omega_\alpha \rho_{bd} / 2 \quad (5.16h)$$

$$\rho_{bc} = [i\Delta_{bc} - \Gamma_b / 2] \rho_{bc} + i [\Omega_\alpha \rho_{ac} - \Omega_\beta (\rho_{bb} - \rho_{cc}) + \Omega_p \rho_{ec}] / 2 \quad (5.16i)$$

$$\rho_{bd} = [i\Delta_{bc} - \Gamma_{bd}] \rho_{bd} + i [\Omega_\alpha \rho_{ad} + \Omega_\beta \rho_{cd} + \Omega_p \rho_{ed}] / 2 \quad (5.16j)$$

$$\rho_{dc} = -\Gamma_d \rho_{dc} / 2 - i\Omega_\beta \rho_{db} / 2 \quad (5.16k)$$

$$\rho_{ea} = [i(\Delta_{eb} - \Delta_{ab}) - \Gamma_{ae}] \rho_{ea} - i [\Omega_\alpha \rho_{eb} + \Omega_p \rho_{ba}] / 2 \quad (5.16l)$$

$$\rho_{eb} = [i\Delta_{eb} - \Gamma_{be}] \rho_{eb} - i [\Omega_\alpha \rho_{ea} - \Omega_\beta \rho_{ec} - \Omega_p (\rho_{ee} - \rho_{bb})] / 2 \quad (5.16m)$$

$$\rho_{ec} = [i(\Delta_{eb} + \Delta_{bc}) - \Gamma_e / 2] \rho_{ec} - i [\Omega_\beta \rho_{eb} + \Omega_p \rho_{bc}] / 2 \quad (5.16o)$$

$$\rho_{ed} = [i(\Delta_{eb} + \Delta_{bc}) - \Gamma_{de}] \rho_{ed} + i\Omega_p \rho_{bd} / 2 \quad (5.16n)$$

where the decay rate

$$\Gamma_e = \gamma_0 Z(\mathcal{E}_{eb})^2$$

The modified probe field detuning is given by:

$$\Delta_{eb} = (\mathcal{E}_p - \mathcal{E}_{eb}) / \hbar$$

and the Rabi frequency

$$\Omega_p = \mu_{eb} E_p / 2\hbar$$

Apart from these exceptions, all other quantities are defined as for the previous nanoparticle configuration.

In this case, we can write the real and imaginary parts of the susceptibility as:

$$\chi_2' = \frac{\chi_0 (G_2' H_1' + G_2'' H_1'')}{(H_1')^2 + (H_1'')^2} \quad (5.17a)$$

$$\chi_2'' = \frac{\chi_0 (G_2'' H_1' - G_2' H_1'')}{(H_1')^2 + (H_1'')^2} \quad (5.17b)$$

where it has been assumed that  $\mu_{eb} = \mu_{ec}$ .

The real-valued terms  $G_2'$  and  $G_2''$  appearing in Eqn. (5.17) are given by:

$$G_2' = \Omega_\beta (\Delta_{ea} P_{cb}' - \Gamma_{ae} P_{cb}') / 2 - \Omega_\alpha (\Gamma_e P_{ab}' / 2 + \Delta_{ec} P_{ab}'') / 2 - \rho_{cc}^{(0)} (\Gamma_e \Delta_{ea} / 2 + \Gamma_{ae} \Delta_{ec}) \quad (5.18a)$$

$$G_2'' = \Omega_\beta (\Delta_{ea} P_{cb}' + \Gamma_{ae} P_{cb}'') / 2 + \Omega_\alpha (\Gamma_e P_{ab}' / 2 + \Delta_{ec} P_{ab}') / 2 - \rho_{cc}^{(0)} (\Gamma_e \Gamma_{ae} / 2 - \Delta_{ea} \Delta_{ec}) \quad (5.18b)$$

where

$$P_{ab}' = X_{ab}' \rho_{bb}^{(0)} + Y_{ab}' \rho_{aa}^{(0)} + S_{ab}' \rho_{dd}^{(0)} + Z_{ab}' \quad (5.19a)$$

$$P_{ab}'' = X_{ab}'' \rho_{bb}^{(0)} + Y_{ab}'' \rho_{aa}^{(0)} + S_{ab}'' \rho_{dd}^{(0)} + Z_{ab}'' \quad (5.19b)$$

The detuning terms in this case are calculated as:

$$\Delta_{ec} = \Delta_{eb} + \Delta_{bc}$$

$$\Delta_{ea} = \Delta_{eb} - \Delta_{ab}$$

The complex-valued terms  $X_{ab}$ ,  $Y_{ab}$ ,  $Z_{ab}$  and  $S_{ab}$  are identical to those in the case of the first nanoparticle scheme. The density matrix elements  $\rho_{aa}^{(0)}$ ,  $\rho_{bb}^{(0)}$ ,  $\rho_{cc}^{(0)}$  and  $\rho_{dd}^{(0)}$  appearing in Eqns. (5.18, 5.19) are also as defined earlier.

## 5.4 Results and Discussions

This section presents numerical simulations of the density matrix elements and the imaginary part of the susceptibility for the isotropic photonic crystal discussed in the previous section.

First, we calculate the time evolution of the level populations of the doped nanoparticles. Our primary aim is to study the effect of the band structure of the crystal reservoir on the population densities of the energy levels of the nanoparticles. The differential equations for the density matrix elements given in Eqn. (5.8) are solved numerically, using a Fehlberg fourth-fifth order Runge-Kutta method (discussed in Appendix J). As an initial condition, it is assumed that  $\rho_{cc}(0) = 1$  and all other levels are unpopulated.

The numerical solutions are obtained for the atomic scheme in Fig. 5-1(a) and are shown in Fig. 5-5. The two pump laser fields are considered to be resonant i.e.:

$$\Delta_{ab} / \gamma_0 = \Delta_{bc} / \gamma_0 = 0$$

and the detuning of the probe field  $\Delta_{ec} / \gamma_0 = 10$ . The Rabi frequencies of the pump and probe fields are taken as:  $\Omega_\alpha / \gamma_0 = \Omega_\beta / \gamma_0 = 2$  and  $\Omega_p / \gamma_0 = 0.2$ . The plots in Figs. (5-5(a)–5-5(d)) show the population densities  $\rho_{aa}$ ,  $\rho_{dd}$ ,  $\rho_{bb}$  and  $\rho_{cc}$ , respectively. The solid and dotted curves in these figures represent the cases where the resonance energy  $\varepsilon_{ad}$  is away from ( $\varepsilon_{ad} / \varepsilon_v = 80.00\%$ ) and close to ( $\varepsilon_{ad} / \varepsilon_v = 99.99\%$ ) the lower edge of the band gap of the photonic crystal, respectively.

After the laser fields are turned on, the population densities of the atomic levels exhibit Rabi oscillations. Eventually, the oscillations are observed to stabilize and the level populations reach steady state.

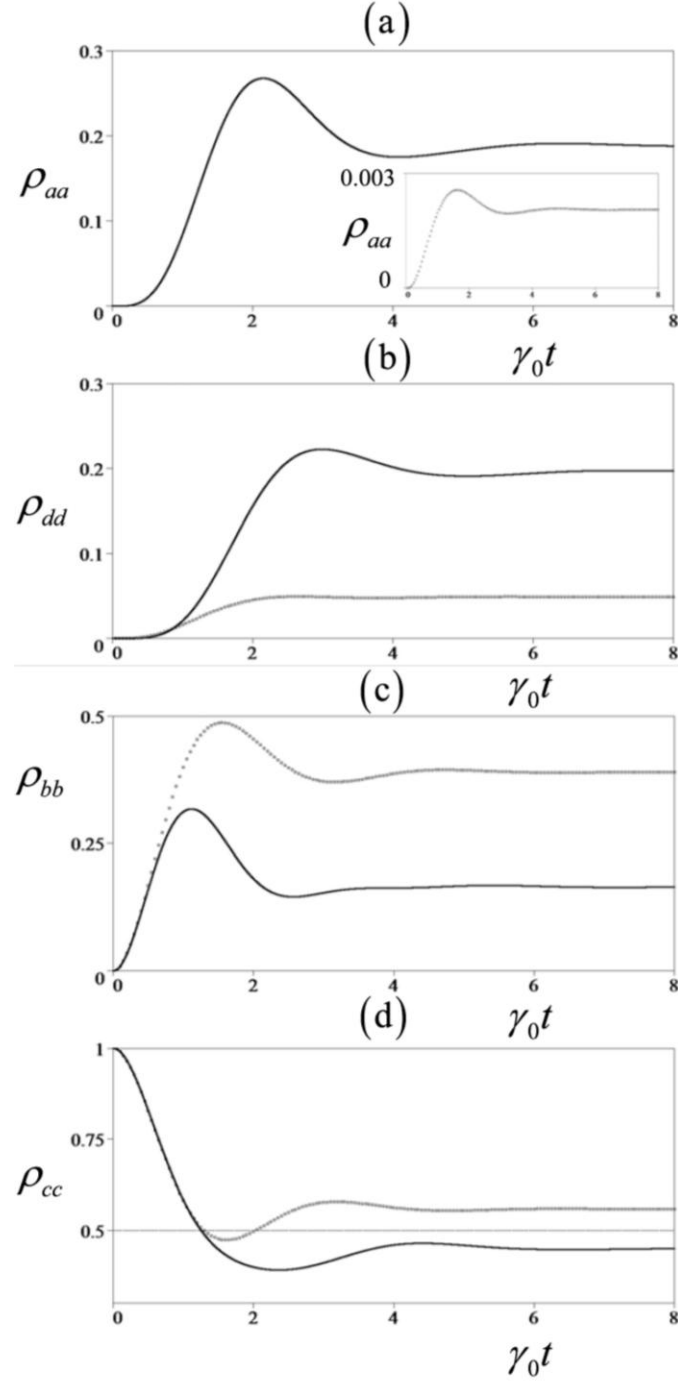


Figure 5-5: Numerical plots of the time evolution of the population densities (a)  $\rho_{aa}$  (b)  $\rho_{dd}$  (c)  $\rho_{bb}$  and (d)  $\rho_{cc}$  of the atom in Fig. 5-1(a). The horizontal axes show dimensionless time  $\gamma_0 t$ . The solid curves are drawn for the case where  $\varepsilon_{ad} / \varepsilon_v = 80.00\%$ . The dotted curves represent the case where  $\varepsilon_{ad} / \varepsilon_v = 99.99\%$ . All other resonance energies are kept far from either of the band edges.

It can be seen from the transient plots in Figs. (5-5(a), 5-5(b)) that the steady-state population densities  $\rho_{aa}$  and  $\rho_{dd}$  decrease as the resonance energy  $\varepsilon_{ad}$  approaches the lower band edge. On the other hand, as seen in the plots in Figs. (5-5(c), 5-5(d)), the population densities  $\rho_{bb}$  and  $\rho_{cc}$  have higher steady-state values, under the same scenario. The explanations behind these observations are given below.

With increasing proximity of the resonance energy  $\varepsilon_{ad}$  to the lower band edge, the decay rate  $\Gamma_a$  given in Eqn. (5.9a) becomes larger due to the growing value of the form factor (see Fig. 5-4). A larger value of  $\Gamma_a$  has the effect of depopulating level  $|a\rangle$  with increasing rapidity, as seen from Eqn. (5.8a). This, in turn, leads to a substantial decline in the steady state level population  $\rho_{aa}$ .

Using Eqn. (5.8d) and assuming steady-state conditions, the population density  $\rho_{dd}$  can be written as  $\rho_{dd} = (\Gamma_a \rho_{aa}) / \Gamma_d$ . This indicates that  $\rho_{dd}$  is directly proportional to both  $\Gamma_a$  and  $\rho_{aa}$ . Although the decay rate  $\Gamma_a$  increases as the resonance energy  $\varepsilon_{ad}$  approaches the lower band edge, the range of its values remains within the same order of magnitude. In contrast, for the same change in the resonance energy, the decrease in  $\rho_{aa}$  is over several orders of magnitude as it is proportional to an exponentially decaying function of  $\Gamma_a$ . Consequently,  $\rho_{dd}$  is observed to decrease.

The reason behind the increase in the steady-state population density  $\rho_{cc}$  is its dependence on  $\rho_{dd}$ , as seen from Eqn. (5.8c). Since level  $|d\rangle$  decays to level  $|c\rangle$ , a decrease in  $\rho_{dd}$  implies an increase in  $\rho_{cc}$ . Similarly, the steady-state population density  $\rho_{bb}$  is observed to increase as  $\varepsilon_{ad}$  approaches the band edge. This is due to the fact that an increase in the population in level  $|c\rangle$  means that more particles are pumped up to level  $|b\rangle$ , as seen from the last term in Eqn. (5.8b). It is worthwhile to note that this effect is also expected in the case of level  $|e\rangle$ , albeit to a much smaller degree (not plotted).

The most important result concerning the steady-state level populations is obtained from Fig. 5-5(d). It can be seen that, as  $\varepsilon_{ad}$  approaches the band edge, an inversion occurs in the population density of the ground level  $|c\rangle$ . Therefore, it is possible to switch the system from an inverted state to a non-inverted state (and vice versa), with respect to level populations, by manipulating the resonance energy between levels  $|a\rangle$  and  $|d\rangle$ . This is a very significant new finding of our theory, which can be used to make new types of photonic switches.

Fig. 5-6 shows the time evolution of  $\chi_1'' / \chi_0$  for the nanoparticle in Fig. 5-1(a), at resonance energies away (solid curve) and close (dotted curve) to the (lower) band edge. The curves are drawn using the same detuning parameters and probe field strength as in Fig. 5-5. The Rabi frequencies of the pump fields in this case are  $\Omega_\alpha / \gamma_0 = \Omega_\beta / \gamma_0 = 15$ . Due to the relatively large values of these frequencies, one can now see a greater number of oscillations. A similar set of values for these Rabi frequencies will be used later in our analyses of the system in the steady state.

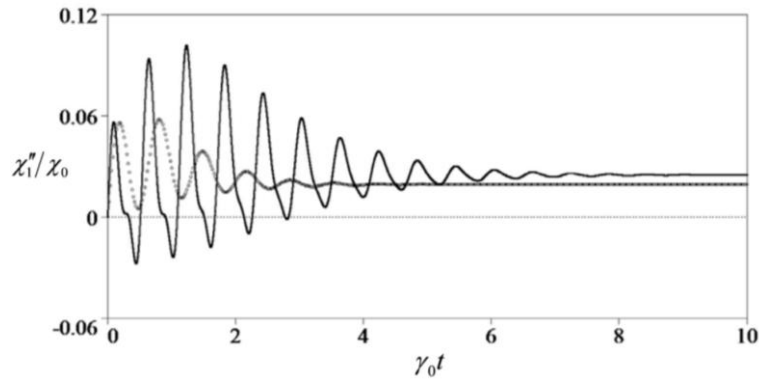


Figure 5-6: Numerical plots of the time evolution of  $\chi_1'' / \chi_0$  for  $\varepsilon_{ad} / \varepsilon_v = 80.00\%$  (solid curve) and  $\varepsilon_{ad} / \varepsilon_v = 99.99\%$  (dotted curve), using the atomic scheme in Fig. 5-1(a). All other resonance energies are kept away from either of the band edges at all times. The horizontal axis shows scaled time  $\gamma_0 t$ .

In Fig. 5-6, it is interesting to note that, as  $\varepsilon_{ad}$  approaches the band edge and the decay rate  $\Gamma_a$  increases,  $\chi_1'' / \chi_0$  reaches its steady-state value comparatively earlier and with fewer oscillations (see dotted curve). This can be understood by considering the fact that

$\chi_1'' / \chi_0$  depends on the level population  $\rho_{cc}$ , which attains steady state earlier for large values of  $\Gamma_a$  [see Eqn. (5.8n) and Fig. 5-5(d)].

Finally, with regards to the transient calculations presented above, it must be noted that similar results can also be obtained for the second atomic scheme given in Fig. 5-1(b).

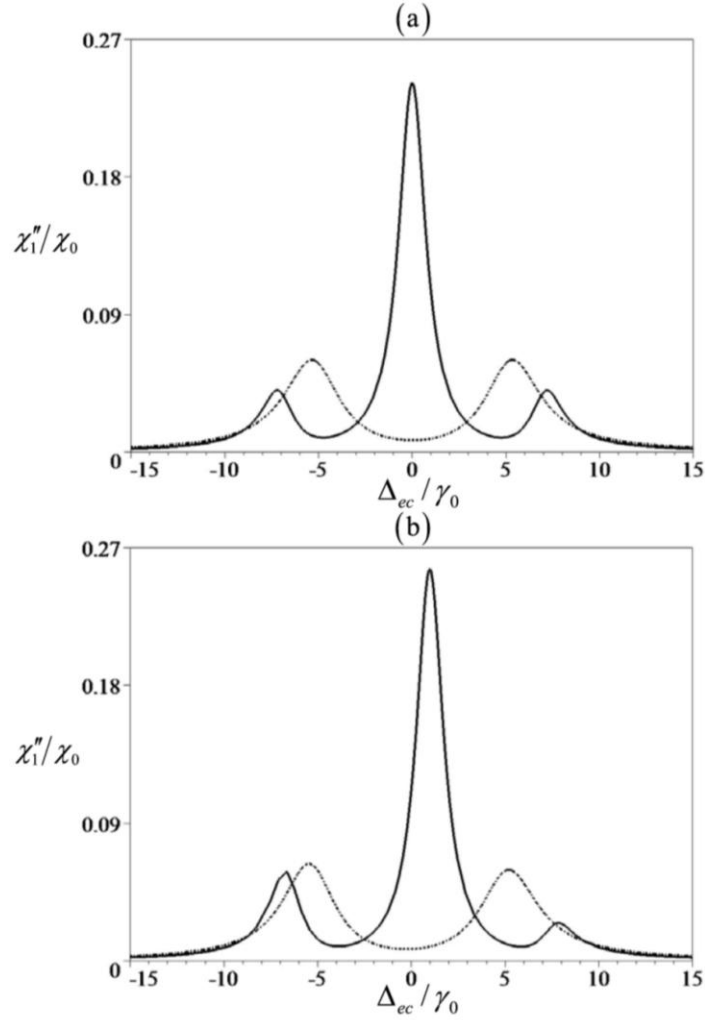


Figure 5-7: Plots of  $\chi_1'' / \chi_0$  against probe field detuning  $\Delta_{ec} / \gamma_0$  for the atom in Fig. 5-1 (a), in steady state. In (a)  $\Delta_{ab} / \gamma_0 = \Delta_{bc} / \gamma_0 = 0$  and in (b)  $\Delta_{ab} / \gamma_0 = 2$  and  $\Delta_{bc} / \gamma_0 = 0$ . The Rabi frequencies of the laser fields are taken as  $\Omega_\alpha / \gamma_0 = \Omega_\beta / \gamma_0 = 10$  and  $\Omega_p / \gamma_0 = 0.2$ . The solid curves are drawn for the case where all resonance energies are away from either of the band edges and  $\epsilon_{ad} / \epsilon_v = 80.00\%$ . The dash-dotted curves represent the case where  $\epsilon_{ad} / \epsilon_v = 99.99\%$  while all other energies remain far from the band edges.



Next, we present an analysis of the ac Stark effect in the doped nanoparticles and study how it is influenced by the band structure of the photonic crystal. The absorption profiles of the probe beams for the two atomic configurations in Fig. 5-1 have been calculated in Figs. (5-7, 5-8), using Eqns. (5.11b, 5.17b), respectively. The Rabi frequencies in this case are:  $\Omega_\alpha / \gamma_0 = \Omega_\beta / \gamma_0 = 10$  and  $\Omega_p / \gamma_0 = 0.2$ . The larger Rabi frequencies for the pump fields have been chosen to make the splitting effect more pronounced. For Figs. (5-7(a), 5-8(a)), the pump fields are considered to be resonant i.e.

$$\Delta_{ab} / \gamma_0 = \Delta_{bc} / \gamma_0 = 0$$

whereas in Figs. 5-7(b) and 5-8(b),  $\Delta_{ab} / \gamma_0 = 2$  and  $\Delta_{bc} / \gamma_0 = 0$ . These parameters are similar to those used in Reference [222].

As before, the solid and dash-dotted curves in Figs. (5-7, 5-8) correspond to the cases when  $\varepsilon_{ad} / \varepsilon_v = 80.00\%$  and  $\varepsilon_{ad} / \varepsilon_v = 99.99\%$ , respectively.

In Fig. 5-7, one can see that the absorption profiles represented by the two solid curves are each characterized by three peaks. This is an evidence of ac Stark splitting (dynamic Stark effect) in this system. The mechanism that gives rise to this effect is briefly explained below.

When  $\varepsilon_{ad}$  lies away from the band edge of the crystal, we have the condition where the decay rate  $\Gamma_a$  is small compared to the Rabi frequencies  $\Omega_\alpha$  and  $\Omega_\beta$ . In this situation, we get strong nanoparticle-field coupling and the dressed state of the system, which are in linear combinations of the states  $|a\rangle$ ,  $|b\rangle$  and  $|c\rangle$ , splits into three states. As a result, one can now observe three transitions from ground level  $|c\rangle$  to excited level  $|e\rangle$  (see solid curves in Fig. 5-7). This splitting of energy levels has also been clearly explained using the idea of dressed states in Reference [222], where similar results were obtained in atomic gases.

In both Figs. (5-7(a), 5-7(b)), as  $\varepsilon_{ad}$  approaches the band edge, the central peak disappears and the heights of the two side peaks increase (dash-dotted curves). In

addition, one can observe shifts in the locations of the side peaks. These are very interesting observations which have not been made previously in this system.

The disappearance of the central peak can be explained as follows. In the presence of strong pump field Rabi frequencies  $\Omega_\alpha$  and  $\Omega_\beta$ , the system has three dressed states, as mentioned before. Note that the three peaks in Fig. 5-7(a) are located at:

$$\begin{aligned}\Delta_{ec} / \gamma_0 &= -\frac{1}{2\gamma_0} \sqrt{\Omega_\alpha^2 + \Omega_\beta^2} \approx -7.07 \\ \Delta_{ec} / \gamma_0 &= 0 \\ \Delta_{ec} / \gamma_0 &= \frac{1}{2\gamma_0} \sqrt{\Omega_\alpha^2 + \Omega_\beta^2} \approx 7.07\end{aligned}$$

When the resonance energy lies near the band edge, we have  $\Gamma_a \geq \Omega_\alpha$  and the effect of  $\Omega_\alpha$  disappears. In other words, the effect of the pump field with Rabi frequency  $\Omega_\alpha$  is inhibited by the band structure of the photonic crystal. Now the system has two dressed states which are in linear combinations of states  $|b\rangle$  and  $|c\rangle$ . As a result, we get two transitions located at:

$$\begin{aligned}\Delta_{ec} / \gamma_0 &= -\Omega_\beta / (2\gamma_0) = -5 \\ \Delta_{ec} / \gamma_0 &= \Omega_\beta / (2\gamma_0) = 5\end{aligned}\tag{.}$$

Similar explanations are applicable to the dash-dotted curve in Fig. 5-7(b), except the locations and the relative heights of the peaks will be different owing to the non-zero detuning parameter  $\Delta_{ab} / \gamma_0$ .

In Fig. 5-8, we have plotted the imaginary part of the susceptibility for the atomic configuration in Fig. 5-1(b), where the probe field sweeps the  $|b\rangle \rightarrow |e\rangle$  transition. For Fig. 5-8(a), both the pump fields are considered to be resonant, whereas for Fig. 5-8(b), the pump field with Rabi frequency  $\Omega_\alpha$  has non-zero detuning. When  $\varepsilon_{ad}$  lies away from the band edge, one can see that the absorption profile seen in the solid curve in Fig. 5-8(a) is characterized by two strong peaks. In contrast, in Fig. 5-8(b), the solid curve has three peaks. However, as the resonance energy approaches the band edge of the crystal,

we observe two peaks for each of the plots in Fig. 5-8 (dash-dotted curves) and the locations of the peaks shift towards the zero detuning mark.

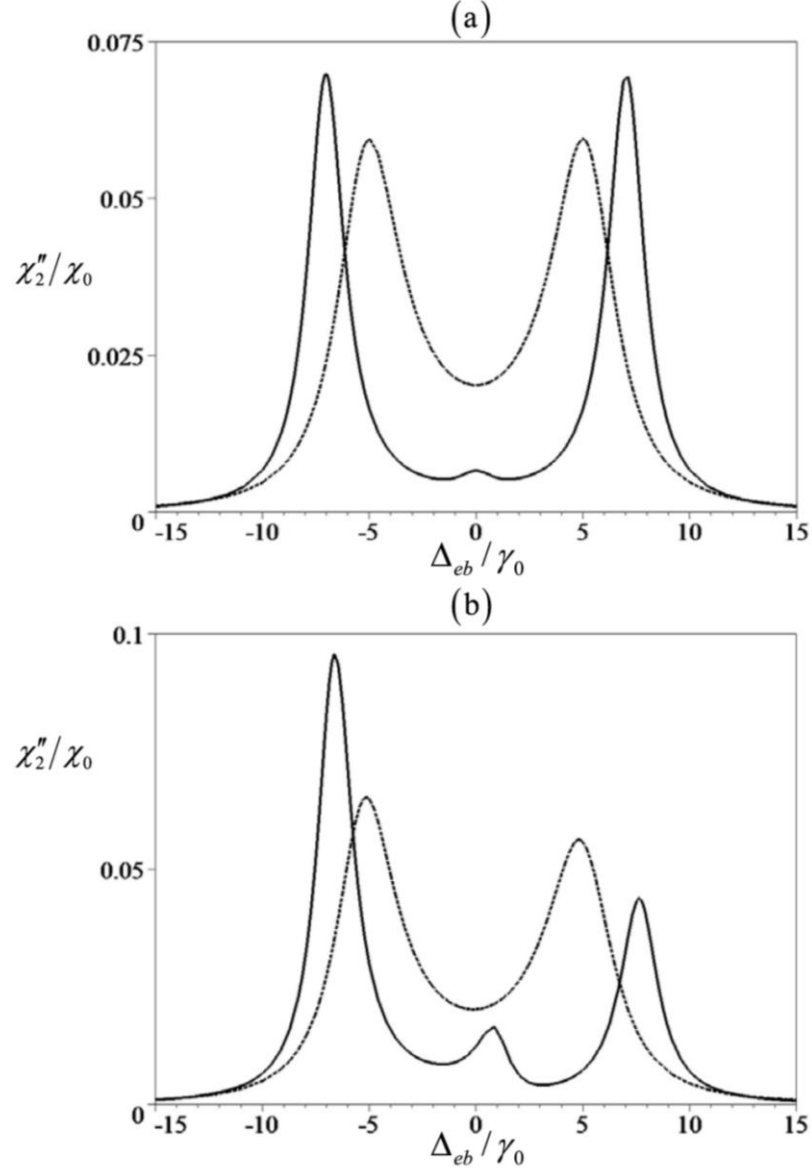


Figure 5-8: Plots of  $\chi_2''/\chi_0$  against probe field detuning  $\Delta_{eb}/\gamma_0$  for the atom in Fig. 5-1 (b), in steady state. In (a)  $\Delta_{ab}/\gamma_0 = \Delta_{bc}/\gamma_0 = 0$  and in (b)  $\Delta_{ab}/\gamma_0 = 2$  and  $\Delta_{bc}/\gamma_0 = 0$ . The Rabi frequencies of the laser fields are taken as  $\Omega_\alpha/\gamma_0 = \Omega_\beta/\gamma_0 = 10$  and  $\Omega_p/\gamma_0 = 0.2$ . The solid curves are drawn for the case where all resonance energies are away from either of the band edges and  $\varepsilon_{ad}/\varepsilon_v = 80.00\%$ . The dash-dotted curves represent the case where  $\varepsilon_{ad}/\varepsilon_v = 99.99\%$  while all other energies remain far from the band edges.

In order to understand the effect in Fig. 5-8(a), we recall that the system can have three dressed states due to the strong coupling of the pump fields. If both pump fields are resonant, the transition from the middle dressed state is forbidden. In this case, the locations of the peaks are:

$$\Delta_{eb} / \gamma_0 = -\frac{1}{2\gamma_0} \sqrt{\Omega_\alpha^2 + \Omega_\beta^2} \approx -7.07$$

$$\Delta_{eb} / \gamma_0 = \frac{1}{2\gamma_0} \sqrt{\Omega_\alpha^2 + \Omega_\beta^2} \approx 7.07$$

When the resonance energy lies near the band edge and the decay rate  $\Gamma_a$  is large compared to  $\Omega_\alpha$ , we get two transitions located at:

$$\Delta_{eb} / \gamma_0 = -\Omega_\beta / 2 = -5$$

$$\Delta_{eb} / \gamma_0 = \Omega_\beta / 2 = 5$$

Fig. 5-8(b) can be explained in a similar way as Fig. 5-7(b). It can also be seen from this figure that the central peak is significantly weak compared to the side peaks. This can be explained by the fact that, at zero detuning, the transition from the middle state of the three dressed states of the system is forbidden (see discussion above). As the detuning is increased, the transition from the middle state becomes allowed. The dash-dotted curve in Fig. 5-8(b) can be explained in the same manner as that in Fig. 5-8(a), except the locations of the peaks will be different due to the non-zero  $\Delta_{ab} / \gamma_0$  parameter.

In all of Figs. 5-7 and 5-8, we have shown that, due to the role played by the band structure of the photonic crystal, the doped nanoparticle effectively becomes transparent to any radiation field tuned to the resonance energy of the probed transition. In fact, we have demonstrated that it is possible to switch from an absorption state to a non-absorption state (and vice versa) for the nanoparticle system, by controlling the resonance energy. More precisely, the transparency is seen to be directly dependent on the location of the resonance energy with respect to the band gap of the crystal. This is a very important finding as techniques of rendering material systems transparent to resonant laser radiation are very desirable for applications in quantum optics and radiation physics.

For example, the transparency effect can be used to enhance the properties and efficiency of physical processes such as nonlinear frequency conversion, optical phase conjugation, squeezed-light generation, low-light level photonic switching, etc. [280].

A survey of relevant studies reveals that the most common techniques employed in producing the transparency effect include the manipulation of atomic response through adjusting the intensity-ratio of pump fields [207, 223–226], changing the amplitude and phase of the driving field(s) [208], tuning the pump field [281], etc. In the calculations presented in this chapter, a new technique for obtaining transparency has been shown, making use of the unique properties of the band structures of photonic crystals. This has great potential for applications in creating new photonic devices for quantum computing.

The discussion in this chapter concerns the ac Stark effect caused by two external strong pump fields in a photonic crystal doped with five-level nanoparticles. The transparency obtained in our theory is an effect of the modified decay rate, the two pump fields and the probe field. There have been many other studies of transparency and splitting of energy levels in doped photonic crystals using physical systems and methods which are different from those considered in this chapter. For example, Petrosyan and Kurizki [282] have studied four-level nanoparticles where they have applied a control probe field and a pump field. They observed electromagnetically induced transparency due to the coupling of a resonant transition of the nanoparticle to the localized density of states within the band gap and at the band edge of the crystal. The splitting of the energy level, in their case, is not due to the external field. It is a result of the coupling to the density of states. Similar studies have also been performed by other researchers [283–286].

In contrast to these works, we do not consider the splitting of the resonance energy due to the coupling of the transition to the density of states. Instead, the A–T splitting demonstrated here occurs due to the external laser fields. This is a very important distinction.

Electromagnetically induced transparency has also been achieved by Singh in four-level nanoparticles doped in a photonic crystal with the application of only one laser field [273]. It is found that the medium can be transformed from a transparent to a non-

transparent state just by changing the location of the resonance energy. More recently, the induced transparency phenomenon have been used in a similar set-up to demonstrate the switching of a single signal photon by a single gating photon of a different frequency, via cross-phase modulation [287]. It has also been shown to feature in the spontaneous emission spectra obtained from both V-type three-level and double V-type four-level nanoparticles embedded in a double-band photonic crystal [234]. The spectra has been observed to contain both dark and narrow spectral lines, arising from a destructive interference or singularities of the density of states of the radiation field and population transfer under joint constructive interferences, respectively.

The isotropic model of the photonic crystal leads to a divergent density of states at a band edge [5–9, 13, 288–293]. It is important to specify how far from the divergent band edge the resonance energy needs to be in order to facilitate the Markovian approximation. Analyses of the decay of a nanoparticle with the resonance energy close to the band-edge energy have shown that the band-edge modes behave like a cavity and the nanoparticle-band-edge modes interaction splits the atomic resonance into a doublet [213–220]. One component of the doublet falls in the continuum of states and decays. The other component falls inside the band gap giving rise to a photon-atom bound state. The magnitude of the splitting is a function of nanoparticle-band-edge detuning. For some values of this detuning, the splitting disappears or its influence on the nanoparticle becomes negligible.

If the resonance energy is inside the band gap, the isotropic model guarantees the existence of a photon-atom bound state. This becomes evident through oscillations in the atomic inversion. However, discussions in the present chapter do not consider cases where the resonance energy lies in the band gap. In fact, the largest value of the resonance energy  $\varepsilon_{ad}$  is  $0.9999\varepsilon_v$ . It is important to note that for large detunings from the band edge, the magnitude of the oscillations in the atomic inversion becomes negligibly small [5].

It is known that the typical signature of non-Markovian effects [5–9, 13, 289–293] is a non-exponential decay [5, 294]. It can be deduced from References [5, 294] that, in the

isotropic photonic crystal considered in this chapter, the system behaves in a Markovian fashion if the detuning  $\Delta \equiv (\varepsilon_v - \varepsilon_{ad}) /$  approximately satisfies the following relation:

$$\frac{\Delta}{\varepsilon_v} \geq \frac{50\beta_I}{\varepsilon_v}$$

where  $\beta_I$  is defined as the characteristic frequency of the nanoparticle-photon interaction [5]. In other words, the Markovian approximation is valid when the density of states can be considered smooth on the frequency scale determined by this characteristic frequency.

Using References [5] and [294],  $\beta_I$  can be approximated as:

$$\beta_I = \left[ \frac{\sqrt{\pi / A_I} (\varepsilon_{ad} \mu_{ad})^2}{12\hbar^2 \varepsilon_0 \varepsilon_v} \right]^{2/3}$$

with the constant  $A_I$  obtained in Reference [18, 19] as:

$$A_I = \left[ -\frac{cL^2}{2a(1+n)^2 \sin(4na\varepsilon_v / ch)} \right] \quad (5.20)$$

By putting the parameters in the equation for  $A_I$  and substituting the value in that for  $\beta_I$ , we found that  $\hbar\Delta / \varepsilon_v \geq 10^{-5}$ , approximately. In this chapter, the largest value of  $\varepsilon_{ad}$  gives  $\hbar\Delta / \varepsilon_v = (\varepsilon_v - 0.9999\varepsilon_v) / \varepsilon_v = 10^{-4}$ . Therefore, from the above calculations, it can be concluded that the Markovian approximation performs relatively well.

Finally, it is interesting to note that the formalism and results obtained for the isotropic model also apply to one-dimensional systems. This can be very advantageous as these systems can be implemented as waveguide channels in three-dimensional photonic crystals [295].

## 5.5 Summary and Conclusion

This chapter details the study of the time evolution of the level populations and both the transient and the steady-state behaviors of the imaginary part of the susceptibility in an isotropic photonic crystal doped with doubly-driven five-level nanoparticles. The nanoparticles in the ensemble interact with the crystal which acts as a reservoir and are

coupled with two strong pump fields and a weak probe field. Each nanoparticle has three levels in cascade configuration. The transition between the bottom level of the cascade and another level with higher energy than that of the cascade levels is studied with a weak probe field. Numerical simulations are performed, using the density matrix method, to obtain the absorption spectrum of this transition at large Rabi frequencies of the driving fields.

It was found that the manipulation of the decay rate offers a new mechanism for switching the nanoparticle system from an inverted to a non-inverted state (and vice versa), with regards to the population of the ground level of the nanoparticle. We have also performed numerical simulations for the imaginary part of the susceptibility. Our calculations have shown that, due to the role played by the band structure of the photonic crystal, the doped nanoparticle effectively becomes transparent to any radiation field tuned to the resonance energy of the probed transition. Therefore, due to the role played by the band structure of the photonic crystal, it is possible to switch between an absorption state and a non-absorption state of the atomic system, by controlling the resonance energy. This is a very important finding as techniques of rendering material systems transparent to resonant laser radiation are very desirable for applications in quantum optics and radiation physics.

This concludes the description of our investigation of the ac Stark effect in photonic crystals when the doped ensemble of nanoparticles are non-interacting. The next chapter details the extension of our study of the splitting phenomenon in these materials to include the effect of DDI between the doped nanoparticles.



## Chapter 6

### 6 Dipole-dipole Interaction and the ac Stark Effect in Photonic Crystals

The previous chapter focused on the study of the ac Stark effect in a doped photonic crystal, neglecting the presence of dipole-dipole interaction (DDI). In this chapter, the work is extended to include the DDI effect.

#### 6.1 Introduction

Chapter 5 detailed our study of the ac Stark effect in a three-dimensional photonic crystal with isotropic geometry. The crystal is doped with an ensemble of identical, non-interacting five-level nanoparticles. These nanoparticles interact with the photonic crystal which plays the role of a reservoir. We have considered two distinct configurations of five-level nanoparticles, driven by two strong pump fields and a weak probe field. Due to the interaction between the particles and the reservoir, the excited energy levels decay spontaneously to the lower levels. It is found that, by manipulating the decay rate with resonance tuning, the nanoparticle can be switched between an inverted and a non-inverted state, with regards to the population of the ground level of the cascade core of the five-level configuration. Furthermore, the band structure of the photonic crystal is found to have a major influence on the ac Stark effect observed in the doped nanoparticles. In particular, the probed transition of a doped nanoparticle could be rendered transparent to any resonant radiation field i.e. the nanoparticle can be switched between an absorption and a non-absorption state, simply by manipulating the location of the resonance energy.

In recent years, there has been considerable interest in studying the role of DDI in multi-level atomic gases [57–61]. For example, Dowling and Bowden [57, 58] have studied the effect of DDI in a three-level atomic gas, and found that the absorption peak changes from a symmetric to an asymmetric shape. Manka et al. [59] have extended the work of Dowling and Bowden [57, 58] to study the effect of atomic nonlinearities on the atomic gas system. They found a density-dependent switching between absorption and

amplification. Calderón et al. [60], on the other hand, have studied DDI in V-type nanoparticles. They found that the system changes from absorption to gain due to the phase difference between the probe and the pump fields, in the presence of DDI.

The effect of DDI on photonic crystals and dispersive materials has also been investigated [13, 69, 70, and 296]. John and Quang [13] have studied the phenomenon of self-induced transparency due to DDI in two-level nanoparticles. Singh and Haque [54] have done some preliminary work on DDI in CPT. Singh [70] has studied the effect of DDI on the enhancement of the refractive index in a photonic crystal doped with five-level nanoparticles.

This discussion in this chapter considers a photonic crystal densely doped with an ensemble of five-level nanoparticles. A schematic diagram of the five-level particle is shown in Fig. 6-1. A probe laser field applied to the system measure its absorption coefficient. The probe induces a dipole moment in each nanoparticle in the ensemble. A pump field and a control laser field are also applied to introduce an interference effect in the system. These fields also induce dipole moments in the nanoparticles. When the concentration of the particles is high, the induced dipoles interact with each other via DDI [272]. We use the mean field approximation in order to include the effect of the DDI in the calculation of the absorption coefficient. Numerical simulations are performed on the absorption coefficient in the presence of DDI. We have observed many interesting effects in the densely doped system. Most notably, we found that the absorption in the system decreases as the strength of the DDI increases. The absorption peaks shift to new positions due to the DDI effect. Furthermore, the widths and the heights of the peaks also depend on the strength of the DDI.

We have also investigated the role of the decay rate in our calculations i.e. the effect of the band structure of the photonic crystal on the doped nanoparticles. We have calculated the absorption coefficient when the relevant resonance energies of the nanoparticles lie away from the band edges of the crystal. Under such conditions, we obtain a pair of peaks in the spectral profile. However, when the resonance energies of the nanoparticles lie near a band edge of the photonic crystal, the system is observed to have only one peak.

We have found that the system can be switched from a one-peak to a three-peak profile, simply by changing the location of the resonance energy. This phenomenon can be used to fabricate novel photonic switching devices.

## 6.2 The Dipole-dipole Interaction Hamiltonian

In a similar vein to the studies presented in preceding chapters, we consider that a photonic crystal is made up of dielectric spheres periodically arranged in air. As mentioned in the previous section, there has been considerable recent interest in doping nanoparticles in photonic crystals. The crystal, in this case, is doped with an ensemble of identical five-level nanoparticles. The energy levels of a five-level nanoparticle in the doped ensemble are denoted by  $|a\rangle$ ,  $|b\rangle$ ,  $|c\rangle$ ,  $|d\rangle$  and  $|e\rangle$ . The level scheme is shown in Fig. 6-1. The Hamiltonians of the doped nanoparticle and the nanoparticle-field interactions are identical to those given by Eqns. (5.2, 5.4), respectively, in Section 5.3 in the previous chapter.

In order to study the ac Stark effect, we apply three external laser fields to the system. A tunable probe field of energy  $\varepsilon_p$  and electric field amplitude  $E_p$  is applied to monitor the absorption coefficient between the ground level  $|c\rangle$  and the excited level  $|e\rangle$ . The magnitude of the corresponding Rabi frequency is denoted as  $\Omega_p$ . A strong pump laser field of energy  $\varepsilon_\beta$  and Rabi frequency  $\Omega_\beta$  is applied between levels  $|c\rangle$  and  $|b\rangle$ . A control field of energy  $\varepsilon_\alpha$  and Rabi frequency  $\Omega_\alpha$  is applied between levels  $|b\rangle$  and  $|a\rangle$ . The application of the three fields leads to the three transitions  $|c\rangle \rightarrow |e\rangle$ ,  $|c\rangle \rightarrow |b\rangle$  and  $|b\rangle \rightarrow |a\rangle$ , which induce the three electric dipole moments  $\mu_{ec}$ ,  $\mu_{bc}$  and  $\mu_{ab}$ , respectively, in each nanoparticle. It is considered that the concentration of the nanoparticles is large enough so that the induced dipoles interact with each other via DDI. The expression of the DDI Hamiltonian has been obtained for a single field and a two-level system, in the mean field approximation, in Section 4.2 in Chapter 4.

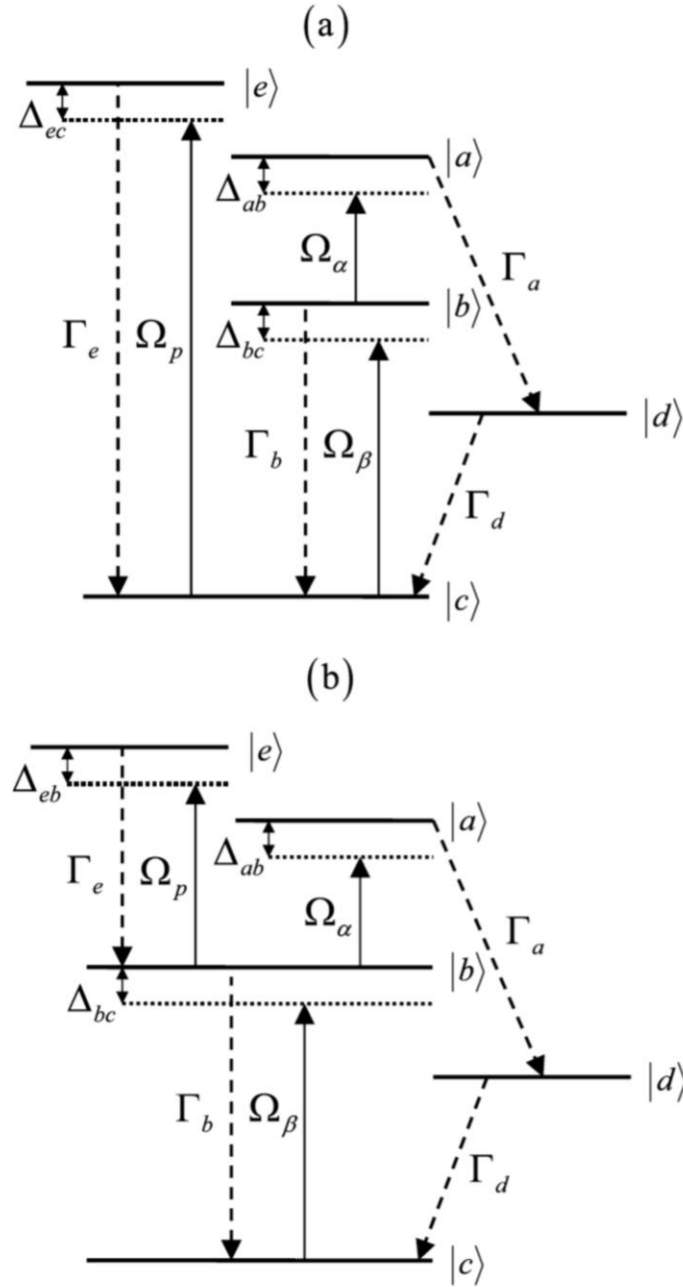


Figure 6-1: Schematic diagram for the five-level nanoparticle, driven by two pump laser fields with Rabi frequencies  $\Omega_\alpha$  and  $\Omega_\beta$ . The levels are denoted as  $|a\rangle$ ,  $|b\rangle$ ,  $|c\rangle$ ,  $|d\rangle$  and  $|e\rangle$ . The probe field with Rabi frequency  $\Omega_p$  drives the  $|c\rangle \rightarrow |e\rangle$  transition. The detuning of the two pump fields and the probe field are denoted as  $\Delta_{ab}$ ,  $\Delta_{bc}$  and  $\Delta_{ec}$ , respectively. The dashed arrows represent the decay channels and  $\Gamma_i$  denotes the decay rate of level  $|i\rangle$ .

The system discussed in this chapter has three external laser fields. We have generalized the theory of Section 4.2 for three fields and have obtained the following DDI Hamiltonian:

$$H_{dd} = - \left( h_{ab} \sigma_{ba}^- e^{i(\varepsilon_a - \varepsilon_{ab})t/\hbar} + h_{bc} \sigma_{cb}^- e^{i(\varepsilon_b - \varepsilon_{bc})t/\hbar} + h_{ec} \sigma_{ce}^- e^{i(\varepsilon_c - \varepsilon_{ec})t/\hbar} \right) + h.c. \quad (6.1)$$

where  $\sigma_{ij}^- = |j\rangle\langle i|$ , with  $i$  and  $j$  denoting  $a, b, c$  and  $e$ . The quantities  $\varepsilon_{ab}$ ,  $\varepsilon_{bc}$  and  $\varepsilon_{ec}$  are the transition energies corresponding to the  $|b\rangle \rightarrow |a\rangle$ ,  $|c\rangle \rightarrow |b\rangle$  and  $|c\rangle \rightarrow |e\rangle$  transitions, respectively. The energy difference between levels  $|a\rangle$  and  $|d\rangle$  is denoted as  $\varepsilon_{ad}$ . The remaining parameters appearing in the above expression are given as:

$$\begin{aligned} h_{ab} &= \Lambda_a \rho_{ab} \\ h_{bc} &= \Lambda_b \rho_{bc} \\ h_{ec} &= \Lambda_c \rho_{ec} \end{aligned}$$

Note that, in the above,  $h_{ji} = (h_{ij})^*$ . The parameters  $\Lambda_a$ ,  $\Lambda_b$  and  $\Lambda_c$ , known as the DDI parameters, are defined as:

$$\begin{aligned} \Lambda_a &= 2\gamma_0 C_a \\ \Lambda_b &= 2\gamma_0 C_b \\ \Lambda_c &= 2\gamma_0 C_c \end{aligned}$$

where

$$\begin{aligned} C_a &= \left( \frac{N_0}{3\epsilon_0 \gamma_0} \right) \mu_{ab}^2 \\ C_b &= \left( \frac{N_0}{3\epsilon_0 \gamma_0} \right) \mu_{bc}^2 \\ C_c &= \left( \frac{N_0}{3\epsilon_0 \gamma_0} \right) \mu_{ec}^2 \end{aligned}$$

In the above,  $N_0$  is the concentration of the doped nanoparticles and  $\epsilon_0$  is the dielectric constant of the medium. The quantity  $\gamma_0$  is the vacuum decay rate, as defined in References [18, 19]. All frequencies discussed in this chapter are measured with respect

to  $\gamma_0$ . In order to get the expression for the DDI, we have neglected the non-diagonal terms as they are much smaller compared to those on the diagonal.

In addition to DDI, the nanoparticles interact with the photonic crystal reservoir. Due to this interaction, level  $|a\rangle$  decays to level  $|d\rangle$  and levels  $|b\rangle$ ,  $|d\rangle$  and  $|e\rangle$  decay to level  $|c\rangle$ . The Hamiltonian of the photonic crystal reservoir and the nanoparticle-reservoir interaction Hamiltonian is written, as in the previous chapter, as follows (discussed in Appendix B):

$$\begin{aligned}
 H = & \int_C \frac{d\varepsilon_k}{2\pi} \varepsilon_k p^\dagger(\varepsilon_k) p(\varepsilon_k) - \int_C \frac{d\varepsilon_k}{2\pi} \sqrt{\gamma_0} Z(\varepsilon_k) p(\varepsilon_k) \sigma_{ad}^+ e^{-i(\varepsilon_k - \varepsilon_{ad})t/\hbar} \\
 & - \sum_{i=b,d} \int_C \frac{d\varepsilon_k}{2\pi} \sqrt{\gamma_0} Z(\varepsilon_k) p(\varepsilon_k) \sigma_{ic}^+ e^{-i(\varepsilon_k - \varepsilon_{ic})t/\hbar} \\
 & - \int_C \frac{d\varepsilon_k}{2\pi} \sqrt{\gamma_0} Z(\varepsilon_k) p(\varepsilon_k) \sigma_{ec}^+ e^{-i(\varepsilon_k - \varepsilon_{ec})t/\hbar} + h.c.
 \end{aligned} \tag{6.2}$$

In the above, the first term is the Hamiltonian of the photonic crystal and the remaining three terms are the Hamiltonian for the nanoparticle-reservoir interaction. The  $p(\varepsilon_k)$  and  $p^\dagger(\varepsilon_k)$  operators denote the annihilation and creation of photons, respectively, where  $\varepsilon_k$  is the energy of the photon with corresponding wave vector  $k$ . As before, the integration contour  $C$  consists of two intervals:  $-\infty < \varepsilon_k \leq \varepsilon_v$  and  $\varepsilon_c \leq \varepsilon_k < \infty$ . The expression for the form factor  $Z(\varepsilon_k)$  is given by Eqn. (5.6) in Chapter 5. A representative plot of the form factor is shown in Fig. 5-4 (bottom panel).

### 6.3 Absorption Coefficient and Density Matrix

The aim of this section is to obtain an expression for the susceptibility due to the weak probe field. For the case of the nanoparticle in Fig. 6-1, the susceptibility can be written as [84]:

$$\chi_1 = \frac{2\mu_{ec}\rho_{ec}}{\epsilon_0 E_p} \tag{6.3}$$

where  $\rho_{ij}$  and  $\mu_{ij}$  denote the elements of the density matrix and the dipole operator, respectively, associated with the transition  $|j\rangle \rightarrow |i\rangle$ . The density matrix elements can be calculated using the master equation method. The system is prepared in such a way that, initially, the nanoparticles are in ground level  $|c\rangle$ . As the pump fields are switched on, the excited levels become populated. Following the master equation method implemented in the previous chapter and Eqns. (6.1, 6.2), the equations of motion for the density matrix elements can be written as follows:

$$\rho_{aa} = -\Gamma_a \rho_{aa} - ix_\alpha (\rho_{ab} - \rho_{ba}) - i(\Pi_{ba} \rho_{ab} - \Pi_{ab} \rho_{ba}) \quad (6.4a)$$

$$\begin{aligned} \rho_{bb} = & -\Gamma_b \rho_{bb} + ix_\alpha (\rho_{ab} - \rho_{ba}) - ix_\beta (\rho_{bc} - \rho_{cb}) + i(\Pi_{ba} \rho_{ab} - \Pi_{ab} \rho_{ba}) \\ & - ix_\beta (\Pi_{cb} \rho_{bc} - \Pi_{bc} \rho_{cb}) \end{aligned} \quad (6.4b)$$

$$\begin{aligned} \rho_{cc} = & \Gamma_b \rho_{bb} + \Gamma_d \rho_{dd} + \Gamma_e \rho_{ee} + ix_\beta (\rho_{bc} - \rho_{cb}) + ix_p (\rho_{ec} - \rho_{ce}) \\ & + ix_\beta (\Pi_{cb} \rho_{bc} - \Pi_{bc} \rho_{cb}) + ix_p (\Pi_{ce} \rho_{ec} - \Pi_{ec} \rho_{ce}) \end{aligned} \quad (6.4c)$$

$$\rho_{dd} = \Gamma_a \rho_{aa} - \Gamma_d \rho_{dd} \quad (6.4d)$$

$$\rho_{ee} = -\Gamma_e \rho_{ee} - ix_p (\rho_{ec} - \rho_{ce}) - ix_p (\Pi_{ce} \rho_{ec} - \Pi_{ec} \rho_{ce}) \quad (6.4e)$$

$$\rho_{ab} = d_{ab} \rho_{ab} - ix_\alpha (\rho_{aa} - \rho_{bb}) - ix_\beta \rho_{ac} - i\Pi_{ba} (\rho_{aa} - \rho_{bb}) - i\Pi_{cb} \rho_{ac} \quad (6.4f)$$

$$\rho_{ac} = d_{ac} \rho_{ac} + ix_\alpha \rho_{bc} - ix_\beta \rho_{ab} - ix_p \rho_{ae} + i\Pi_{ba} \rho_{bc} - i\Pi_{cb} \rho_{ab} - i\Pi_{be} \rho_{ae} \quad (6.4g)$$

$$\rho_{ad} = d_{ad} \rho_{ad} + ix_\alpha \rho_{bd} + i\Pi_{ba} \rho_{bd} \quad (6.4h)$$

$$\rho_{bc} = d_{bc} \rho_{bc} + ix_\alpha \rho_{ac} - ix_\beta (\rho_{bb} - \rho_{cc}) + ix_p \rho_{be} + i\Pi_{ba} \rho_{ac} - i\Pi_{cb} (\rho_{bb} - \rho_{cc}) + i\Pi_{ea} \rho_{be} \quad (6.4i)$$

$$\rho_{bd} = d_{bd} \rho_{bd} + ix_\alpha \rho_{ad} + ix_\beta \rho_{cd} + i\Pi_{ba} \rho_{ad} + i\Pi_{cb} \rho_{cd} \quad (6.4j)$$

$$\rho_{dc} = -d_{dc} \rho_{dc} - ix_\beta \rho_{db} + ix_p \rho_{de} - i\Pi_{cb} \rho_{db} + i\Pi_{ea} \rho_{de} \quad (6.4k)$$

$$\rho_{ea} = d_{ea} \rho_{ea} - ix_\alpha \rho_{eb} + ix_p \rho_{ca} - i\Pi_{ba} \rho_{eb} + i\Pi_{ea} \rho_{ca} \quad (6.4l)$$

$$\begin{aligned} \rho_{eb} = & d_{ec} \rho_{eb} - ix_\alpha \rho_{ea} - ix_\beta \rho_{ec} + ix_p \rho_{cb} - i\Pi_{ba} \rho_{ea} - i\Pi_{cb} \rho_{ec} \\ & + i\Pi_{ea} \rho_{cb} \end{aligned} \quad (6.4m)$$

$$\rho_{ec} = d_{ec} \rho_{ec} - ix_\beta \rho_{eb} + ix_p (\rho_{cc} - \rho_{ee}) - i\Pi_{cb} \rho_{eb} + i\Pi_{ea} (\rho_{cc} - \rho_{ee}) \quad (6.4n)$$

$$\rho_{ed} = d_{ed} \rho_{ed} + ix_p \rho_{cd} + i\Pi_{ea} \rho_{cd} \quad (6.4o)$$

The complex detuning terms appearing in Eqn. (6.4) are given by:

$$d_{ij} = i\Delta_{ij} - \Gamma_{ij}$$

where

$$\begin{aligned}\Delta_{ab} &= (\varepsilon_a - \varepsilon_{ab}) / \hbar \\ \Delta_{bc} &= (\varepsilon_b - \varepsilon_{bc}) / \hbar \\ \Delta_{ec} &= (\varepsilon_p - \varepsilon_{ec}) / \hbar\end{aligned}$$

The remaining parameters are defined as:

$$\begin{aligned}x_i &= \Omega_i / 2 \\ \Omega_p &= \mu_{ec} E_p / 2\hbar \\ \Gamma_{ij} &= (\Gamma_i + \Gamma_j) / 2 \\ \Pi_{ij} &= \frac{h_{ij}}{2\gamma_0}\end{aligned}$$

where the  $\Gamma_i$  terms are the reservoir-mediated decay rates:

$$\begin{aligned}\Gamma_a &= \gamma_0 Z(\varepsilon_{ad})^2 \\ \Gamma_b &= \gamma_0 Z(\varepsilon_{bc})^2 \\ \Gamma_d &= \gamma_0 Z(\varepsilon_{dc})^2 \\ \Gamma_e &= \gamma_0 Z(\varepsilon_{ec})^2\end{aligned}$$

The  $\Pi_{ij}$  terms appearing in Eqn. (6.4) account for the inclusion of the DDI effect. The absorption coefficient can then be calculated by evaluating the value of  $\rho_{ec}$  from these density matrix equations.

## 6.4 Results and Discussions

This section presents our numerical simulations on the absorption coefficient for the photonic crystal. The parameters of the crystal are taken as in Reference [24]:

$$\begin{aligned}n &= 1.082 \\ L &= 300 \text{ nm} \\ a / L &= 0.24\end{aligned}$$

All the energies in the calculation are measured with respect to the decay rate energy  $\gamma_0$  of a nanoparticle in free space. The Rabi frequencies used in these calculations are:  $\Omega_a / \gamma_0 = \Omega_b / \gamma_0 = 10$  and  $\Omega_p / \gamma_0 = 0.02$ . Also, the pump fields are considered to be resonant.



In these calculations, we have used the normalized susceptibility ( $\chi / \chi_0$ ) and the normalized detuning parameter ( $\delta_{ab} / \gamma_0$ ). The imaginary susceptibility ( $\chi'' / \chi_0$ ) is calculated both in the absence and presence of DDI due only to the probed transition (DDI parameter  $C_c$ ). It is directly related to the absorption coefficient.

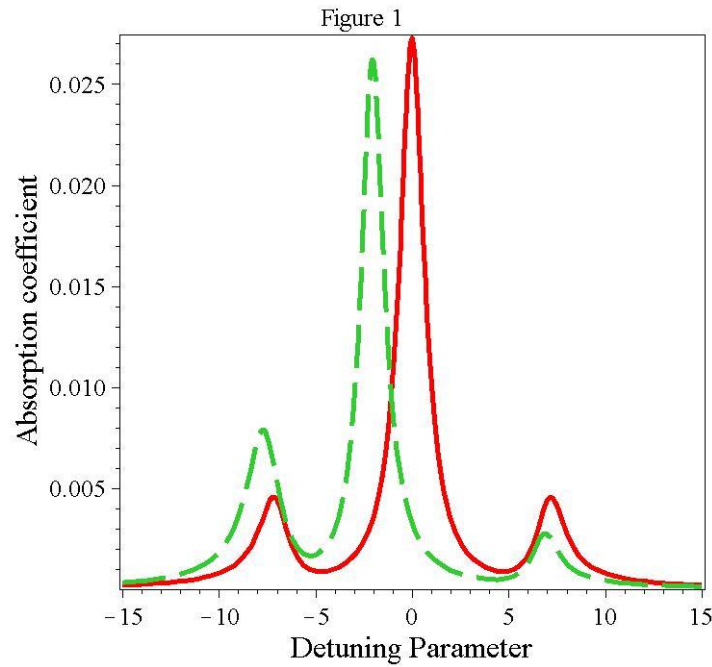


Figure 6-2: Plots of the absorption coefficient against the detuning parameter. The solid and the dashed curves correspond to  $C_c = 0$  and  $C_c = 5$ , respectively.

The absorption coefficient is plotted as a function of the detuning parameter ( $\delta_{ab} / \gamma_0$ ) in Fig. 6-2. The solid and the dashed curves correspond to  $C_c = 0$  and  $C_c = 5$ , respectively.

The solid curve has three peaks and two minima. The peaks are located symmetrically about the zero detuning mark. In the presence of DDI, the peaks become asymmetric. This behavior has also been found in other systems [57–60, 296].

Note that the positions of the peaks shift towards the left in the presence of DDI. The height of the left peak decreases as opposed to that of the right peak. This is due to the presence of an extra detuning term appearing in the absorption coefficient. The type of behaviour described above has also been found in atomic gases.

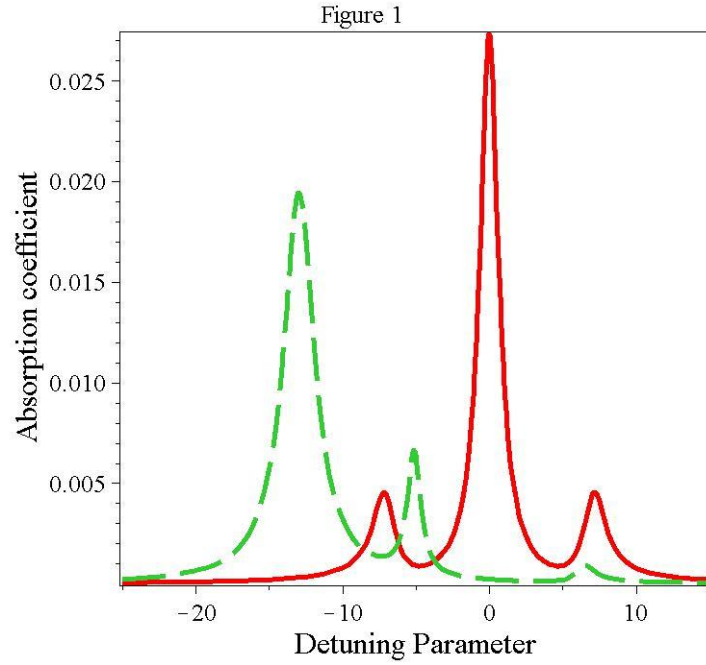


Figure 6-3: Plots of the absorption coefficient against the detuning parameter. The solid and the dashed curves correspond to  $C_c = 5$  and  $C_c = 10$ , respectively.

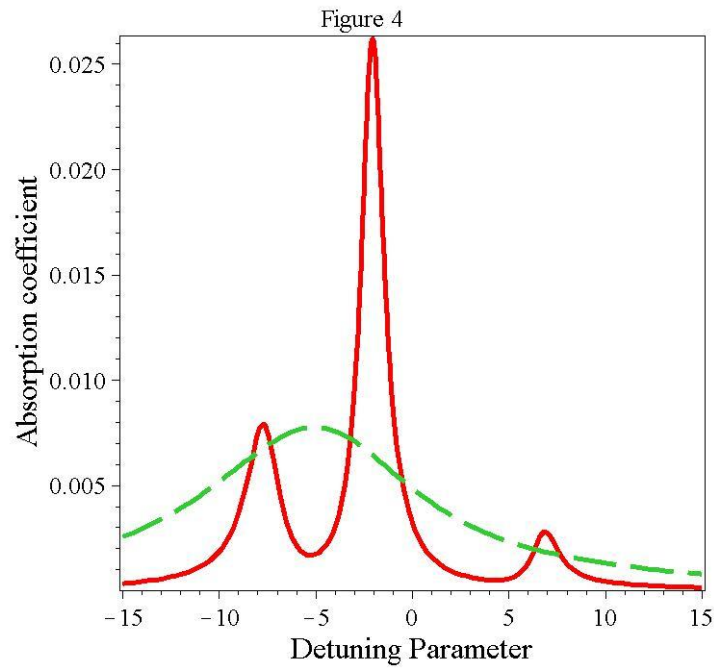


Figure 6-4: Plots of the absorption coefficient against the detuning parameter when the relevant resonance energy of the nanoparticle lies away from (solid curve) and near a band edge (dashed curve) of the photonic crystal. The DDI parameter  $C_c = 5$ .

We have also plotted the absorption coefficient under strong DDI coupling conditions. The results are shown in Fig 6.3. The solid and the dashed curves correspond to  $C_c = 5$  and  $C_c = 10$ , respectively. Note that, in the presence of strong DDI coupling, the right peak disappears and the absorption spectrum has only two peaks. This means that the system can be changed from a three-peak spectral profile to that featuring two peaks by increasing the strength of the DDI coupling.

In addition to the above, we have also investigated the role of the band structure of the photonic crystal in our calculations. In Fig. (6.2), we have calculated the influence of the DDI effect on the absorption coefficient when the relevant resonance energy of the nanoparticle lies away from either of the band edges of the photonic crystal. Next, we consider that this resonance energy lies near the lower band edge. The results are shown in Fig 6.4 (with  $C_c = 5$ ).

The solid curve in Fig. 6-4 corresponds to when the resonance energy lies away from the band edge (dashed curve in Fig. 6-2). Note that this curve has three peaks. The dashed curve in the figure is plotted when the resonance energy lies near the lower band edge. In contrast, this curve has only one peak. The physics behind the disappearing side peaks is explained below.

The decay rate of an energy level of a doped nanoparticle is very large when the corresponding resonance energy lies near one of the band edges of the photonic crystal. Consequently, all three peaks merge into one solitary spectral feature. This means that, by moving the resonance energy, the number of absorption peaks appearing in the spectrum can be controlled. Therefore, the system can be switched from a one-peak to a three-peak profile, simply by changing the location of the relevant resonance energy.

## 6.5 Summary and Conclusion

This chapter details our study of the effect of DDI on the ac Stark effect in a photonic crystal doped with an ensemble of five-level nanoparticles. A probe laser field is applied to measure the absorption coefficient by inducing a dipole moment in each particle. A pump and a control laser field are applied to introduce an interference effect in the

system. They also induce dipole moments in each nanoparticle in the ensemble. When the concentration of the nanoparticles is high, the induced dipoles interact with each other via DDI [272]. The mean field approximation is used to include the effect of DDI.

Numerical simulations are performed on the absorption coefficient in the presence of DDI. We found that the absorption in the system decreases as the strength of the DDI increases. The absorption peaks also shift to new positions due to the effect of DDI. Moreover, the system can be switched from a three-peak profile to that featuring two peaks (and vice versa) by changing the DDI parameter. The width and the height of the peaks are also found to depend on the strength of the DDI. From the point of view of the influence of the photonic crystal band structure, we also found that the system can be switched from a one-peak to a three-peak profile by changing the location of the relevant resonance energy.

This concludes our study of the ac Stark effect in a photonic crystal doped with an interacting ensemble of nanoparticles.

## Chapter 7

### 7 Concluding Remarks

In the works presented in this thesis, we have studied the phenomenon of coherent population trapping (CPT) and the ac Stark effect in photonic crystals and dispersive materials doped with nanoparticles. The nanoparticles are interacting with the photonic crystal and dispersive material reservoirs. In certain cases, they are also taken to be interacting with each other via dipole-dipole interaction (DDI). Both of these materials have energy gaps in their dispersion relation. We have used the density matrix method to facilitate our investigation of these phenomena.

First, we have investigated the phenomenon of photon trapping in nanoparticles doped in photonic crystals. These materials feature energy gaps due to the periodicity of the dielectric constant. We found that, in photonic crystals, when the resonance energy lies within the lower and upper bands, one observes the CPT effect at certain values of the relative Rabi frequency for a given initial configuration of the energy levels of the nanoparticle. The CPT effect can be controlled by moving the resonance energies of the nanoparticles within the lower and upper bands of the photonic crystal.

We have also investigated the CPT effect in dispersive materials. These materials have energy gaps in their dispersion spectra as well. However, the band gap in these materials is due to phonon and photon coupling. The most useful thing we found from our calculations is that the steady-state population on the upper level of a doped nanoparticle depends very sensitively on the coherence conditions. It is also found that increasing the decay rate can increase the fraction of population trapped in the system. In this way, the same population density in the upper level can be obtained for a range of values of the resonance energy simply by adjusting the intensities of the coupled field.

The influence of DDI has also been investigated on the CPT effect. For a photonic crystal, we found that, when the resonance energies lie away from the band edges and within the lower or upper bands, trapping is observed at certain values of the relative

Rabi frequency. Moreover, this effect varies depending on the strength of the dipole-dipole interaction between the nanoparticles.

For a dispersive material, it can be seen that when the resonance energy lies within the lower and upper bands, one observes the CPT effect at certain values of the relative Rabi frequency, which vary depending on the strength of the DDI between the nanoparticles. Also, in both media, as this interaction becomes stronger, the population density of the uppermost level increases. We have also observed that the CPT effect can be switched on and off due to the presence of DDI.

We proceed to extend our study of doped nanoparticles in these materials to include nonlinear quantum optical phenomena – in particular, the ac Stark Effect. We found that manipulation of the decay rate offers a new mechanism for switching the doped nanoparticle from an inverted to a non-inverted state (and vice versa), with regards to the population of the ground level of the nanoparticle. Our calculations have also shown that, due to the role played by the band structure of the photonic crystal, the doped nanoparticle effectively becomes transparent to any radiation field tuned to the resonance energy of the probed transition.

We also study the effect of DDI on dynamic Stark splitting in a photonic crystal doped with an ensemble of five-level nanoparticles. It is found that, when the concentration of the particles is high, the induced dipoles – interacting with each other via DDI – decreases the absorption in the system with increasing interaction strength. The absorption peaks shift to new positions due to the effect of DDI. The system can also be switched from a three-peak spectral profile to that featuring two peaks simply by changing the DDI parameter.

In the latter works presented in this thesis, we have used the density matrix formulation in order to calculate the absorption coefficients of applied probe fields. The method of density matrix is developed from the Schrödinger equation, accounting for the temperature of the system. As a result, the density matrix contains correlations functions between its elements (referred to as coherence terms of the density matrix), which are time-dependent. In the literature, most works use the Markovian approximation in order

to simplify the time-dependent correlation functions. In this approximation, the damping present in the system is assumed to destroy the *memory* of the past, leading to a very short correlation time, i.e. the state of the system at any given time is taken to depend only on the state immediately preceding it. The theory presented in this thesis for the five-level nanoparticles take the Markovian approximation into account. Furthermore, in all the calculations presented in the thesis, we account for the decay rates of the energy levels of the nanoparticles analytically.

Due to the two approximations mentioned above (the Markovian approximation and the analytical inclusion of the decay rates), our proposed theories have a number of limitations insomuch as that they may not be able to predict experimental outcomes with quantitative accuracy. But, importantly, the qualitative aspects of the findings of the works in this thesis remain perfectly valid and provide very useful insights into the behaviours of the systems under study.

It is useful to note here that, for most modern optoelectronic devices, the energy required per switching operation is an important consideration in studying light-matter interactions. Consequently, it is crucial and, indeed, very informative to estimate the switching power required by the systems studied in this thesis, in relation specifically to the photonic crystal reservoir. This has been done in Appendix K.

The present work can quite easily be extended to metallic photonic crystals (MPCs). Recently, there has been considerable experimental and theoretical research done on MPCs because of their ability to control electronic and photonic resonances simultaneously [297]. They are more reflective than the crystals made of dielectric or semiconductor materials over a broader range of frequencies. Therefore, they are more likely to possess a complete photonic band gap compared to their dielectric counterparts.

The presence of band gaps in MPCs is the result of a combination of plasma screening effects and Bragg scattering. In order to have a complete photonic band gaps in a dielectric photonic crystal, a high dielectric contrast is required. This restriction causes a great deal of difficulty in the fabrication of these crystals. Materials with energy-dependent dielectric constants are the best alternative to overcome this obstacle and

metals are known to possess this much desired property. Also, photons interact much more strongly with metals than dielectrics, making MPCs more useful for developing integrated photonic devices.

MPCs are fabricated with the combination of dielectric and metallic nano-layers or spheres in the form of one-, two-, or three dimensional systems. For example, Kuo et al. [297] fabricated opaline gold photonic crystals possessing complete photonic band gaps in the optical regime. Recently, Hatef and Singh [298] have studied the effect of plasma energy on the absorption coefficient of MPCs doped with an ensemble of three-level nanoparticles, which are taken to interact with each other via DDI. It should be emphasized here that the phenomenon of CPT and the ac Stark effect have not been studied in these crystals.

The present work can also be extended to dispersive material nanowires. Recently there has been considerable interest in studying the optoelectronic properties of waveguides and nanowires made from polaritonic materials [299]. Most commonly, polaritonic waveguides and nanowires are fabricated through the femtosecond laser machining of holes or trenches which are carved through  $\text{LiNbO}_3$  or  $\text{LiTaO}_3$  host crystals [300].

Recently, Singh [299] has proposed the fabrication of polaritonic nanowires and wave guides by embedding one polaritonic material into another. He has considered that the embedded polaritonic material has a smaller band gap than the host material. For example, the semiconductor GaP has a smaller band gap than that of MgO. Because of this band-gap engineering, the polaritons have bound states in the embedded materials. It is found that the number of bound polariton states depends on the size of the nanowire. It has also been found that the absorption spectrum splits into many peaks due to the coupling between the nanoparticles and the bound polariton states. In other words, the polaritonic nanowire can be switched from one transparent state to another. This is a very interesting discovery which can be used to make polaritonic switches and transistors.

The study of polaritonic nanowires and waveguides is a new field of research which will prove to be very useful as the field of electronics faces increasingly insurmountable technological and physical barriers in increasing the speed of processing networks,



whereas photonics requires lossy integration of a light source and guiding structures. This field bridges the gap between electronics and photonics. It has a wide range of applications, including high bandwidth signal processing, THz imaging and THz spectroscopy. However, the phenomenon of CPT and the ac Stark effect have not been studied in these crystals. Such future investigations have great potentials for developing new types of quantum optical devices in these new polaritonic systems.

## Bibliography

- [1] Z. Ficek and S. Swain, *J. Mod. Opt.* **49**, 3 (2002).
- [2] S. John, *Phys. Rev. Lett.* **58**, 2486 (1987).
- [3] E. Yablonovitch, *Phys. Rev. Lett.* **58**, 2059 (1987).
- [4] E. Yablonovitch, T. J. Gmitter, and K. M. Leung, *Phys. Rev. Lett.* **67**, 2295 (1991).
- [5] M. Florescu and S. John, *Phys. Rev. A* **64**, 033801 (2001).
- [6] N. Vats, S. John, and K. Busch, *Phys. Rev. A* **65**, 043808 (2002).
- [7] M. Florescu and S. John, *Phys. Rev. A* **69**, 053810 (2004).
- [8] O. Toader and S. John, *Phys. Rev. E* **71**, 036605 (2005).
- [9] T. Y. M. Chan, O. Toader, and S. John, *Phys. Rev. E* **73**, 046610 (2006).
- [10] S. John, *Phys. Rev. Lett.* **53**, 2169 (1984).
- [11] J. D. Joannopoulos, R. D. Meade, and J. N. Winn, *Photonic Crystals* (Princeton University Press, New Jersey, 1995).
- [12] J.-M. Lourtioz, H. Benisty, V. Berger, J.-M. Gerard, D. Maystre, A. Tchebnokov, and P.-N. Favenec, *Photonic Crystals: Towards Nanoscale Photonic Devices* (Springer, Berlin, 2005).
- [13] S. John and T. Quang, *Phys. Rev. Lett.* **76**, 2484 (1996).
- [14] T. Quang, M. Woldeyohannes, S. John, and G. S. Agarwal, *Phys. Rev. Lett.* **79**, 5238 (1997).
- [15] M. Woldeyohannes and S. John, *Phys. Rev. A* **60**, 5046 (1999).
- [16] M. Woldeyohannes, S. John, and V. I. Rupasov, *Phys. Rev. A* **63**, 013814 (2000).
- [17] M. Woldeyohannes and S. John, *J. Opt. B* **5**, R43 (2003).
- [18] S. John and J. Wang, *Phys. Rev. Lett.* **64**, 2418 (1990).
- [19] S. John and J. Wang, *Phys. Rev. B* **43**, 12772 (1991).
- [20] V. I. Rupasov and M. R. Singh, *Phys. Rev. Lett.* **77**, 338 (1996).
- [21] V. I. Rupasov and M. R. Singh, *Phys. Rev. A* **56**, 898 (1997).
- [22] V. I. Rupasov and M. R. Singh, *Phys. Rev. A* **54**, 3614 (1996).
- [23] M. R. Singh, *J. Mod. Opt.* **50**, 1319 (2003).
- [24] M. R. Singh and I. Haque, *J. Mod. Opt.* **52**, 1857 (2005).
- [25] M. R. Singh, *J. Phys. B: At. Mol. Opt. Phys.* **42**, 065503 (2009).
- [26] A. Hatef, S. M. Sadeghi, and M. R. Singh, *Nanotechnology* **23**, 065701 (2012).
- [27] C. Ding, J. Li, A. Zheng, and X. Yang, *Physica E* **43**, 1494 (2011).

- [28] C. Ding, J. Li., X. Yang, and X.-Y. Lü, *Phys. Scr.* **83**, 055405 (2011).
- [29] M. R. Singh, *J. Mod. Opt.* **56**, 758 (2009).
- [30] W.-H. Chang, W.-Y. Chen, H.-S. Chang, T.-P. Hsieh, J.-I. Chyi, and T.-M. Hsu, *Phys. Rev. Lett.* **96**, 117401 (2006).
- [31] M. Barth, R. Schuster, A. Gruber, and F. Cichos, *Phys. Rev. Lett.* **96**, 243902 (2006), and references therein.
- [32] X. Zhang, Y. Liu, S.-T. Lee, S. Yang, and Z. Kang, *Energy Environ. Sci.* **7**, 1409 (2014).
- [33] X. Zhang, S. Feng, J. Zhang, T. Zhai, H. Liu, and Z. Pang, *Sensors* **12**, 12082 (2012).
- [34] T. van der Sar, J. Hagemeier, W. Pfaff, E. Heeres, S. Thon, H. Kim, P. Petroff, O. Tjerk, D. Bouwmeester, and R. Hanson, *J. Opt. Soc. Am. B* **29**, 698 (2012).
- [35] Y. Liu, H. Yu, S. Chen, X. Quan, and H. Zhao, *Environ. Sci. Technol.* **46**, 1724 (2012).
- [36] K. Busch and S. John, *Phys. Rev. Lett.* **83**, 967 (1999).
- [37] O. Toader and S. John, *Science* **292**, 1133 (2001).
- [38] P. Yeh, *Optical Waves In Layered Media* (John Wiley & Sons, New York, 1988), p.337.
- [39] M. Plihal and A. A. Maradudin, *Phys. Rev. B* **44**, 8565 (1991).
- [40] P. Villeneuve and M. Piche, *Phys. Rev. B* **46**, 4969 (1992).
- [41] D. R. Smith, R. Dalichaouch, N. Kroll, S. Schultz, S. L. McCall, and P. M. Platzman, *J. Opt. Soc. Am. B* **10**, 314 (1993).
- [42] S. Noda, N. Yamamoto, H. Kobayashi, M. Okano, and K. Tomoda, *App. Phys. Lett.* **75**, 905 (1999).
- [43] A. Feigel, Z. Kotler, B. Sfez, A. Arsh, M. Klebanov, and V. Lyubin, *App. Phys. Lett.* **77**, 3221 (2000).
- [44] A. Chelnokov, K. Wang, S. Rowson, P. Garoche, and J.-M. Lourtioz, *App. Phys. Lett.* **77**, 2943 (2000).
- [45] C. Cuisin, A. Chelnokov, D. Decanini, D. Peyrade, Y. Chen, and J.-M. Lourtioz, *Optical and Quantum Electronics* **34**, 13 (2002).
- [46] S. M. Sadeghi and W. Li, *Phys. Rev. B* **69**, 045311 (2004).
- [47] H. Y. Ling, P. Maenner, and H. Pu, *Phys. Rev. A* **72**, 013608 (2005).
- [48] B. P. Hou, S. J. Wang, W. L. Yu, and W. L. Sun, *Phys. Rev. A* **69**, 053805 (2004).
- [49] C. Kittel, *Introduction to Solid State Physics* (John Wiley & Sons, New York, 1996), p.287.
- [50] V. I. Rupasov and M. R. Singh, *Phys. Lett. A* **222**, 258 (1996).

- [51] A. Godone, F. Levi, S. Micalizio, and C. Calosso, *Phys. Rev. A* **70**, 012508 (2004).
- [52] A. B. Post, Y.-Y. Jau, N. N. Kuzma, and W. Happer, *Phys. Rev. A* **72**, 033417 (2005).
- [53] R. Santra, E. Arimondo, T. Ido, C. H. Greene, and J. Ye, *Phys. Rev. Lett.* **94**, 173002 (2005).
- [54] M. R. Singh and W. Lau, *Phys. Stat. Sol. (b)* **203**, 401 (1997).
- [55] M. R. Singh and W. Lau, *Phys. Lett. A* **231**, 115 (1997).
- [56] M. R. Singh, *Phys. Rev. B* **75**, 155427 (2007).
- [57] J. P. Dowling and C. M. Bowden, *Phys. Rev. Lett.* **70**, 1421 (1993)
- [58] J. P. Dowling and C. M. Bowden, *Phys. Rev. A* **47**, 1247 (1993).
- [59] A. S. Manka, J. P. Dowling, C. M. Bowden, and M. Fleischhauer, *Phys. Rev. Lett.* **73**, 1789 (1994).
- [60] O. G. Calderón, M. A. Anton, and F. Careno, *Eur. Phys. J. D* **25**, 77 (2003).
- [61] A. A. Afansev, L. S. Gaida, and A. I. Martinovich, *J. Appl. Spectrosc.* **72**, 68 (2005).
- [62] J.-H. Li, J.-B. Liu, J.-M. Luo, and X.-T. Xie, *Commun. Theor. Phys.* **45**, 1102 (2006).
- [63] G.-F. Zhang and Z.-Y. Chen, *Opt. Comm.* **275**, 274 (2007).
- [64] M. Reboiro, *Phys. Scr.* **78**, 045006 (2008).
- [65] O. Civitarese, M. Reboiro, L. Rebón, and D. Tielas, *Phys. Lett. A* **374**, 2117 (2010).
- [66] R. A. Vlasov, A. M. Lemeza, and M. G. Gladush, *J. Appl. Spectrosc.* **80**, 698 (2013).
- [67] F. M. Ablayev, S. N. Andrianov, S. A. Moisev, and A. V. Vasiliev, *Lobachevskii J. Math.* **34**, 291 (2013).
- [68] I. Haque and M. R. Singh, *AIP Conf. Proc.* **772**, 1246 (2005).
- [69] M. R. Singh and I. Haque, *Phys. Stat. Sol. (c)* **2**, 2998 (2005).
- [70] M. R. Singh, *Phys. Rev. A* **69**, 023807 (2004).
- [71] M. R. Singh, *J. Phys. B: At. Mol. Opt. Phys.* **39**, 5131 (2006).
- [72] M. R. Singh, *Phys. Lett. A* **363**, 177 (2007).
- [73] M. R. Singh, *J. Phys. B: At. Mol. Opt. Phys.* **40**, 675 (2007).
- [74] M. R. Singh, *Phys. Lett. A* **372**, 5083 (2008).
- [75] D. V. Novitsky and S. Y. Mikhnevich, *Optika I Spektroskopiya* **104**, 987 (2008).
- [76] D. V. Novitsky and S. Y. Mikhnevich, *J. Appl. Spectrosc.* **77**, 232 (2010).
- [77] J. Wang, L. Jiang, H. Zhang, T.-H. Huang, and H.-Z. Zhang, *Opt. Comm.* **284**, 5323 (2011).

- [78] M. R. Singh, *J. Mod. Opt.* **56**, 758 (2009).
- [79] M. R. Singh, C. Racknor, and D. Schindel, *Appl. Phys. Lett.* **101**, 051115 (2012).
- [80] J. D. Cox, M. R. Singh, G. Gumbs, M. A. Anton, and F. Carreno, *Phys. Rev. B* **86**, 125452 (2012).
- [81] E. Arimondo, *Progress in Optics* **35**, edited by E. Wolf (Elsevier, Amsterdam, 1996), p. 257, and references therein.
- [82] J. Mompart and R. Corbalán, *J. Opt. B* **2**, R7 (2000), and references therein.
- [83] S. E. Harris and J. H. Macklin, *Phys. Rev. A* **40**, 4135 (1989).
- [84] M. O. Scully and M. S. Zubairy, *Quantum Optics* (Cambridge University Press, Cambridge, 1997).
- [85] G. Alzetta, A. Gozzini, L. Moi, and G. Orriols, *Nuovo Cimento B* **36**, 5 (1976).
- [86] R. Whitley and C. Stroud, *Phys. Rev. A* **14**, 1498 (1976).
- [87] H. Gray, R. M. Whitley, and C. R. Stroud, Jr., *Opt. Lett.* **3**, 218 (1978).
- [88] G. P. Agrawal, *Phys. Rev. A* **24**, 1399 (1981).
- [89] G. S. Agarwal and W. Harshawardhan, *Phys. Rev. Lett.* **77**, 1039 (1996).
- [90] W. Guerin, N. Mercadier, F. Michaud, D. Brivio, L. S. Froufe-Pérez, R. Carminati, V. Ereameev, A. Goetschy, S. E. Skipetrov, and R. Kaiser, *J. Opt.* **12**, 024002 (2010).
- [91] J.-Y. Gao, S.-H. Yang, D. Wang, X.-Z. Guo, K.-X. Chen, Y. Jiang, and B. Zhao, *Phys. Rev. A* **61**, 023401 (2000).
- [92] V. G. Arkhipkin and I. V. Timofeev, *Phys. Rev. A* **73**, 025803 (2006).
- [93] M. Paternostro and M. S. Kim, *Phys. Rev. A* **67**, 023811 (2003).
- [94] S. Scheel, J.K. Pachos, E.A. Hinds, and P.L. Knight, *Quantum Gates and Decoherence, Lect. Notes Phys.* **689**, 47 (2006).
- [95] S. Gateva, E. Alipieva, and E. Taskova, *Phys. Rev. A* **72**, 025805 (2005).
- [96] S. Gateva, L. Petrov, E. Alipieva, G. Todorov, V. Domelunksen, and V. Polischuk, *Phys. Rev. A* **76**, 025401 (2007).
- [97] S. Gateva, L. Gurdev, E. Alipieva, E. Taskova, and G. Todorov, *J. Phys. B: At. Mol. Opt. Phys.* **44**, 035401 (2011).
- [98] H. Guo, G. Li, and J. Peng, *Phys. Lett. A* **300**, 147 (2002).
- [99] C. Affolderbach, S. Knappe, R. Wynands, A. V. Taichenachev, and V. I. Yudin, *Phys. Rev. A* **65**, 043810 (2002).
- [100] A.-S. F. Obada, H. A. Hessian, and A.-B. A. Mohamed, *J. Mod. Opt.* **56**, 881 (2009).
- [101] A. Mortezaipoor, M. Abedi, M. Mahmoudi, and M. R. H. Khajepour, *J. Phys. B: At. Mol. Opt. Phys.* **44**, 085501 (2011).

- [102] M. Macovei, J. Evers, and C. H. Keitel, *Phys. Rev. Lett.* **91**, 233601 (2003).
- [103] S.-Y. Gao, F.-L. Li, and D.-L. Cai, *J. Phys. B: At. Mol. Opt. Phys.* **40**, 3893 (2007).
- [104] G. Morigi, *Phys. Rev. A* **67**, 033402 (2003).
- [105] V. G. Arkhipkin and I. V. Timofeev, *Phys. Rev. A* **64**, 053811 (2001).
- [106] B. P. Hou, S. J. Wang, W. L. Yu, and W. L. Sun, *J. Phys. B: At. Mol. Opt. Phys.* **39**, 2335 (2006).
- [107] G. Yang, M. Xie, Z. Zhang, and K. Wang, *Phys. Rev. A* **77**, 063825 (2008).
- [108] B.-Q. Ou, L.-M. Liang, and C.-Z. Li, *Opt. Comm.* **281**, 4940 (2008).
- [109] X. Q. Jiang and X. D. Sun, *Opt. Comm.* **282**, 922 (2009).
- [110] F. Li and S.-Y. Zhu, *Opt. Comm.* **162**, 155 (1999).
- [111] A. Imamoğlu, H. Schmidt, G. Woods, and M. Deutsch, *Phys. Rev. Lett.* **79**, 1467 (1997).
- [112] A. Karawajczyk, J. Zakrzewski, and W. Gawlik, *Phys. Rev. A* **45**, 420 (1992).
- [113] S. Rebić, A. S. Parkins, and S. M. Tan, *Phys. Rev. A* **65**, 043806 (2002).
- [114] S. Rebić, D. Vitali, C. Ottaviani, P. Tombesi, M. Artoni, F. Cataliotti, and R. Corbalán, *Phys. Rev. A* **70**, 032317 (2004).
- [115] M. L. Ladrón de Guevara, and M. Orszag, *Opt. Comm.* **202**, 303 (2002).
- [116] S. N. Sandhya, *J. Phys. B: At. Mol. Opt. Phys.* **40**, 837 (2007).
- [117] S. R. Entezar, H. Vahed, and H. Tajalli, *J. Phys. B: At. Mol. Opt. Phys.* **40**, 2927 (2007).
- [118] R. Yu, J. Li, P. Huang, A. Zheng, and X. Yang, *Phys. Lett. A* **373**, 2992 (2009).
- [119] M. Xie and G. Yang, *Opt. Comm.* **282**, 1819 (2009).
- [120] X. Yang, Y. Huang, Z. Zhang, and X. Yan, *Opt. Comm.* **285**, 2101 (2012).
- [121] B.-Q. Ou, L.-M. Liang, and C.-Z. Li, *J. Phys. B: At. Mol. Opt. Phys.* **42**, 205503 (2009).
- [122] M. Mahmoudi, S. M. Mousavi, and M. Sahrai, *Eur. Phys. J. D* **57**, 241 (2010).
- [123] D. Aumiler, *Phys. Rev. A* **82**, 055402 (2010).
- [124] J. Q. Shen, *Opt. Comm.* **283**, 4546 (2010).
- [125] J. Qi, *Phys. Scr.* **81**, 015402 (2010).
- [126] L. Fang and J. Gao, *Optik* **124**, 6539 (2013).
- [127] M. R. Doery, R. Gupta, T. Bergeman, and H. Metcalf, *Phys. Rev. A* **51**, 2334 (1995).
- [128] H. Kanokogi and K. Sakurai, *Phys. Rev. A* **53**, 2650 (1996).

- [129] Y. Gu, L. Wang, K. Wang, C. Yang, and Q. Gong, *J. Phys. B: At. Mol. Opt. Phys.* **39**, 463 (2006).
- [130] J. F. Dynes, M. D. Frogley, J. Rodger, and C. C. Phillips, *Phys. Rev. B* **72**, 085323 (2005).
- [131] A. Imamoğlu, *Phys. Stat. Sol. (b)* **243**, 3725 (2006).
- [132] W. Chua, S. Duan, and J.-L. Zhua, *Appl. Phys. Lett.* **90**, 222102 (2007).
- [133] A. K. Patnaik, P. S. Hsu, G. S. Agarwal, G. R. Welch, and M. O. Scully, *Phys. Rev. A* **75**, 023807 (2007).
- [134] M. Z. Maialle and M. H. Degani, *Phys. Rev. B* **83**, 155308 (2011).
- [135] A. N. Litvinov, K. A. Barantsev, B. G. Matisov, G. A. Kazakov, and Y. V. Rozhdestvensky, *Opt. Comm.* **305**, 155 (2013).
- [136] L. E. E. de Araujo, *Phys. Rev. A* **69**, 013408 (2004).
- [137] K. C. Fu, C. Santori, C. Stanley, M. C. Holland, and Y. Yamamoto, *Phys. Rev. Lett.* **95**, 187405 (2005).
- [138] G. Bevilacqua, V. Biancalana, E. Breschi, Y. Dancheva, L. Moi, C. Andreeva, S. Cartaleva, and T. Karaulanov, *Phys. Rev. Lett.* **95**, 123601 (2005).
- [139] R. Kolesov, *Phys. Rev. A* **72**, 051801 (2005).
- [140] L. Margalit, M. Rosenbluh, and A. D. Wilson-Gordon, *Phys. Rev. A* **85**, 063809 (2012).
- [141] L. Margalit, M. Rosenbluh, and A. D. Wilson-Gordon, *Phys. Rev. A* **87**, 033808 (2013).
- [142] L. Margalit, M. Rosenbluh, and A. D. Wilson-Gordon, *Phys. Rev. A* **88**, 023827 (2013).
- [143] J. Yang, Y. Tian, B. Tan, P. Yun, and S. Gu, *J. Appl. Phys.* **115**, 093109 (2014).
- [144] E. Arimondo, *Progress in Optics* **35**, edited by E. Wolf (Elsevier Science, Amsterdam, 1996).
- [145] J. P. Marangos, *J. Mod. Opt.* **45**, 471 (1998).
- [146] M. D. Lukin, *Rev. Mod. Phys.* **75**, 457 (2003).
- [147] S. E. Harris, *Phys. Rev. Lett.* **62**, 1033 (1989).
- [148] L. M. Narducci, H. M. Doss, P. Ru, M. O. Scully, S.-Y. Zhu, and C. Keitel, *Opt. Comm.* **81**, 379 (1991).
- [149] O. A. Kocharovskaya, A. B. Matsko, and Y. Rostovtsev, *Phys. Rev. A* **65**, 013803 (2001).
- [150] K.-J. Boller, A. Imamoğlu, and S. E. Harris, *Phys. Rev. Lett.* **66**, 2593 (1991).
- [151] S. E. Harris, *Physics Today* **50**, 36 (1997).
- [152] C. L. Bentley, Jr., J. Liu, and Y. Liao, *Phys. Rev. A* **61**, 023811 (2000).

- [153] M. Fleischhauer, A. Imamoglu, and J. P. Marangos, *Rev. Mod. Phys.* **77**, 633 (2005).
- [154] M. O. Scully, *Phys. Rev. Lett.* **67**, 1855 (1991).
- [155] S. E. Harris, J. E. Field, and A. Kasapi, *Phys. Rev. A* **46**, R29 (1992).
- [156] C. Szymanowski and C. H. Keitel, *J. Phys. B* **27**, 5795 (1994).
- [157] A. S. Zibrov, M. D. Lukin, L. Hollberg, D. E. Nikonov, M. O. Scully, H. G. Robinson, and V. L. Velichansky, *Phys. Rev. Lett.* **76**, 3935 (1996).
- [158] S. H. Autler and C. H. Townes, *Phys. Rev.* **100**, 703 (1955).
- [159] C. Cohen-Tannoudji and S. Reynaud, *J. Phys. B* **10**, 345 (1977), and references therein.
- [160] N. B. Delone and V. P. Kraĭnov, *Phys. Usp.* **42**, 669 (1999), and references therein.
- [161] A. Schabert, R. Keil, and P. E. Toschek, *Opt. Comm.* **13**, 265 (1975).
- [162] B. R. Mollow, *Phys. Rev. A* **5**, 1522 (1972).
- [163] C. Delsart and J.-C. Keller, *J. Phys. B* **9**, 2769 (1976).
- [164] J. E. Bjorkholm and P. F. Liao, *Opt. Comm.* **21**, 132 (1977).
- [165] H. R. Gray and C. R. Stroud, Jr., *Opt. Comm.* **25**, 359 (1978).
- [166] P. T. H. Fisk, H.-A. Bachor, and R. J. Sandeman, *Phys. Rev. A* **34**, 4762 (1986).
- [167] M. Jakob and G. Y. Kryuchkyan, *Phys. Rev. A* **57**, 1355 (1998).
- [168] X.-F. He, P. T. H. Fisk, and N. B. Manson, *J. Appl. Phys.* **72**, 211 (1992).
- [169] P. Yi, M. Song, Y. Liu, R. W. Field, L. Li, and A. M. Lyyra, *Opt. Comm.* **233**, 131 (2004).
- [170] V. A. Sautenkov, Y. V. Rostovtsev, and E. R. Eliel, *Phys. Rev. A* **78**, 013802 (2008).
- [171] Y. Li, L. Li, and Y. Zhang, *J. Mod. Opt.* **57**, 885 (2010).
- [172] A. D. Slepikov, A. R. Bhagwat, V. Venkataraman, P. Londero, and A. L. Gaeta, *Phys. Rev. A* **81**, 053825 (2010).
- [173] D. E. Sikes and D. D. Yavuz, *Opt. Comm.* **283**, 556 (2010).
- [174] D. Miletić, T. Bandi, C. Affolderbach, and G. Mileti, *Phys. Scr.* **T149**, 014012 (2012).
- [175] Y. O. Dudin, L. Li, and A. Kuzmich, *Phys. Rev. A* **87**, 031801(R) (2013).
- [176] J.-L. Robyr, P. Knowles, and A. Weis, *Phys. Rev. A* **90**, 012505 (2014).
- [177] B. K. Teo, D. Feldbaum, T. Cubel, J. R. Guest, P. R. Berman, and G. Raithel, *Phys. Rev. A* **68**, 053407 (2003).
- [178] R. Garcia-Fernandez, A. Ekers, J. Klavins, L. P. Yatsenko, N. N. Bezuglov, B. W. Shore, and K. Bergmann, *Phys. Rev. A* **71**, 023401 (2005).



- [179] C. Ates, T. Pohl, T. Pattard, and J. M. Rost, *Phys. Rev. Lett.* **98**, 023002 (2007).
- [180] P. Bohlouli-Zanjani, J. A. Petrus, and J. D. D. Martin, *Phys. Rev. Lett.* **98**, 203005 (2007).
- [181] J. A. Petrus, P. Bohlouli-Zanjani, and J. D. D. Martin, *J. Phys. B: At. Mol. Opt. Phys.* **41**, 245001 (2008).
- [182] P. J. Windpassinger, D. Oblak, U. B. Hoff, J. Appel, N. Kjærgaard, and E. S. Polzik, *New J. Phys.* **10**, 053032 (2008).
- [183] A. Tauschinsky, C. S. E. van Ditzhuijzen, L. D. Noordam, and H. B. van Linden van den Heuvell, *Phys. Rev. A* **78**, 063409 (2008).
- [184] B. M. Sparkes, M. Hosseini, G. Hétet, P. K. Lam, and B. C. Buchler, *Phys. Rev. A* **82**, 043847 (2010).
- [185] D. Farkas, A. Zozulya, and D. Anderson, *Appl. Phys. B* **101**, 705 (2010).
- [186] N. Souther, R. Wagner, P. Harnish, M. Briel, and S. Bali, *Laser Phys. Lett.* **7**, 321 (2010).
- [187] V. V. Ivanov and S. Gupta, *Phys. Rev. A* **84**, 063417 (2011).
- [188] F. L. Kien, P. Schneeweiss, and A. Rauschenbeutel, *Phys. Rev. A* **88**, 033840 (2013).
- [189] V. V. Ivanov, *Opt. Comm.* **324**, 258 (2014).
- [190] J. von Zanthier, C. Skornia, G. S. Agarwal, and H. Walther, *Phys. Rev. A* **63**, 013816 (2000).
- [191] J. A. Sherman, T. W. Koerber, A. Markhotok, W. Nagourney, and E. N. Fortson, *Phys. Rev. Lett.* **94**, 243001 (2005).
- [192] M. Haas, U. D. Jentschura, and C. H. Keitel, *Am. J. Phys.* **74**, 77 (2006).
- [193] J.-M. Pirkkalainen, S. U. Cho, J. Li, G. S. Paraoanu, P. J. Hakonen, and M. A. Sillanpää, *Nature* **494**, 211 (2013).
- [194] B. Girard, G. O. Sitz, R. N. Zare, N. Billy, and J. Vigué, *J. Chem. Phys.* **97**, 26 (1992).
- [195] S. Xu, G. Sha, B. Jiang, W. Sun, X. Chen, and C. Zhang, *J. Chem. Phys.* **100**, 6122 (1994).
- [196] J. Qi, G. Lazarov, X. Wang, L. Li, L. M. Narducci, A. M. Lyyra, and F. C. Spano, *Phys. Rev. Lett.* **83**, 288 (1999).
- [197] X. Xu, B. Sun, P. R. Berman, D. G. Steel, A. S. Bracker, D. Gammon, and L. J. Sham, *Science* **317**, 929 (2007).
- [198] B. J. Sussman, D. Townsend, M. Y. Ivanov, and A. Stolow, *Science* **314**, 278 (2006).
- [199] B. J. Sussman, *Am. J. Phys.* **79**, 477 (2011).

- [200] B. Y. Changa, H. Choia, S. Shina, S. Leeb, and I. R. Sola, *J. Mod. Opt.* **56**, 811 (2009).
- [201] R. Shimano and M. Kuwata-Gonokami, *Phys. Rev. Lett.* **72**, 530 (1994).
- [202] C. J. M. Tavares, M. A. Costa Neto, R. Sitters, N. B. Manson, and M. Glasbeek, *Phys. Rev. B* **50**, 13795 (1994).
- [203] A. N. Vamivakas, Y. Zhao, C.-Y. Lu, and M. Atatüre, *Nature Physics* **5**, 198 (2009).
- [204] L. Yang, L. Zhang, X. Li, L. Han, G. Fu, N. B. Manson, D. Suter, and C. Wei, *Phys. Rev. A* **72**, 053801 (2005).
- [205] Y. S. Bai, T. W. Mossberg, N. Lu, and P. R. Berman, *Phys. Rev. Lett.* **57**, 1692 (1986).
- [206] S. Qamar, S.-Y. Zhu, and M. S. Zubairy, *J. Opt. B* **5**, 175 (2003).
- [207] D. McGloin, *J. Phys. B* **36**, 2861 (2003).
- [208] X.-M. Hu, J. Xiong, and J.-S. Peng, *Eur. Phys. J. D* **13**, 401 (2001).
- [209] F. W. Strauch, S. K. Dutta, H. Paik, T. A. Palomaki, K. Mitra, B. K. Cooper, R. M. Lewis, J. R. Anderson, A. J. Dragt, C. J. Lobb, and F. C. Wellstood, *IEEE Transactions on Applied Superconductivity* **17**, 105 (2007).
- [210] T. Y. Abi-Salloum, *J. Mod. Opt.* **57**, 1366 (2010).
- [211] D. Bimberg, M. Grundmann, and N. N. Ledentsov, *Quantum Dot Heterostructures* (John Wiley & Sons, Chichester, 1999).
- [212] P. Harrison, *Quantum Wells, Wires and Dots* (John Wiley & Sons, Chichester, 2005).
- [213] A. Barenco, D. Deutsch, A. Ekert, and R. Jozsa, *Phys. Rev. Lett.* **74**, 4083 (1995).
- [214] M. Bayer, O. Stern, P. Hawrylak, S. Fafard, and A. Forchel, *Nature* **405**, 923 (2000).
- [215] P. Michler, A. Imamoğlu, M. D. Mason, P. J. Carson, G. F. Strouse, and S. K. Buratto, *Nature* **406**, 968 (2000).
- [216] H. Kamada, H. Gotoh, J. Temmyo, T. Takagahara, and H. Ando, *Phys. Rev. Lett.* **87**, 246401 (2001).
- [217] D. V. Regelman, U. Mizrahi, D. Gershoni, E. Ehrenfreund, W. V. Schoenfeld, and P. M. Petroff, *Phys. Rev. Lett.* **87**, 257401 (2001).
- [218] W. W. Chow, H. C. Schneider, and M. C. Phillips, *Phys. Rev. A* **68**, 053802 (2003).
- [219] T. Y. Zhang, W. Zhao, J. C. Cao, and G. Qasim, *J. Appl. Phys.* **98**, 094311 (2005).
- [220] T. Y. Zhang and W. Zhao, *Phys. Rev. B* **73**, 245337 (2006).
- [221] J. F. Dynes, M. D. Frogley, M. Beck, J. Faist, and C. C. Phillips, *Phys. Rev. Lett.* **94**, 157403 (2005).

- [222] C. Wei, D. Suter, A. S. W. Winsdor, and N. B. Manson, *Phys. Rev. A* **58**, 2310 (1998).
- [223] A. Narayanan, R. Srinivasan, U. K. Khan, A. Vudayagiri, and H. Ramachandran, *Eur. Phys. J. D* **31**, 107 (2004).
- [224] A. Narayanan, *Eur. Phys. J. D* **39**, 13 (2006).
- [225] J. Sun, Z. Zuo, X. Mi, Z. Yu, Q. Jiang, Y. Wang, L.-A. Wu, and P. Fu, *Phys. Rev. A* **70**, 053820 (2004).
- [226] M. R. Singh, *Opt. Lett.* **19**, 2909 (2009).
- [227] A. Hatef and M. R. Singh, *Opt. Comm.* **284**, 2363 (2011).
- [228] J. D. Cox, M. R. Singh, C. Racknor, and R. Agarwal, *Nano Letters* **11**, 5284 (2011).
- [229] A. Goban, C.-L. Hung, S.-P. Yu, J. D. Hood, J. A. Muniz, J. H. Lee, M. J. Martin, A. C. McClung, K. S. Choi, D. E. Chang, O. Painter, and H. J. Kimble, *Nature Communications* **5**: 3808 (2014).
- [230] H. Nihei and A. Okamoto, *J Mod. Opt.* **51**, 1983 (2004).
- [231] H.-Z. Zhang, J. B. Yang, and S. H. Tang, *J. Mod. Opt.* **50**, 1649 (2003).
- [232] H.-Z. Zhang, S. H. Tang, P. Dong, and J. He, *Phys. Rev. A* **65**, 063802/1 (2002).
- [233] S.-Y. Zhu, H. Chen, and H. Huang, *Phys. Rev. Lett.* **79**, 205 (1997).
- [234] Y. Yang and S.-Y. Zhu, *Phys. Rev. A* **61**, 043809/1 (2000).
- [235] J.-P. Xu, N.-H. Liu, and S.-Y. Zhu, *Phys. Rev. E* **73**, 016604 (2006).
- [236] J.-P. Xu and Y.-P. Yang, *Opt. Comm.* **268**, 99 (2006).
- [237] C.-H. Huang, S.-C. Cheng, J.-N. Wu, and W.-F. Hsieh, *J. Phys.: Condens. Matter* **23**, 225301 (2011).
- [238] J.-N. Wu, C.-H. Huang, S.-C. Cheng, and W.-F. Hsieh, *Phys. Rev. A* **81**, 023827 (2010).
- [239] K. Zhang, H. Zhang, and H.-Z. Zhang, *J. Mod. Opt.* **54**, 33 (2007).
- [240] S. Yang, M. Al-Amri, S.-Y. Zhu, and M. S. Zubairy, *Phys. Rev. A* **87**, 033818 (2013).
- [241] C.-H. Huang, J.-N. Wu, Y.-Y. Li, S.-C. Cheng, and W.-F. Hsieh, *Phys. Rev. A* **84**, 013802 (2011).
- [242] S. Y. Xie and Y. P. Yang, *Eur. Phys. J. D* **42**, 163 (2007).
- [243] L. Jiang, S. Du, R.-G. Wan, J. Kou, H. Zhang, and H.-Z. Zhang, *Opt. Comm.* **283**, 3714 (2010).
- [244] X.-S. Huang, H.-L. Liu, and C.-X. Ding, *J. Mod. Opt.* **60**, 128 (2013).
- [245] L. Jiang, H. Zhang, and H.-Z. Zhang, *J. Mod. Opt.* **56**, 1713 (2009).
- [246] C. Ding, J. Li, and X. Yang, *Opt. Comm.* **284**, 4550 (2011).

- [247] D. Zhang, J. Li, C. Ding, and X. Yang, *Phys. Lett. A* **376**, 1978 (2012).
- [248] C. Ding, J. Li, and X. Yang, *Appl. Phys. B* **103**, 669 (2011).
- [249] I. de Vega and D. Alonso, *Phys. Rev. A* **77**, 043836 (2008).
- [250] S. R. Entezar, *Phys. Lett. A* **373**, 3413 (2009).
- [251] H. Takeda and S. John, *Phys. Rev. A* **83**, 053811 (2011).
- [252] X. Sun, B. Zhang, and X. Jiang, *Opt. Comm.* **281**, 5194 (2008).
- [253] N. Foroozani, M. M. Golshan, and M. Mahjoei, *Phys. Rev. A* **76**, 015801 (2007).
- [254] S.-C. Cheng, J.-N. Wu, T.-J. Yang, and W.-F. Hsieh, *Phys. Rev. A* **79**, 013801 (2009).
- [255] H. Zhang, G. Qiang Liu, and H.-Z. Zhang, *Can. J. Phys.* **85**, 981 (2007).
- [256] D. Yang, J. Wang, H.-Z. Zhang, and J. Yao, *J. Phys. B: At. Mol. Opt. Phys.* **40**, 1719 (2007).
- [257] X. Q. Jiang, B. Zhang, and X. D. Sun, *J. Phys. B: At. Mol. Opt. Phys.* **41**, 065508 (2008).
- [258] C.-X. Song, J.-H. Huang, and N.-H. Liu, *Opt. Comm.* **284**, 1598 (2011).
- [259] B. Zhang, X. Sun, and X. Jiang, *Optik* **122**, 1262 (2011).
- [260] D. Zhang, J. Li, C. Ding, and X. Yang, *Opt. Comm.* **285**, 3612 (2012).
- [261] M. R. Singh, *Phys. Rev. B* **80**, 195303 (2009).
- [262] M. R. Singh and C. Racknor, *Phys. Rev. B* **82**, 155130 (2010).
- [263] S. Gozzini, S. Cartaleva, A. Lucchesini, C. Marinelli, L. Marmugi, D. Slavov, and T. Karaulanov, *Eur. Phys. J. D* **53**, 153 (2009).
- [264] G. P. Zhang and T. F. George, *Phys. Rev. A* **88**, 063808 (2013).
- [265] M. R. Singh, *Research Topics and Developments in Chemical Physics: From Quantum Scale to Macroscale*, edited by A. F. Terzis and E. Paspalakis (Transworld Research Network, Kerala, 2008), Chap. 5.
- [266] A. D. Greentree, D. Richards, J. A. Vaccaro, A. V. Durrant, S. R. de Echaniz, D. M. Segal, and J. P. Marangos, *Phys. Rev. A* **67**, 23818 (2003).
- [267] Y. V. Rostovtsev, A. B. Matsko, and M. O. Scully, *Phys. Rev. A* **57**, 4919 (1998).
- [268] H. F. Zhang, J.-H. Wu, X.-M. Su, and J.-Y. Gao, *Phys. Rev. A* **66**, 53816 (2002).
- [269] A. D. Wilson-Gordon, and H. Friedmann, *J. Mod. Optics* **49**, 125 (2002).
- [270] M. R. Singh, *J. Mod. Opt.* **54**, 1739 (2007).
- [271] D. Suter, *The Physics of Laser-Atom Interactions* (Cambridge University Press, Cambridge, 1997).
- [272] G. F. Mazenko, *Quantum Statistical Mechanics* (Wiley Inc., New York, 2000).
- [273] M. R. Singh, *Phys. Rev. A* **70**, 033813 (2004).

- [274] M. D. Lukin and P. R. Hemmer, *Phys. Rev. Lett.* **84**, 2818 (2000).
- [275] M. Weissbluth, *Photon-Atom Interactions* (Academic Press, San Diego, 1988), Chap. 7.
- [276] C. Santori and Y. Yamamoto, *Nature Physics* **5**, 173 (2009).
- [277] B. R. Mollow, *Phys. Rev.* **188**, 1969 (1969).
- [278] E. Ahmed, A. Hansson, P. Qi, T. Kirova, A. Lazoudis, S. Kotochigova, A. M. Lyyrab, L. Li, J. Qi, and S. Magnier, *J. Chem. Phys.* **124**, 084308 (2006).
- [279] M. R. Singh, *Phys. Rev. A* **75**, 033810 (2007).
- [280] R. W. Boyd, *IEEE Journal on Selected Topics in Quantum Electronics* **6**, 881 (2000), and references therein.
- [281] D. Bhattacharyya, *J. Opt. B* **6**, 563 (2004).
- [282] D. Petrosyan and G. Kurizki, *Phys. Rev. A* **64**, 023810 (2001).
- [283] A. G. Kofman, G. Kurizki, and B. Sherman, *J. Mod. Opt.* **41**, 353 (1994).
- [284] S. John and T. Quang, *Phys. Rev. A* **50**, 1764 (1994).
- [285] E. Paspalakis, N. J. Kylstra, and P. L. Knight, *Phys. Rev. A* **60**, R33 (1999).
- [286] C. Du, Z. Hu, and S. Li, *J. Opt. B: Quantum Semiclass. Opt.* **6**, 263 (2004).
- [287] P. Bermel, A. Rodriguez, S. G. Johnson, J. D. Joannopoulos, and M. Soljacic, *Phys. Rev. A* **74**, 043818 (2006).
- [288] T. Quang and S. John, *Phys. Rev. A* **56**, 4273 (1997).
- [289] I. de Vega, D. Alonso, and P. Gaspard, *Phys. Rev. A* **71**, 023812 (2005).
- [290] D. Mogilevtsev, S. Kilin, S. B. Cavalcanti, and J. M. Hickmann, *Phys. Rev. A* **72**, 043817 (2005).
- [291] D. Mogilevtsev and S. Kilin, *Phys. Rev. A* **69**, 053809 (2004).
- [292] D. Mogilevtsev, S. Kilin, and S. B. Cavalcanti, *Photonics Nanostr. - Fund. Appl.* **2**, 161 (2004).
- [293] D. Mogilevtsev, S. Kilin, and S. B. Cavalcanti, *Photonics Nanostr. - Fund. Appl.* **3**, 38 (2005).
- [294] M. Florescu, Private Communications, 2007.
- [295] M. Florescu, S. Scheel, H. Haeffner, H. Lee, D. Strekalov, P. L. Knight, and J. P. Dowling, *Europhys. Lett.* **69**, 945 (2005).
- [296] I. Haque and M. R. Singh, *Photonics 2004 – 7th International Conference on Optoelectronics, Fiber Optics & Photonics, Cochin, SPIE Elec. Conf. Proc.* (2004).
- [297] C. Y. Kuo and S. Y. Lu, *Appl. Phys. Lett.* **92**, 121919 (2008).
- [298] A. Hatef and M. R. Singh, *Phys. Rev. A* **81**, 063816 (2010).
- [299] M. R. Singh, *Phys. Rev. B* **80**, 195303 (2009), and references therein.

- [300] T. Feurer, N. S. Stoyanov, D. W. Ward, J. C. Vaughan, E. R. Statz, and K. A. Nelson, *Annu. Rev. Mater. Res.* **37**, 317 (2007).
- [301] N. W. Ashcroft and N. D. Mermin, *Solid State Physics* (Saunders College, Philadelphia, 1976), pp.146-147.
- [302] E. Merzbacher, *Quantum Mechanics* (Wiley, New York, 1980), p.108.
- [303] M. R. Singh, *Electronic, Photonic, Polaritonic and Plasmonic Materials* (John Wiley & Sons, Inc., London, 2014).
- [304] J. Mathews and R. L. Walker, *Mathematical Methods of Physics* - 2nd edition (Addison-Wesley, California, 1971).
- [305] E. Fehlberg, *Low-order Classical Runge-Kutta Formulas with Step Size Control and their Application to some Heat Transfer Problems* (NASA Technical Report 315, 1969).
- [306] A. Majumdar, N. Manquest, A. Faraon, and J. Vučković, *Opt. Express* **18**, 3974 (2010).
- [307] D. Englund, A. Faraon, I. Fushman, N. Stoltz, P. Petroff and J. Vučković, *Nature* **450**, 857 (2007).
- [308] I. Fushman , D. Englund, A. Faraon, , N. Stoltz, P. Petroff and J. Vučković, *Science* **320**, 769 (2008).

## Appendices

### Appendix A: One-dimensional Scalar Wave Equation

The one-dimensional scalar wave equation is obtained from the general Maxwell equation for electromagnetic waves in a medium with three-dimensional dielectric function  $\epsilon(\bar{x})$  [12]:

$$\nabla \times [\nabla \times E(\bar{x})] = \frac{\omega^2}{c^2} \epsilon(\bar{x}) E(\bar{x})$$

But, according to the property of the del operator:

$$\nabla \times [\nabla \times E(\bar{x})] = \nabla(\nabla \cdot E(\bar{x})) - \nabla^2 E(\bar{x})$$

Using the result on right hand side of this equation and simplifying to a scalar potential  $\phi$  in one dimension, we get:

$$\nabla(\nabla \phi) - \nabla^2 \phi = \frac{\omega^2}{c^2} \epsilon(x) \phi$$

Rearranging, we can write:

$$-\nabla^2 \phi - \frac{\omega^2}{c^2} \epsilon(x) \phi = -\nabla(\nabla \phi)$$

But the gradient of  $\nabla \phi = -\frac{\omega^2}{c^2} \epsilon(x) \phi$  [11], which gives:

$$-\nabla^2 \phi - \frac{\omega^2}{c^2} \epsilon(x) \phi = \frac{\omega^2}{c^2} \epsilon(x) \phi$$

### Appendix B: Photon Dispersion Relation in the Photonic Crystal Reservoir

The derivation of the photon dispersion relation is given in the Appendix of Reference [18]. The author considers the well-known Schrödinger equation in one dimension with a single potential well  $V(x) = -V_0$  for  $|x| < a$  ( $V(x) = 0$  otherwise):

$$-\frac{\hbar^2}{2m} \nabla^2 \phi + V(x) \phi = E \phi$$

where  $a$ , the diameter of the dielectric spheres in the photonic crystal, establishes the analogy between the sphere and the potential well. From Reference [301], the dispersion relation can then be obtained in terms of the transmission and reflection coefficients  $t$  and  $r$ , respectively, as follows:

$$\cos(kL) = -\frac{t^2 - r^2}{2t} e^{-i\kappa L} + \frac{1}{2t} e^{i\kappa L}$$

with

$$\kappa = \frac{\sqrt{2mE}}{\hbar}$$

Then, using the scattering matrix approach of Reference [302], the transmission and reflection coefficients can be determined from the wave function  $\varphi$  (since

$\varphi(x) = e^{i\kappa x} + r e^{-i\kappa x}$  for  $x < -a$  and  $\varphi(x) = t e^{i\kappa x}$ , for  $x > a$ ) as follows:

$$\begin{bmatrix} r \\ 1 \end{bmatrix} = \begin{bmatrix} \left\{ \cos(2\kappa'a) - \frac{i\eta^+}{2\kappa\kappa'} \sin(2\kappa'a) \right\} e^{2i\kappa a} & \frac{i\eta^-}{2\kappa\kappa'} \sin(2\kappa'a) \\ -\frac{i\eta^-}{2\kappa\kappa'} \sin(2\kappa'a) & \left\{ \cos(2\kappa'a) + \frac{i\eta^+}{2\kappa\kappa'} \sin(2\kappa'a) \right\} e^{-2i\kappa a} \end{bmatrix} \begin{bmatrix} 0 \\ t \end{bmatrix}$$

with  $\eta^\pm = (\kappa^2 \pm \kappa'^2) / \kappa\kappa'$ , where  $\kappa' = \sqrt{2m(E + V_0)} / \hbar$ .

Multiplying the matrices on the right-hand side of this equation, equating corresponding components of the resulting matrix to those of the matrix on the left-hand side, and rearranging, the following relations can be obtained:

$$\frac{t^2 - r^2}{2t} = e^{2i\kappa a} \left\{ 2 \cos(2\kappa'a) - i \frac{\eta^+}{\kappa\kappa'} \sin(2\kappa'a) \right\} = \left( \frac{1}{2t} \right)^*$$

The superscript \* denotes the complex conjugate. Using these in the expression for the dispersion relation gives:

$$\cos(kL) = \cos(2\kappa a - \kappa L) \cos(2\kappa'a) + \frac{\eta^+}{2} \sin(2\kappa a - \kappa L) \sin(2\kappa'a)$$



For the model of the photonic crystal used in this thesis (see the Appendix of Reference [18]),  $\kappa = \varepsilon_k / (ch)$ ,  $\kappa' = n\varepsilon_k / (ch)$  and  $\eta^+ = (1+n^2)/n$ . Substituting these expressions in the preceding equation:

$$\cos(kL) = \cos\left[\frac{(2a-L)\varepsilon_k}{ch}\right] \cos\left(\frac{2na\varepsilon_k}{ch}\right) + \frac{(1+n^2)}{2n} \sin\left[\frac{(2a-L)\varepsilon_k}{ch}\right] \sin\left(\frac{2na\varepsilon_k}{ch}\right)$$

But,  $L = 2a + b$ ,  $\sin(-\theta) = -\sin(\theta)$  and  $\cos(-\theta) = \cos(\theta)$ . Therefore:

$$\cos(kL) = \cos\left(\frac{b\varepsilon_k}{ch}\right) \cos\left(\frac{2na\varepsilon_k}{ch}\right) - \frac{(1+n^2)}{2n} \sin\left(\frac{b\varepsilon_k}{ch}\right) \sin\left(\frac{2na\varepsilon_k}{ch}\right)$$

or

$$2n \cos(kL) = 2n \cos\left(\frac{b\varepsilon_k}{ch}\right) \cos\left(\frac{2na\varepsilon_k}{ch}\right) - (1+n^2) \sin\left(\frac{b\varepsilon_k}{ch}\right) \sin\left(\frac{2na\varepsilon_k}{ch}\right)$$

Using the trigonometric identities  $\cos(\theta_1)\cos(\theta_2) = [\cos(\theta_1 - \theta_2) + \cos(\theta_1 + \theta_2)]/2$  and  $\sin(\theta_1)\sin(\theta_2) = [\cos(\theta_1 - \theta_2) - \cos(\theta_1 + \theta_2)]/2$ , the preceding equation can be written as follows:

$$\begin{aligned} 4n \cos(kL) = 2n & \left( \cos\left[\frac{(2na-b)\varepsilon_k}{ch}\right] + \cos\left[\frac{(2na+b)\varepsilon_k}{ch}\right] \right) \\ & - (1+n^2) \left( \cos\left[\frac{(2na-b)\varepsilon_k}{ch}\right] - \cos\left[\frac{(2na+b)\varepsilon_k}{ch}\right] \right) \end{aligned}$$

Noting that  $(1+n)^2 = 1+2n+n^2$  and  $(1-n)^2 = 1-2n+n^2$ , the expression finally yields:

$$4n \cos(kL) = \left( (1+n)^2 \cos\left[\frac{\varepsilon_k(2na+b)}{ch}\right] - (1-n)^2 \cos\left[\frac{\varepsilon_k(2na-b)}{ch}\right] \right)$$

### Appendix C: Reservoir, Field, and Interaction Hamiltonians

Without loss of generality, we consider a two-level atom as the doped nanoparticle, with states  $|a\rangle$  and  $|b\rangle$ .

The interaction between the doped nanoparticle and the photonic crystal is written in the dipole approximation as [303]:

$$H_{AR} = -p \cdot E_p$$

where  $p$  is the dipole moment induced in the nanoparticle due to a reservoir photon with field amplitude  $E_p$ . Then, using the raising and lowering operators:

$$H_{AR} = -\sum_i \sum_j |i\rangle \langle i| p |j\rangle \langle j| E_p = -\sum_{i=a,b} \sum_{j=a,b} |i\rangle \langle j| p_{ij} E_p = -\sum_{i=a,b} \sum_{j=a,b} \sigma_{ij} p_{ij} E_p$$

where  $p_{ij} = \langle i| p |j\rangle$  are the matrix elements of the dipole operator.

But, since  $p_{aa} = p_{bb} = 0$ :

$$H_{AR} = -p_{ab} (\sigma_{ba}^+ + \sigma_{ba}^-) E_p$$

with

$$\begin{aligned} \sigma_{ij}^+ &= |i\rangle \langle j| \\ \sigma_{ij}^- &= |j\rangle \langle i| \end{aligned}$$

These are the raising and lowering operators, respectively.

The interaction Hamiltonians can now be obtained by considering the electric field of the reservoir photon in the second quantized form.

#### Appendix D: Hamiltonian of the Nanoparticle I

Without loss of generality, we consider a two-level atom as the doped nanoparticle, with states  $|a\rangle$  (ground) and  $|b\rangle$  (excited), and the preserving, raising and lowering operators, respectively, as:

$$\begin{aligned} \sigma^z &= |b\rangle \langle b| - |a\rangle \langle a| \\ \sigma^+ &= |b\rangle \langle a| \\ \sigma^- &= |a\rangle \langle b| \end{aligned}$$

These are Pauli operators, obeying the following commutation relations:

$$\begin{aligned} [\sigma^z, \sigma^+] &= +2i\sigma^- \\ [\sigma^z, \sigma^-] &= -2i\sigma^+ \\ [\sigma^+, \sigma^-] &= \sigma^z \end{aligned}$$

Then, the Hamiltonian of the two-level nanoparticle can be written as:

$$H_A = \varepsilon_{ab} \left( \sigma^z + \frac{1}{2} \right)$$

where  $\varepsilon_{ab} = \varepsilon_b - \varepsilon_a$ .

## Appendix E: Dipole Approximation

In the dipole (or E1) approximation [60], for a vector potential

$$A(\mathbf{r}_0 + \mathbf{r}, t) = A(t)e^{ik \cdot (\mathbf{r}_0 + \mathbf{r})} = A(t)e^{ik \cdot \mathbf{r}_0} e^{ik \cdot \mathbf{r}} = A(t)e^{ik \cdot \mathbf{r}_0} (1 + ik \cdot \mathbf{r} + \dots)$$

the  $k \cdot \mathbf{r}$  and higher terms are ignored, reducing the potential to

$$A(\mathbf{r}_0 + \mathbf{r}, t) \approx A(t)e^{ik \cdot \mathbf{r}_0}$$

## Appendix F: Rotating Wave Approximation (RWA)

In the rotating wave approximation (RWA) [60], in deriving the interaction Hamiltonian between an atom and a field, the counter-rotating terms proportional to  $e^{\pm i(\omega + \nu)t}$  in the equations of motion of the amplitudes of the wave functions representing the atom pumped to different levels are ignored. In fact, in many cases, the counter-rotating terms never appear. Nevertheless, in all cases, the RWA gives a very good approximation for simplifying the analysis of complex atom-field systems

## Appendix G: Photonic Crystal Form Factor

The form factor of the photonic crystal is related to its density of states (DOS). Its derivation is as follows [303]:

In the equation for the density of states for photons in a photonic crystal, the summation over the photon wave vector  $k$  is written as

$$\sum_k = \int D(\varepsilon_k) d\varepsilon_k$$

where  $D(\varepsilon_k)$  is density of states. The summation over  $k$  can be replaced by

$$\sum_k = 2 \int \frac{\frac{4\pi}{3} k^2 dk}{(2\pi)^3 / \Omega}$$

where  $\Omega$  is the volume of the photonic crystal. The integration over  $k$  can be replaced by that over the photon energy  $\varepsilon_k$  as follows

$$\sum_k = \int \left( \frac{\Omega}{3\pi^2} k^2 \frac{dk}{d\varepsilon_k} \right) d\varepsilon_k = \int D(\varepsilon_k) d\varepsilon_k$$

So,  $D(\varepsilon_k)$  is written as:

$$D(\varepsilon_k) = \frac{\Omega}{3\pi^2} k^2 \frac{dk}{d\varepsilon_k}$$

This expression can be rewritten in the following form:

$$D(\varepsilon_k) = \frac{\Omega \varepsilon_k^2}{3\pi^2 (\hbar c)^2} \frac{dk}{d\varepsilon_k}$$

$$D(\varepsilon_k) = \left( \frac{\Omega \varepsilon_k^2}{3\pi^2 (\hbar c)^3} \right) \left( (\hbar c) \frac{dk}{d\varepsilon_k} \right)$$

where we have replaced  $k^2$  as  $\varepsilon_k^2 / (\hbar c)^2$ .

The expression within the first bracket above is the DOS of photons in free space. We denote it as  $D_0$  and write it as

$$D_0(\varepsilon_k) = \frac{\Omega \varepsilon_k^2}{3\pi^2 (\hbar c)^2}$$

Now, the DOS of photons in the photonic crystal can be written as

$$D(\varepsilon_k) = D_0(\varepsilon_k) \left( (\hbar c) \frac{dk}{d\varepsilon_k} \right)$$

The expression in the bracket above is expressed as

$$Z(\varepsilon_k) = \sqrt{(\hbar c) \frac{dk}{d\varepsilon_k}}$$

This is called the form factor of the photonic crystal. Now the DOS can be expressed in terms of the form factor as

$$D(\varepsilon_k) = D_0 Z^2(\varepsilon_k)$$

The form factor can also be expressed in terms of  $D(\varepsilon_k)$  as

$$Z(\varepsilon_k) = \sqrt{\frac{D(\varepsilon_k)}{D_0}}$$

Note that the form factor depends on the DOS.

Now, the band structure of photonic crystals made from dielectric spheres (refractive index  $n_s$  and diameter  $a$ ) and a background material (refractive index  $n_b$  and spacing  $b$ ) can be obtained as

$$\cos kL = F(\varepsilon_k)$$

where

$$F(\varepsilon_k) = \sum_{\pm} \left[ \pm \left( \frac{(n_s(\varepsilon_k) \pm n_b)^2}{4n_s(\varepsilon_k)n_b} \right) \cos \left( \frac{2\varepsilon_k(n_s(\varepsilon_k)a \pm n_b b)}{c} \right) \right]$$

This equation can be re-written as: can rewrite the eqn. (A9) in the following form

$$k = \frac{1}{L} \cos^{-1}(F(\varepsilon_k))$$

Finally, the form factor is calculated by differentiating this expression with respect to  $\varepsilon_k$ .

## Appendix H: The Laplace Transform Method

The Laplace Transform Method [304] is an algebraic technique of obtaining a particular solution of a differential equation given specific initial conditions. The Laplace transform  $L(f(t))$  of a function  $f(t)$  is defined as the function  $F(s)$  given as follows:

$$F(s) = L(f(t)) = \int_0^{\infty} e^{-st} f(t).dt$$

The transforms used in this thesis make use of following two properties:

$$\begin{aligned} L(a f(t) + b g(t)) &= a L(f(t)) + b L(g(t)) \\ L(f'(t)) &= \int_0^{\infty} e^{-st} f'(t).dt \end{aligned}$$

These give the following results:

$$L(f'(t)) = sL(f(t)) - f(0)$$

The particular transforms of interest as far as the calculations in chapters 2 – 4 are concerned can be found in Reference [304].

### **Appendix I: Hamiltonian of the Nanoparticle II**

Without loss of generality, we consider a two-level atom as the doped nanoparticle, with states  $|a\rangle$  and  $|b\rangle$ , having energies  $\varepsilon_a$  and  $\varepsilon_b$ , respectively.

The Hamiltonian of the nanoparticle is written as:

$$H_A = \sum_{i=a,b} \varepsilon_i \sigma_{ii}$$

where  $\sigma_{ii}$  is the number operator giving  $\sigma_{ii}|i\rangle = \varepsilon_i|i\rangle$ .

This gives:

$$H_A = \varepsilon_a |a\rangle\langle a| + \varepsilon_b |b\rangle\langle b|$$

### **Appendix J: Fehlberg Fourth-fifth Order Runge-Kutta Method (RK45)**

This method is widely used to ensure accuracy in obtaining the solutions of systems of ordinary differential equations [305]. It is based on the precept of solving the system twice using step sizes  $S$  and  $S/2$ . This is followed by a comparison of the solutions at the mesh points associated to the larger step size  $S$ . The comparison process is the key behind the efficiency of this method as it determines if the step size being used is optimum.

At each step of the procedure, two different approximations for the solution are obtained.

The subsequent comparison process has three possible outcomes:

1. If the two approximations are in agreement within the specified order (in this case, fifth) of accuracy, they are accepted as solutions.
2. If the preceding is not true, the step size is decreased.
3. If the approximations agree to within a higher order of accuracy than required, the step size is increased.

## Appendix K: Switching Power

In Reference [306], Majumdar et al. have analyzed the performance of an electro-optic modulator based on a single quantum dot (nanoparticle) strongly coupled to a nano-resonator. They have obtained the following formula for the control energy per switching operation ( $U_{dev}$ ) as follows:

$$U_{dev} = \frac{1}{2} \epsilon_0 \epsilon_r V_d E_{ext}^2$$

where  $V_d$  is the volume (in cubic nanometer units) of the nanoparticle,  $E_{ext}$  is the external laser field applied to the nanoparticle (in V/m),  $\epsilon_0 = 8.85 \times 10^{-12}$  F/m is the absolute permittivity constant and  $\epsilon_r$  is the dielectric constant of the material constituting the resonator.

For the pulse frequency  $f_l$  (in Hz) of the applied laser field, Majumdar et al. [306] have calculated the operating power of the device (nanoparticle) as

$$O_{power} = f_l U_{dev} = \frac{1}{2} \epsilon_0 \epsilon_r f_l V_d E_{ext}^2$$

Using the above equation, they have estimated the operating power for a device with volume  $V_d = 1 \mu\text{m} \times 1 \mu\text{m} \times 200 \text{ nm}$  when an external laser field with  $E_{ext} = 5 \times 10^4$  V/cm is applied. They have taken  $\epsilon_r = 13$  and  $f_l = 10$  GHz.

Putting the above parameters in the preceding equation, they found that  $U_{dev} = 0.5$  femto-Joules and  $O_{power} = 5 \mu\text{W}$ . These energy scales are of the same order of magnitude as all other optical switching devices operating at the single-photon level [307, 308].

In the present thesis, we have studied systems consisting of nanoparticles (QDs) and photonic crystals. The advantage of using a photonic crystal reservoir is that one can easily manipulate the dielectric constant of the system and the intensity of the radiation fields within the crystal reservoir. In Chapter 2, we have shown that there is a band gap present in the photon dispersion relation of the photonic crystal, which can be used to change the intensity of the radiation field within the crystal. This is due to the fact that the

density of states within the photonic crystal is very large near the upper and lower band edges and has a value of zero within the band gap. This means that an external radiation field applied to the system having frequencies lying within the band gap does not propagate within the device; hence, the device will not operate. Conversely, if the frequency of the external field lies outside the band gap, the field will propagate freely. This property can be used for making switching devices by changing the frequencies of the applied fields.

Note that the expressions of the  $U_{dev}$  and  $O_{power}$  given above are expressed in terms of amplitude  $E_{ext}$  of the laser field. In the works presented in this thesis, we have denoted the amplitude of the laser field in terms of the Rabi frequency  $\Omega_{ext}$ . This can be defined, in general, as:

$$\Omega_{ext} = \frac{P_{ab} E_{ext}}{\hbar}$$

where  $P_{ab}$  refers to the dipole moment between states  $|a\rangle$  and  $|b\rangle$ . The value of  $P_{ab}$  is in the order of magnitude of the product between the electronic charge ( $1.602 \times 10^{-19}$  C) and the Bohr radius ( $5.29 \times 10^{-11}$  m).

We can use the above equation for  $\Omega_{ext}$  to rewrite the expressions for  $U_{dev}$  and  $O_{power}$ , in terms of the Rabi frequency:

$$U_{dev} = \frac{\epsilon_0 \epsilon_r V_d \hbar^2 \Omega_{ext}^2}{2 P_{ab}^2}$$

$$O_{power} = \frac{f_l \epsilon_0 \epsilon_r V_d \hbar^2 \Omega_{ext}^2}{2 P_{ab}^2}$$

Now, we can calculate the energy per switching operation  $U_{dev}$  and the operating power  $O_{power}$  of our optoelectronic device consisting of the QD and the photonic crystal reservoir. The typical size (volume) of our device is taken as  $V_d = 10^9$  cubic nm. Without loss of generality and accounting for the most intense laser field considered in the thesis, we have calculated the Rabi frequency of the external field  $\Omega_{ext} = 2.6 \times 10^6$  Hz (the



magnitude of the electric field is taken as  $2.0 \times 10^6$  V/m, as in the literature), where the vacuum decay rate  $\gamma_0$  is taken as in Reference [306]. The dielectric constant of the spheres constituting the photonic crystal is taken as  $\epsilon_r = 5.5$  and  $f_l = 15$  GHz. Using these values, we estimate the values of  $U_{dev}$  and  $O_{power}$  as 0.097 femto-Joules and 1.46  $\mu$ W, respectively. These values, crucially, are well within the acceptable limit of energy and power consumption mentioned earlier in this appendix.

## Curriculum Vitae

|  |   |
|--|---|
| <b>Name:</b>                                 | Iftekhar Haque  |
| <b>Post-secondary Education and Degrees:</b> | <p>Western University<br/>London, Ontario, Canada<br/>2003-Present Ph.D.</p> <p>University of Toronto<br/>Toronto, Ontario, Canada<br/>1998-2003 B.Sc.</p>  |
| <b>Honours and Awards:</b>                   | <p>National Science and Engineering Research Council (NSERC)<br/>Postgraduate Scholarship (PGS D)<br/>2006-2009</p> <p>Faculty of Science Graduate Student Teaching Award<br/>Western University, London, Ontario<br/>2007</p> <p>Province of Ontario Graduate Scholarship (OGS)<br/>2005-2006</p> <p>Dept. of Physics and Astronomy Award of Excellence in Teaching<br/>Western University, London, Ontario<br/>2005</p> <p>Graduate Student Teaching Award<br/>SOGS, GTA and FGS, Western University, London, Ontario<br/>2004</p> <p>Undergraduate Teaching Assistant Award<br/>University of Toronto, Toronto, Ontario<br/>2002</p> |
| <b>Related Work Experience</b>               | <p>Mathematics Technologist (Full-time)<br/>The Learning Centre, Fanshawe College<br/>2014-Present</p> <p>Professor (Mathematics and Physics)<br/>School of Applied Science and Technology, Fanshawe College<br/>2013-Present</p>   |

Teaching Assistant  
Department of Physics and Astronomy, Western University  
2003-2007

Teaching Assistant  
Department of Physical Sciences, University of Toronto  
2000-2003

#### **Publications in Refereed Journals:**

1. **Haque, I.** and Singh, Mahi R. (2007). A Study of the ac Stark Effect in Doped Photonic Crystals. J. Phys.: Condens. Matter, 19, 156229, 1-18.
2. Singh, Mahi R. and **Haque, I.** (2005). Coherent Population Trapping in Photonic and Dispersive Band-gap Materials. J. Mod. Opt. 52, 1857.
3. Singh, Mahi R. and **Haque, I.** (2005). Numerical Simulations of Photon Trapping in Doped Photonic Crystals Doped with Multi-level Atoms. Phys. Stat. Sol. (c) 2, 2998.

#### **Publications in Refereed Conference Proceedings:**

4. **Haque, I.** and Singh, Mahi R. (2005). Coherent Photon Trapping in Doped Photonic Crystals and Dispersive Semiconductor Materials. AIP Conf. Proc. 772, 1246.

#### **Publications in Conference Proceedings:**

5. Singh, Mahi R., Zinke-Allmang, M., To, C., **Haque, I.**, and Maszko, A. (2006). Computing by Thermal Hopping: DNA as a Biomolecular Conductor. 25th Annual Meeting of the Canadian Biomaterials Society, Calgary.
6. Singh, Mahi R. and **Haque, I.** (2005). Numerical Simulations on Transient Polariton Linewidth in Dispersive Band-gap Materials. Proc. SPIE 5971, 59711H.
7. **Haque, I.** and Singh, Mahi R. (2004). Self-consistent Numerical Simulation of Dipole-dipole Interaction between Impurity Quantum Dots in Dispersive Materials.

Photonics 2004 -- 7th International Conference on Optoelectronics, Fiber Optics & Photonics, Cochin, SPIE Elec. Conf. Proc.